University of Pavia
Department of Molecular Medicine

PhD course in Translational Medicine

XXXIV cycle

PhD thesis on

Role of HGF/SF in tissue regeneration

Tutor:
Prof. Hugo de Jonge
Prof. Ermanno Gherardi

Candidate:
Dr. Enrica Bovio

Academic year 2020-2021

Dedicated to…..

Lorenzo, my family, my friends, Murphy's law, and bad planning

Index

Abstract

Nonalcoholic fatty liver disease (NAFLD), and the more advanced stage nonalcoholic steatohepatitis (NASH), is nowadays a major health problem with a global prevalence estimated at 25%. NAFLD patients have an increased risk to develop cirrhosis, end stage liver disease, and hepatocellular carcinoma. While there is an urgent need for effective treatment, unfortunately, there are no approved drugs for this condition.

Hepatocyte apoptosis and inflammatory response are key events for NASH development. It was therefore hypothesized that combination therapy with Hepatocyte Growth Factor/Scatter Factor (HGF/SF), the most potent liver survival-promoting factor, and a macrophage-focused immunotherapeutic drug able to switch M1 macrophages to M2 phenotype can cure NASH. Unfortunately, HGF/SF is unsuitable for therapy because it has a limited tissue/organ penetration and distribution due to its high affinity for heparan sulphate proteoglycans (HSPG). Moreover, it has a short half-life and is unstable in physiological buffers. Therefore, our laboratory in collaboration with the group of Dr. Vicogne at Pasteur Institute in Lille designed and produced K1K1, a new engineered fragment of HGF/SF able to overcome the limitations of the parent molecule and to be more suitable as a drug candidate.

The stability and the biological activity of K1K1 were compared to HGF/SF, highlighting K1K1 superiority. Furthermore, we investigated the activation of signaling pathways in two liver cell lines after stimulation with K1K1, HGF/SF, and other recombinant proteins, showing that K1K1 was as good as HGF/SF.

In order for K1K1 treatment to work, it was important to confirm that the receptor is present, and the pathway is relevant in the diseased tissue. Assessment of MET protein expression with immunohistochemistry (IHC) in formalin-fixed paraffin-embedded (FFPE) liver samples of patients with NAFLD showed that MET receptor is expressed on the hepatocytes and therefore K1K1 could be regarded a good drug candidate for use in future therapy.

Finally, we have evaluated the protective effect of K1K1 alone or in combination with macrophage-focused immunotherapeutic drugs on a NASH-on-a-chip model. The combination therapy was found to be the most effective in reducing steatosis, apoptosis, and fibrosis. These promising results highlight K1K1 potential as a new drug candidate for NASH treatment.

Introduction

Chronic diseases

In 2017 non-communicable diseases (NCDs) represented the greatest fraction of deaths (73.4%) while communicable, maternal, neonatal, and nutritional (CMNN) causes accounted for 18.6%. In ten years (2007-2017) there was a 22.7% increase in total numbers of deaths from NCDs while the number of deaths for CMNN causes decreased by 22.2% [1].

Degenerative diseases of epithelial organs such as chronic obstructive pulmonary disease (COPD), acute kidney injury (AKI), alcoholic and non-alcoholic steatohepatitis (ASH and NASH) are nowadays a major cause of mortality and new therapeutic strategies are needed [1 2].

Regenerative medicine is a rapidly evolving field, the goal of this young discipline is to develop new therapies to restore cells, tissues and organs that have been harmed by aging or disease. Regenerative medicine therapies frequently involved the use of stem cells but currently the scientific, financial, and regulatory challenges make the application of these therapies to diseases affecting millions of people very difficult [3]. Alternative approaches are therefore necessary and protein-based therapy could be a promising option in diseases lacking effective treatment. Growth factors are particularly interesting molecules, they can stimulate many cellular processes including cell proliferation, migration, differentiation, and multicellular morphogenesis, therefore growth factors are essential molecules for tissue repair and regeneration [4].

Our laboratory worked extensively on growth factors, here a novel MET receptor agonist based on Hepatocyte Growth Factor/Scatter Factor (HGF/SF) was developed, and this new molecule has the potential to be used for regenerative medicine purposes.

Hepatocyte Growth Factor/Scatter Factor (HGF/SF)

HGF/SF has a double name because the protein was discovered independently by two research groups. The first group identified a mitogenic protein for hepatocytes [5], later called HGF, while the second one discovered the *scatter* factor that promotes the migration of epithelial cells [6].

The human gene for *HGF/SF* is located on the long arm of chromosome 7 at q21.1 and it is formed by 18 exons and 17 introns [7].

HGF/SF is biosynthesized as a single-chain prepro-form of 728 amino acids, including a signal sequence and both α and β-chains. After cleavage of the first 31 amino acids signal sequence, a single-chain pro-HGF is further cleaved between Arg494 and Val495. This processing is coupled to the conversion of biologically inactive pro-HGF to active HGF and it has been proposed that several proteases in the serum or cell membranes are involved in the activation of single-chain HGF, such as urokinase-type plasminogen activator, plasma kallikrein, coagulation factors XII and XI, matriptase, hepsin, and HGF activator (HGF-A) [8].

HGF-A plays an important role, this protein is biosynthesized mainly by hepatocytes and circulates in the plasma as an inactive single-chain proHGF-A. Inside injured tissues, prothrombin is converted to thrombin which in turn activates proHGF-A, leading to HGF/SF activation in response to tissue damage [8].

The activity of HGF-A is also regulated by HGF-A inhibitor-1 (HAI-1) which is not only a specific inhibitor but also a cell-associated reservoir of HGF-A. In conclusion, the regulatory mechanism for the activation of pro-HGF can be considered a link between inflammation and tissue regeneration [8].

The active and final form of HGF/SF is glycosylated and composed of two chains linked by a disulfide bond [7]. The 69 kDa α-chain has an N-terminal hairpin loop and four kringle domains while the 34 kDa β-chain has a serine protease homology (SPH) domain (**Fig. 1**) [9].

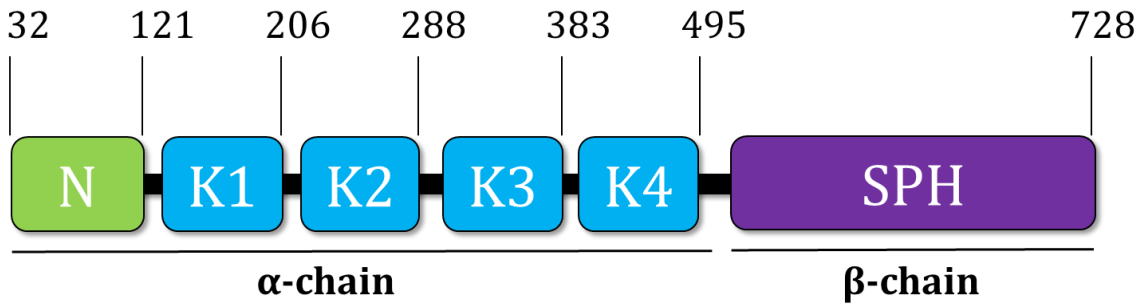

Fig. 1 Schematic structure representing HGF/SF domains.

HGF/SF belongs to the family of plasminogen-related growth factors with a SPH domain that does not show proteolytic activity because of specific substitutions of important amino acids within the catalytic site [7].

HGF/SF is mainly synthetized by mesenchyme-derived cell types such as smooth muscle cells and fibroblasts and especially these last ones are present in different tissues including liver, skin, kidney, lung, heart, and brain [10].

In contrast to other growth factors HGF/SF binds to only one receptor, the Mesenchymal Epithelial Transition (MET) receptor [11].

MET receptor

In 1984, human *MET* oncogene was first discovered due to its transforming activity caused by a gene fusion between *MET* and the translocated promoter region (*TPR*). Isolation of the full-length human *MET* proto-oncogene sequence was possible in 1987, revealing this gene encoded a transmembrane receptor tyrosine kinase [12].

The human *MET* gene is located on chromosome 7q21-q31, it is formed by 21 exons and the protein is biosynthesized as a single chain precursor of 1,390 aa [13 14] . Immediately after translation, the protein is glycosylated inside Golgi reticulum and later, in the post-Golgi compartment, the cellular protease furin cleaves MET precursor between residues 307 and 308. The result of the cleavage are two chains named alpha and beta linked by a disulphide bond [14]. The mature MET receptor is a 190 kDa glycosylated protein with a 50 kDa extracellular α-chain and a 145 kDa β-chain that contains most of the extracellular domain, the transmembrane domain, and the intracellular domain (**Fig. 2**) [9].

The MET extracellular portion is composed of a semaphorin (SEMA) domain, a plexin-semaphorin-integrin (PSI) domain and four immunoglobulin-plexin-transcription (IPT) repeats. The SEMA domain includes the entire α-chain and part of the β-chain and it is HGF/SF binding site (**Fig. 2**) [14].

The receptor intracellular domain is composed of a juxtamembrane domain, a kinase domain, and a carboxyl-terminal domain. The juxtamembrane domain is involved in MET signal downregulation through two residues, Ser975 and Tyr1003 while phosphorylation of Tyr1234 and Tyr1235 within the kinase domain increase MET signaling. The carboxyl-terminal domain function as a docking site for the recruitment of many transducers and adaptors and Tyr1349 and Tyr1356 are two important sites for this process (**Fig. 2**) [11 14].

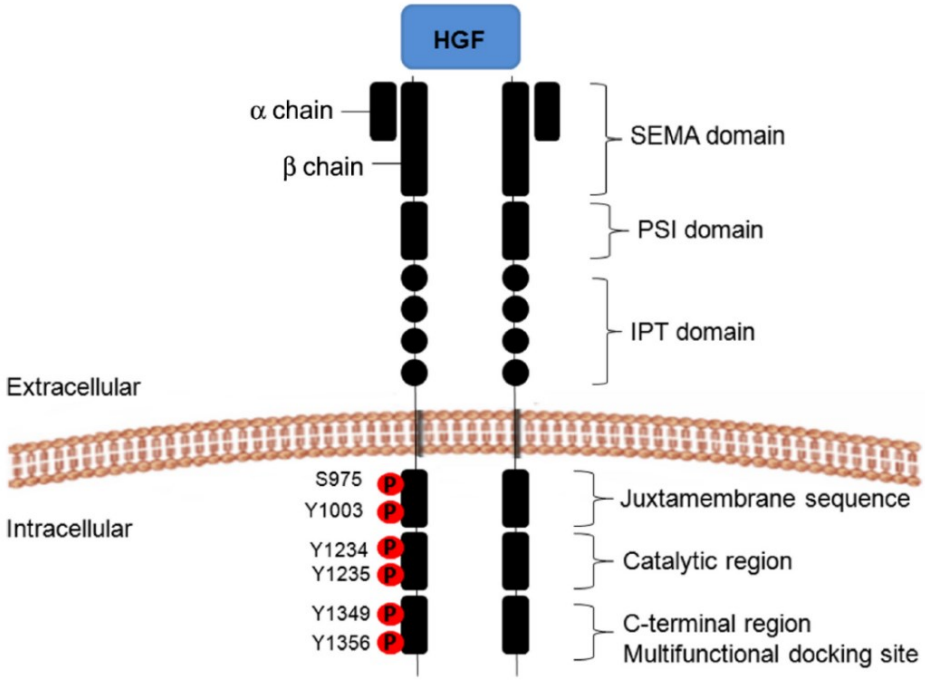

Fig. 2 Schematic structure of MET domains [11].

MET, unlike HGF/SF, is mainly expressed on the surface of epithelial and endothelial cells and the unique distribution of cells expressing MET or HGF/SF facilitates paracrine signaling [9 11].

HGF/SF-MET signaling pathways

MET signaling starts when HGF/SF binds to the MET receptor, leading to the stable homo-dimerization of two receptors. Immediately after, the intracellular domain is activated due to trans-phosphorylation of Tyr1234 and Tyr1235 in the kinase domain, followed by a second trans-phosphorylation of Tyr1349 and Tyr1356 within the carboxyl-terminal domain [11].

Tyr1349 and Tyr1356 are necessary to form the multifunctional docking site which is essential for the activation of multiple signaling pathways directly or are used by adaptors such as growth factor receptor-bound protein 2 (GRB2) and GRB2-associated-binding protein 1 (GAB1). Subsequently, many different intracellular signaling pathways are activated such as the Mitogen-activated protein kinases (MAPK), that is involved in the regulation of normal cell proliferation, survival, and differentiation [8 11].

The (MAPK)s are a family of serine/threonine protein kinases, that propagate a cascade starting from the MAPK kinase kinase (MAPKKK) group, the MAPK kinase (MAPKK), to the MAPK that are partially controlled by their phosphorylation. There are several

isoforms of MAPKs for each group, the best studied are extracellular signal-regulated kinases (ERKs). MET signaling activates rat sarcoma virus (RAS) protein through the GRB2–SOS complex which can interact directly with MET docking site or can be associated indirectly. RAS can be also activated in a different way, through Src homology phosphatase 2 (SHP2) dephosphorylation of GAB1 binding site. In this pathway, MET activation triggers guanosine triphosphate (GTP) loading of the RAS GTPase which can recruit and activate RAF kinases. When RAF moves to the membrane, it becomes activated leading to kinases MEK1 and MEK2 phosphorylation and activation. These two kinases then phosphorylate the final effectors ERK1/ERK2 [11].

The second pathway is the PI3K–AKT pathway. PI3K can be activated directly by MET and/or indirectly by RAS. After MET activation, the lipid kinase PI3K phosphorylates phosphatidylinositol (4,5)-bisphosphate (PIP2) to synthesize the second messenger phosphatidylinositol (3,4,5)-triphosphate (PIP3). PIP3 recruits AKT to the plasma membrane where it is phosphorylated and activated by phosphoinositide-dependent kinase-1 (PDK-1). Activated AKT phosphorylates many targets such as the mammalian target of rapamycin (mTOR), pro-apoptotic protein BAD, anti-apoptotic protein BCL2, E3 ubiquitin-protein ligase MDM2 and glycogen synthase kinase 3β (GSK3β). All these proteins can interfere with important cell cycle regulators such as myc and cyclin D [11].

The third pathway activated is the Janus kinase (JAK)–signal transducer and activator of transcription (STAT) pathway. There are seven members of the STAT protein family, the phosphorylation of the docking site of MET is followed by STAT3 phosphorylation which causes dissociation from the receptor. STAT3 mainly acts as a direct transcription factor, promoting cell proliferation, survival, and invasion [11].

The fourth pathway is nuclear factor-kappaB (NF-κB) pathway, which regulates gene expression by binding to their promoters/enhancers. The NF-κB family consists of five proteins that form homo and heterodimeric complexes by associating with each other. The NF-κB system is inactive in the cytoplasm due to the action of the inhibitor of κB (IκB) but NF-κB can be activated after inhibitor destruction, leading to the unmask of the nucleus localization signal (NLS) and NF-κB release. Then NF-κB is free to translocate to the nucleus and to transactivate target genes by binding to gene promoter/enhancer regions [11].

In conclusion, HGF/SF- MET signaling causes proliferation, cell survival, division, and migration (**Fig. 3**) [11 13].

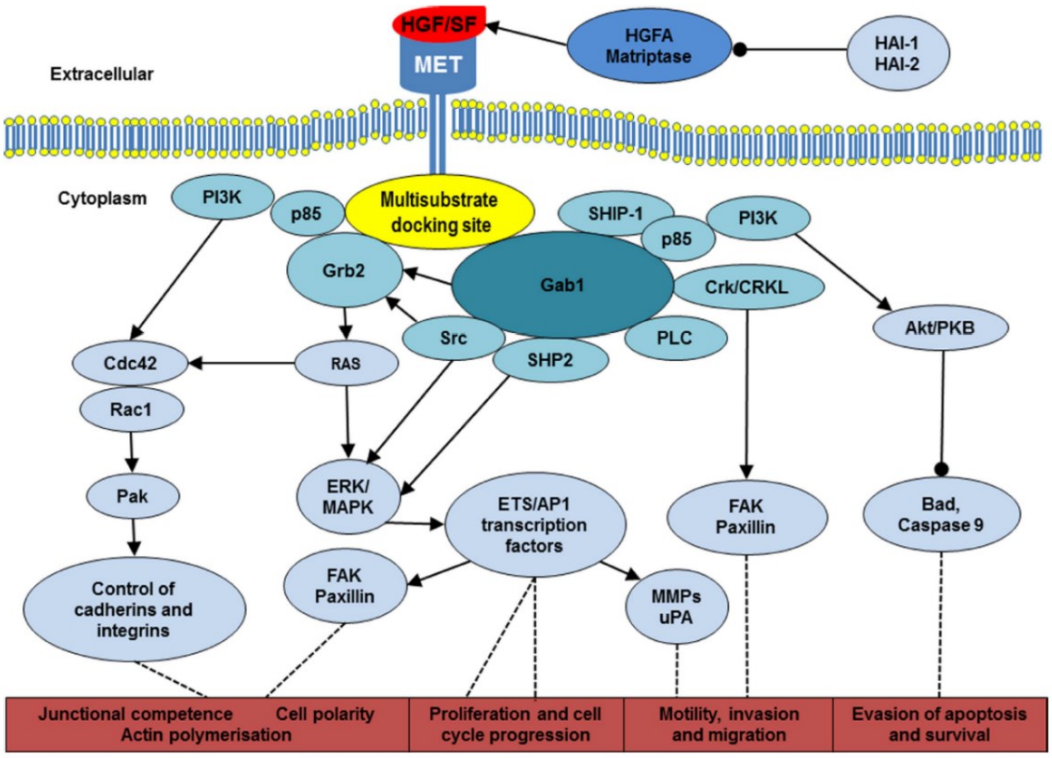

Fig. 3 The HGF/SF-MET pathway [13].

HGF/SF-MET pathway in development and in adult tissues

HGF/SF-MET pathway is essential both during embryogenesis and in adult life. Knockout mice for HGF/SF die in utero after 13.5-15.5 days, both placenta and liver development is impaired [9 14]. Similarly, knockout mice for MET also die in utero, and they also have liver development problems [9].

HGF/SF works as a chemoattractant signal for myogenic precursor cells and in embryos lacking MET expression, migration of myogenic precursor cells from the dermomyotome in the somite to the limb buds and diaphragm is impaired. Therefore, the skeletal muscles of the limbs and diaphragm are not formed [9].

HGF/SF is also implicated in neuronal and glial development [8]. HGF/SF acts as a chemoattractant for spinal motor neurons and for the projection of motor neurons to limb muscle and it is also involved in the development of sensory, sympathetic, parasympathetic, and cortical neurons. In the end, HGF/SF regulates proliferation and differentiation of oligodendrocyte progenitor cells [8].

Activation of HGF/SF-MET pathway is vital also in adult life and it is involved in many physiological processes. HGF/SF can not only stimulate proliferative, mitogenic, motogenic, 3-D morphogenic activities but it can also act suppressing apoptotic cell death in many tissues [8].

The involvement of HGF/SF-MET pathway in tissue protection and regeneration was particularly studied in liver tissue. HGF/SF expression increases in response to liver injuries while conversely, neutralization of endogenous HGF/SF increases hepatocytes apoptosis, necrosis, and suppressed liver regeneration [8] .

HGF/SF connection to liver functioning was demonstrated using conditional knockout of the *MET* gene in mice [15] [16] [17]. In these mice, administration of a low-dose of agonistic anti-Fas antibody in mice with hepatocyte-specific *MET*-/- caused hypersensitivity even to mild liver injury, demonstrating the antiapoptotic activity of HGF/SF in liver protection [15].

Delayed liver regeneration, persistent inflammatory reaction and susceptibility to fibrotic change was also observed in liver or hepatocyte-specific *MET-/-* mice [16].

In another experiment, chronic cholestatic liver injury was induced after bile duct ligation and mice with hepatocyte-specific M*ET*-/- showed increased hepatocyte apoptosis, inflammation, profibrogenic responses, and were more susceptible to chronic inflammation and fibrotic change when compared to controls [17].

The hepatotropic and hepatoprotective roles of HGF/SF were well studied but HGF/SF-MET pathway is also able to support the protection and regeneration of other tissues such as kidney, lung, nervous system, cardiovascular, cutaneous, and gastrointestinal tissues [8].

HGF/SF-MET pathway also plays an important role in repressing fibrosis and inflammation in different cell and tissue types as demonstrated in studies using tissue-specific *MET* knockout mice [8].

Chronic tissue injury is tightly associated with fibrotic change, and this is particularly important for liver cirrhosis and chronic kidney disease. Nowadays, there are no effective treatments for these diseases but, at least in animal models, HGF-treatment is highly effective on chronic fibrosis in various disease models, including liver cirrhosis, chronic kidney disease, dilated cardiomyopathy, and lung fibrosis [8].

HGF/SF has an important role in tissues protection and regeneration as stated before, but it can also be involved in tumor biology because in cancer tissues the pathways physiologically activated by MET can be adopted for invasion and metastasis [8].

HGF/SF could be a potential drug candidate to treat chronic disease considering the essential roles in the regeneration of epithelial organs but there are several drawbacks in using this protein for therapy. First, mammalian expression systems need to be used to produce HGF/SF because of its complex structure and the presence of posttranslational

modification, and unfortunately, the yield is limited and the costs are high [18]. Second, HGF/SF has a very short half-life [19] and it is unstable in physiological buffers [18]. Third, the protein acts only locally because it has a high affinity for heparan sulphate proteoglycans (HSPG), which limit penetration and distribution *in vivo* [20].

The goal was therefore to overcome these limitations through the design and production of a novel, minimal MET agonist. This process started with the discovery of alternative spliced isoforms of HGF/SF called NK1 and NK2.

NK1 and NK2

Shortly after the discovery of HGF/SF two isoforms were identified, NK1 and NK2. The NK1 variant is a 21 kDa protein containing the *N*-terminal hairpin and the first kringle domain [21], while NK2 is a 33 kDa protein extending through the second kringle domain [22] [23].

The *NK1* isoform is the shortest functionally active isoform of *HGF/SF*, it is transcribed as a 2079 nucleotides mRNA of five exons encoding a 201 aa polypeptide [10].

The other functionally active isoform of *HGF* is *NK2*, it is transcribed as a 1292 or 1307 nucleotides mRNA of seven exons, encoding a 284 aa or a 290 aa protein [10].

Both NK2 and NK1 are able to bind MET receptor and to compete with HGF/SF for the binding, inducing a comparable MET phosphorylation. NK1 and NK2 are also expressed in human tissues during development and in adults but the biological and cellular activities of these two isoforms differ from the ones of the full length HGF/SF [10].

NK1 can recapitulate most of the actions of full-length HGF/SF in cell lines (motility, proliferation, morphogenesis), but little is known about whether the signaling induced by NK1 in cells is the same of HGF/SF [10].

The situation is even more complex with NK2 because this protein is not able to induce proliferation and branching morphogenesis in any cell type tested. NK2 can still induce motility in MDCK cells but not in other cell types and NK2 can competitively inhibit HGF/SF-induced proliferation and morphogenesis. NK2 signal transduction is still poorly understood [10].

Little is known about NK1 and NK2 biological functions and their over-expression *in vivo* have varying effects on cellular proliferation, survival, and migration.

NK1 over-expression in transgenic mice was similar to HGF/SF over-expression in many aspects because in both cases “enlarged livers, ectopic skeletal-muscle formation,

progressive renal disease, aberrant pigment cell localization, precocious mammary lobuloalveolar development" were reported by Jakubczak et al. (Jakubczak et al., 1998). However, in mice over-expressing NK1 livers were only 1.5-fold enlarged, compared with 2–3-fold increases observed in mice over-expressing HGF/SF, and cancers incidence were lower [24] .

Mice over-expressing NK1 also had increased hepatocyte proliferation and reduced liver fibrosis after partial hepatectomy [10].

NK2 over-expression in transgenic mice did not show the phenotypic consequences observed in response to HGF/SF over-expression. Metastasis had lower or increased incidence according to different studies [10].

When both NK2 and HGF/SF were over-expressed, HGF/SF alterations did not show, indicating a potential blocking effect of NK2 on over-expressed HGF/SF [10].

NK2 over-expression in murine models of liver injury have mixed results even if in all of them NK2 seems to be involved in tissue repair inhibition [10].

In conclusion, NK1 can recapitulate most of HGF/SF biological activities, while NK2 appears to be a partial antagonist of HGF/SF as it does not induce proliferation of normal cells and may also contribute to the inhibition of tissue repair [10].

From NK1 to 1K1 and K1K1

Structural studies dedicated to the understanding of the HGF/SF-MET interaction made possible to identify two binding sites for the MET receptor on HGF/SF molecule, a low-affinity binding site in the SPH domain and a high-affinity binding site within the N-domain and the K1 domain [25]. Using deletion mutagenesis, the MET binding site for HGF/SF and heparin were also discovered, both of them were located within the SEMA domain, in a region spanning the α-chain (amino acids 25-307) and the β-chain (first 212 amino acids) [26].

HGF/SF has a high-affinity for HSPG and its analogue heparin, and two binding sites were identified, a high-affinity binding site in the N-domain and a low-affinity binding site within the K1 domain [18].

NK1 can recapitulate most of HGF/SF biological activities [10], and this protein has both the high-affinity heparin binding site within the N-domain and the high-affinity binding site for MET [27] [28]. Using protein engineering, HSPG binding sites were changed to improve the protein activity and tissue/organ distribution and a new HGF/SF derivate molecule was created, 1K1 [18]. Both 1K1 and NK1 were produced in yeast and 1K1 is a mutant of NK1

with a reduced affinity for HSPG because the low-affinity binding site for HSPG on K1 domain is disrupted through two reverse charge mutations (K132E:R134E) [18].

First, analytical ultracentrifugation was used to compare 1K1, NK1 and HGF/SF stability showing 1K1 and NK1 were more stable than the full-length protein. Second, proliferative, and anti-apoptotic effects of these variants were tested in primary human hepatocytes and in rodents. *In vitro* experiments with human hepatocytes showed all HGF/SF forms induced similar levels of DNA synthesis and reduced levels of Fas ligand-mediated apoptosis. *In vivo* experiments showed 1K1 was more active than NK1 in healthy mice where it significantly increased hepatocyte DNA synthesis, and in mice treated with carbon tetrachloride, where it reduced fibrosis. In rats, after 70% partial hepatectomy, daily administration of 1K1 for 5 days was significantly superior to NK1 treatment in increasing liver mass and bromodeoxyuridine labeling index [18].

1K1 was active both *in vitro* and *in vivo* and it has many advantages if compared to the full-length protein HGF/SF. The main advantages of 1K1 are better stability, it can be produced in high yield and at low costs in yeast, and has improved tissue penetration due to the reduced affinity for HSPG and a smaller molecular size [18].

NK1 was believed to be the smallest possible agonist but after extensive structural studies on HGF/SF-MET and NK1-MET complexes, the high-affinity binding site for MET was identified within K1 domain, opening therefore new perspectives [25 29 30 31 32]. This finding together with the observation that streptavidin-induced multimerization of a single biotinylated synthetic K1 domain resulted in a complex with potent biological activities, opened the way to the creation of K1K1 [33].

It was hypothesized that two K1 domains in tandem, forming a covalent K1K1 dimer with reduced heparin affinity, could behave as a minimal receptor agonist [34].

K1K1

To design K1K1, the spatial positions of the two K1 domains in the crystal structure of the NK1 dimer was studied [29 35]. Observing the NK1 dimer structure, the distance between the last cysteine in one K1 domain and the first cysteine in the other K1 domain was approximately 9 angstroms. A linker to bridge the K1 domains was therefore used and the four amino acids SEVE linker, which naturally occurs between K1 and K2 domains in HGF/SF, was chosen. The SEVE sequence was also introduced at the C-terminus. The result of this design was therefore a covalent K1 dimer that presents two receptor binding sites on opposite ends, and it no longer dependents on dimerization for its biological

activity, as is the case for NK1 [36] [37]. The other innovations of K1K1 are a significantly reduced heparin affinity due to the elimination of the N-domain and the possibility to produce this molecule in bacterial cells, therefore with high yields and at low costs compared to the parent molecule [34].

After preliminary studies, K1K1 was selected to assess its neuroprotective effect in *in vitro* and *in vivo* models of amyotrophic lateral sclerosis (ALS) [38].

ALS is a fatal motoneuron disease that lack effective treatments. Multiple mechanisms are responsible for motor neuron (MN) death and for the loss of muscular innervation, in particular there could be an activation of signaling pathways promoting cell death or a loss of activation of pro-survival pathways. The alteration of these pathways could be also detected together with the loss of the anti-inflammatory protective environment around damaged motor neurons [38].

HGF/SF interaction with MET receptor can activate survival pathways for sensory and motor neurons in case of tissue damage, both during the development and in adult. It was therefore interesting to test K1K1, the HGF/SF engineered protein with superior potency and stability described above, as a potential drug candidate for the treatment of ALS [38].

In vitro experiments showed K1K1 was ten times more effective than HGF/SF in preventing MNs loss. Indeed, when motor neurons were treated with K1K1, there was a total recovery of the viability at a ten-times lower concentration compared to HGF/SF treatment. The K1K1 neuroprotective effect was also tested *in vivo,* using a superoxide dismutase 1 G93A (SOD1G93A) transgenic mice, a frequently used ALS animal model. Here, K1K1 was able to postpone the onset of muscular impairment and it worked in reducing MN loss and skeletal muscle denervation [38]. Other important positive effects were associated with these first findings, there was an increased level of p-ERK in the spinal cord and sciatic nerves, and the activation of non-myelinating Schwann cells was reported. In the lumbar spinal cord of treated mice, reduced microglia and astroglia activation was reported, together with lower T cells infiltration and increased levels of interleukin 4. Finally, K1K1 was also effective in preventing T cells infiltration in skeletal muscle [38].

Unfortunately, these promising protective effects of the treatment were lost in long term, probably because of the insurgence of drug tolerance mechanisms [38]. In a separate study, the regenerative potential of K1K1 was more extensively tested both *in vitro* and on *in vivo* models of alcoholic steatohepatitis (ASH) [34].

In vitro experiments on Hela cells were performed to analyze MET receptor activation and downstream signaling after stimulation with recombinant human HGF/SF, K1K1, and other engineered proteins at different concentrations. P-MET, p-AKT, and p-ERK were detected by Western blot and K1K1 was able to stimulate phosphorylation down to 100 pM concentrations like HGF/SF. Precise quantification of AKT and ERK activation was possible using ALPHAScreen™ technology. For p-AKT, K1K1 showed lower maximum activation values compared to HGF/SF while for p-ERK there was no significant differences between the two proteins [34].

K1K1 and HGF/SF biological activities were also evaluated with different biological assays. First, a cell viability assay was performed. The assay was based on metabolic activity on MDCK cells incubated overnight in the presence of apoptosis inducer (anisomycin) or apoptosis inducer plus HGF/SF or K1K1 at different concentrations [34].

HGF/SF was more effective than K1K1 in preventing cell death but K1K1 was in turn much more potent than NK1 [34].

In the end, MDCK cells were also used for scatter assay, a powerful assay to determine the minimal concentration needed to induce the epithelial-mesenchymal transition. K1K1 was able to induce cell scattering down to 1 pM concentration, ten times lower than HGF/SF and one thousand times lower than NK1 [34].

In vivo experiments were performed, in which 8-week-old FVB mice were injected with different amounts of K1K1 (0.1 to 5 μg), the animals were sacrificed after 10 minutes, and p-MET, p-AKT and p-ERK were detected by Western blot on liver homogenates. No detectable phosphorylation signal was present in control and 0.1 μg of K1K1 while injection of 0.5, 1, and 5 μg gave uniform activation of the pathway [34].

After verifying the activation of MET receptor *in vivo,* 5 μg of K1K1 were injected to determine the duration of the stimulation by sacrificing the animals at different time points. The signal decreased over time, but it was detectable up to 60 min.

In the end, K1K1 *in vivo* efficacy was tested on a validated mouse model of subchronic alcohol exposure, the adapted Lieber DeCarli (LDC) model. The treatments with different doses of K1K1 (0.4, 2 and 10 μg) were significantly effective in decreasing the steatosis in mice fed with alcohol (LDC +K1K1). K1K1 treatment was not only able to decrease steatosis, but the highest doses of K1K1 (2 and 10μg) were also able to significantly decrease the mRNA expression of the proinflammatory cytokines TNFα and IL-6 [34].

The results obtained using K1K1 in *in vivo* models of ALS and ASH showed its therapeutic potential and the possibility to use this molecule as a drug candidate for other chronic diseases of epithelial organs such as nonalcoholic steatohepatitis (NASH).

NASH

Nonalcoholic fatty liver disease (NAFLD) is : "an increasingly common condition defined by the presence of ≥5% liver steatosis in the absence of significant alcohol consumption, steatogenic medication, or monogenic hereditary disorders" as stated by Romero et al. (Romero et al., 2020) [39].

NAFLD is a definition that comprises a continuum of liver conditions varying in severity. Hepatic steatosis (fatty liver) alone is named as nonalcoholic fatty liver (NAFL) while the term NASH is used to identify a more serious process where inflammation and hepatocyte damage, known as ballooning, are present [39 40].

Pericellular fibrosis is also typically identified in patients with NASH. Currently, imaging and clinical features are not sufficient for NASH diagnosis, it can only be definitively diagnosed after histological examination of a liver biopsy [39 40] .

In 1980 NAFLD was recognized as a distinct condition not caused by alcohol consumption but for more than 10 years there was an underestimation of this pathology, as a diagnosis of steatosis was considered a benign diagnosis. Many studies were necessary to point out that fatty liver not related to excessive alcohol consumption can lead to serious pathologies [41].

NAFLD and in particular NASH have become a global health problem for multiple reasons. In 2018 the global prevalence of NAFLD was estimated at 25%, with the highest values in South America, Asia and Middle East (**Fig. 4**) [42].

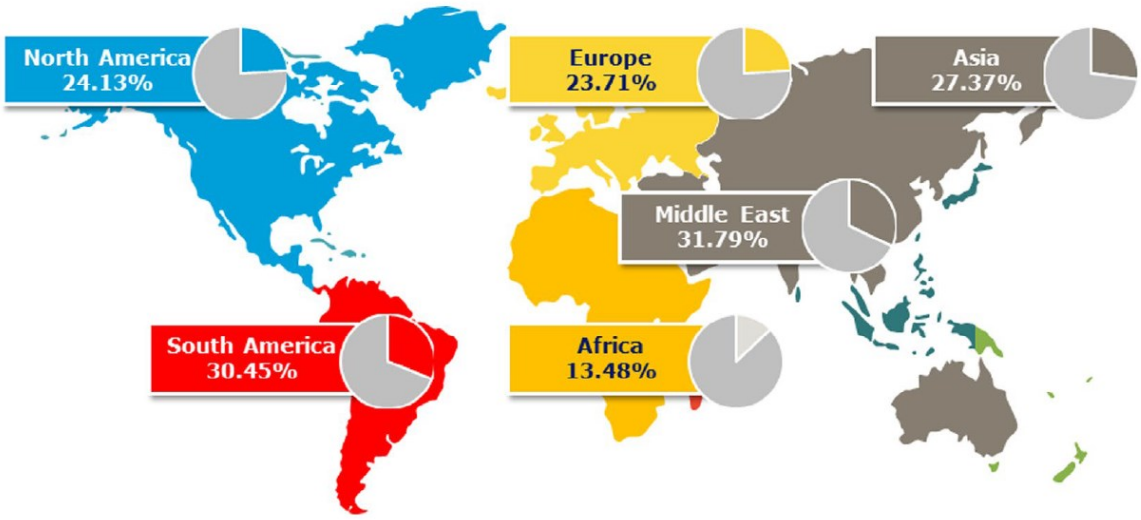

Fig. 4 NAFLD global prevalence [42].

NASH prevalence estimation is not so accurate because of histologic requirements, but in the US the prevalence of individuals with NASH is estimated between 1.5% and 6% [42].

Metabolic syndrome (MS), which includes obesity, type 2 diabetes mellitus, dyslipidemia, hyperglycemia and systemic hypertension is the most important risk factor for NAFLD development [39 40]. There is a strong link between metabolic syndrome factors and NAFLD, it was estimated that up to 75% of individuals with type 2 diabetes and 50% of patients with systemic hypertension have NAFLD [40].

Patients with NAFLD/NASH can experience important and even life-threatening clinical complications, indeed patients with NAFLD and primarily those with NASH have an increased risk of liver-specific death (> 6-fold) [42].

The increased risk of liver-specific death is deeply related to the stage of fibrosis and although cardiovascular disease is the first cause of death in NAFLD, in patients with advanced fibrosis mortality due to liver failure is predominant [42].

NAFLD is the seventh-most common cause of cancer death in US and the third one worldwide, indeed subjects with NAFLD can develop hepatocellular carcinoma (HCC) with a prevalence estimated between 2.4% and 12.8%. Liver transplantation represents another important clinical complication in patients with NASH, indeed NASH is now the second-leading indication for liver transplantation in the US [42].

NAFLD is an extremely complex pathology and in 2021 there are still no approved drugs for its treatment. Current strategies to treat NASH are the same used for type 2 diabetes and obesity, therefore a lifestyle change, with increasing physical exercise and weight loss. Weigh loss in particular can have therapeutic effects, improving all the parameters of

NASH, inflammation and fibrosis included. Dietary interventions and increased physical activity are effective in clinical trials but most of the times these conditions are not applicable to real life because NAFLD patients have a low compliance with diets and exercise [39] [43].

NAFLD has different rates of progression among individuals which show variegate clinical manifestation. These differences in clinical manifestations can be explained considering the complex natural history of this pathology where numerous risk factors are present. It will be extremely important to have a better understanding of these factors to establish NAFLD subtypes, therefore improving the prediction of disease progression and the choice of the most effective treatments [40].

NASH pathogenesis is complicated, many molecular pathways are involved, and it is not sure if NAFL always precedes NASH. Until a few years ago, the "two-hit" theory was used to explain NASH pathogenesis. The first "hit" was steatosis, the second "hit" was necessary for NASH development and involved other factors such as oxidative stress. This theory is now outdated, leaving space to more complex interpretations (**Fig. 5**) [40].

Free fatty acids (FFA) have a central role in NASH pathogenesis. FFA have different provenience, they are generated from lipolysis of triglyceride in adipose tissue and delivered to the liver or they can be synthesized from glucose and fructose by de novo lipogenesis (DNL) in hepatocytes. FFA within the hepatocytes have two possible fates: mitochondrial beta-oxidation or re-esterification to form triglyceride (**Fig. 5**) [40].

Triglycerides can be exported into the blood as very-low-density lipoprotein (VLDL) or they can form lipid droplets in hepatocytes, a hallmark of NAFLD. When beta-oxidation and re-esterification pathways are saturated, lipotoxic species can form from FFA, causing multiple consequences. Insulin resistance can contribute to the overload of FFA because there is a reduced glucose disposal in non-hepatic tissues, including adipose tissue where the inappropriate release of fatty acids takes place. The consequent accumulation of lipotoxic species leads to ER stress, oxidant stress, and inflammasome activation (**Fig. 5**) [40].

The inflammasome is a cytoplasmic complex composed of multiple proteins, activated by danger-associated molecular patterns (DAMPs), including saturated fatty acids, and by pathogen-associated molecular protein (PAMPs), which are the products of gut microbiota. The activation of hepatocyte inflammasome can be an important step between the first manifestation of NAFLD and later hepatocytes death and liver fibrogenesis, indeed in experiments with mice, it was demonstrated that hepatocytes

inflammasome activation cause both the expression of pro-inflammatory cytokines, such as interleukin (IL)-1β and IL-18, and the induction of apoptosis through caspase-1 activation (**Fig. 5**) [40].

Stressed or injured hepatocytes together with activated Kupffer cells can induce the activation of hepatic stellate cells into myofibroblasts that start producing matrix proteins faster than they are degraded. The progressive accumulation of the extracellular matrix leads to fibrosis, cirrhosis, and with time, to liver failure (**Fig. 5**) [40].

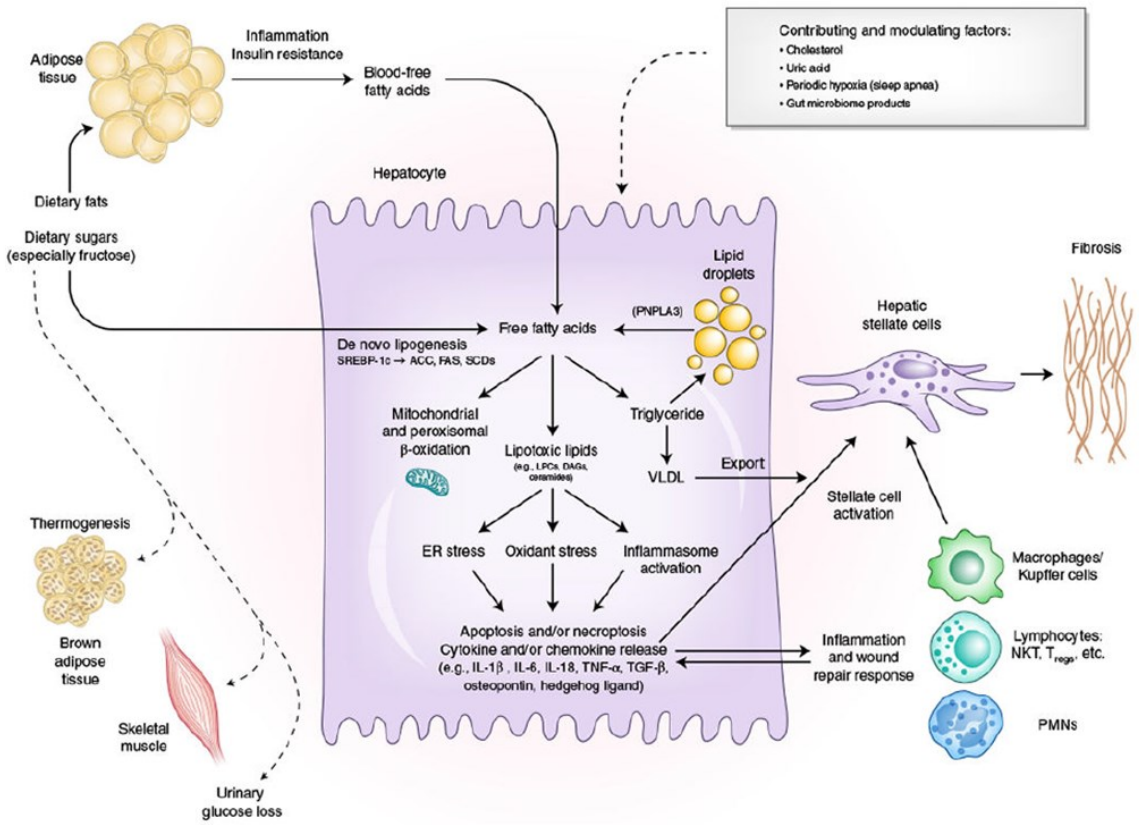

Fig. 5 Model of NASH pathogenesis [40] .

In 2022 more than 200 clinical trials are ongoing to test new drugs to cure NASH (https://clinicaltrials.gov). The drugs can be divided in 3 main groups based on their goal: those that target metabolic stress, the ones that act on reducing inflammation, and the ones that try to stop or reverse the progression of fibrosis (**Fig. 6**) [39].

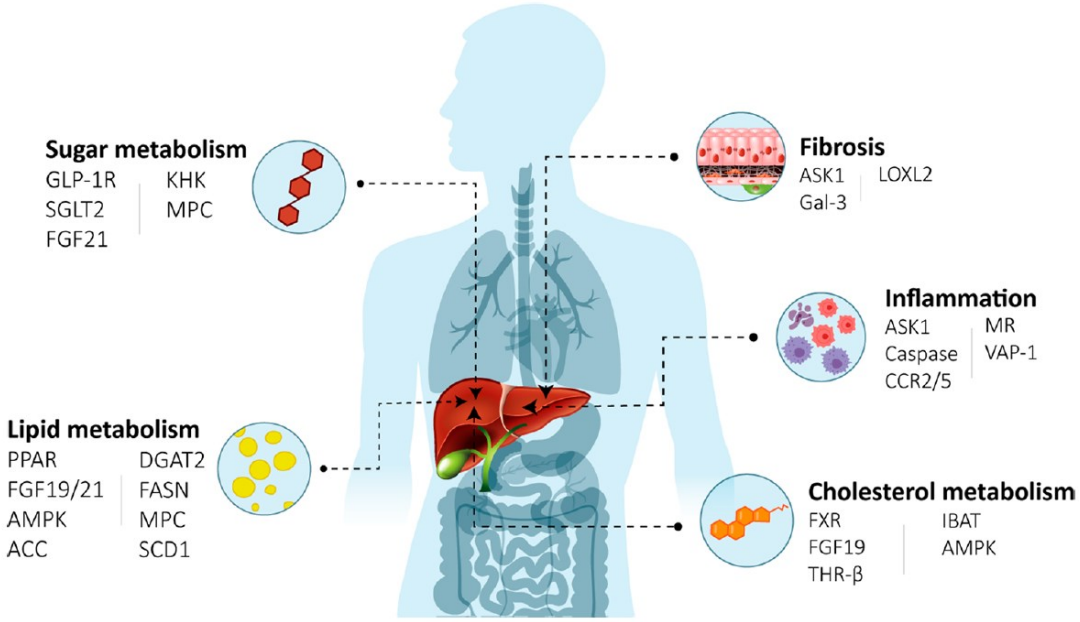

Fig. 6 Drugs that are under investigation for NASH and their modes of action [39].

Many factors make NASH drug development very complicated. First, NASH pathogenesis is complex, and patients have different rates of progression with variegate clinical manifestation, therefore they may respond very differently to the same treatment, even with similar clinical diagnoses. Second, a long treatment duration (>1 year) is needed in clinical trials to achieve NASH resolution, and invasive procedures like liver biopsy are required for the evaluation of the treatment. Third, there is still a lack of valuable in *vitro* and *in vivo* models that can fully recapitulate all the aspects of NASH [39].

Considering all these factors, it will be necessary to find better *in vivo* and *in vitro* models that can fully recapitulate the complexity of the disease, to have a better knowledge of NASH pathogenesis mechanisms to discover useful therapy targets and to evaluate drugs combinations that can target multiple interconnected pathways related to the disease [39].

New strategies

During the years NAFLD *in vitro* models' complexity evolved rapidly. 2D monoculture cell models with primary human hepatocytes were once considered the gold standard for short-term experiments. They have high functionality relative to the human organ *in vivo* but they have a very limited life span in culture and genetic variability is present due to the different donors. Alternatives to primary human hepatocytes are 2D monocultures of hepatocyte-like cells (HLCs) derived from induced pluripotent stem cells and human hepatoma cell lines such as HepG2. These two monocultures are easy to use but again there are some drawbacks for both, such as the difficulty to obtain large volumes of HLCs, and the risk of teratoma formation. A drawback with the use of HepG2 cells is that they have a low expression of drug-metabolizing enzymes [44].

In vitro NAFLD models of 2D monocultures are attractive systems because they are easy to use and, especially for cell lines, there is a possibility of scaling up to high throughput experiments. Unfortunately, these models cannot fully recapitulate NAFLD because multiple cell types are involved in disease progression, and they interact with each other and with the matrix forming a complex and unique 3D architecture [44 45].

A first step forward for *in vitro* NAFLD models was the creation of the 2D coculture, rapidly followed by 3D monoculture models with cell lines or primary human hepatocytes. A third step was the development of 3D cocultures of human hepatocytes, hepatic stellate cells, endothelial cells, and Kupffer cells [44 45].

All the models described lack dynamic perfusion and are therefore static models. More recently, microfluidic-based 3D organ-on-a-chip platforms have been developed making possible the creation of 3D organs in miniature able to recapitulate key physiological features of the liver microenvironment and overcoming therefore the limitations of the previous 2D and 3D models. These new 3D organ-on-a-chip platforms have the potential to fill the gap between *in vitro* and *in vivo* models, becoming a valuable platform for preclinical studies [45 46].

Identifying new and valuable *in vitro* models is one of the challenges, together with the identification of new potential drug candidates. Several studies highlighted hepatocyte apoptosis due to lipotoxic stress as a key element in NASH development so preventing hepatocytes death and promoting liver regeneration can be an effective treatment.

The hepatotropic and hepatoprotective roles of HGF/SF were studied for more than 30 years showing this is the leading protein for hepatocyte viability and regeneration [8 15 16 17]. The protective role of the HGF/SF-MET pathway in NASH was also studied in *in vivo*

mice models, showing that the genetic knockout of MET receptor triggers NASH progression [47] [48]. Considering these findings, there is a strong rationale for the use of K1K1 as a drug candidate for NASH treatment.

Another key element of NASH is the inflammatory response of immune cells which, together with hepatocyte apoptosis, leads to fibrosis development. The inflammasome response activates Kupffer cells and causes monocyte recruitment, that differentiate in M1 macrophages. M1 macrophages secrete pro-inflammatory cytokines that can stimulate stellate cells to differentiate into myofibroblasts leading to fibrosis development [40] [49] [50]. Recently, the role of M1 and M2 macrophages in NASH has been studied, revealing the protective role of the M2 phenotype [49] [51] [52]. Therefore, using drugs such as TAK-242 [53] [54] and SR1078 [55] with the potential to switch M1 to M2 can have an anti-NASH effect [56] [57] [58]. Furthermore, it has been recently found that treatment with HGF/SF not only promotes tissue regeneration, but it is also able to switch M1 macrophages/ Kupffer cells to an M2-like phenotype [59].

NASH is a multifactorial disease and targeting multiple processes using both K1K1 to inhibit hepatocyte apoptosis and a panel of drugs able to polarize M1 to M2 can be an innovative and effective treatment.

Objective of the thesis research

1. Large scale recombinant production of K1K1, 1K1 and MET567.
2. Compare HGF/SF, K1K1 and 1K1 protein stability.
3. Assessment of MET and HGF/SF protein expression with immunohistochemistry (IHC) in formalin-fixed paraffin-embedded (FFPE) liver samples of patients with steatosis or NASH.
4. Study of pathways activation in human and murine liver cell lines (HepG2 and AML12) after stimulation with K1K1, HGF/SF and other recombinant proteins.
5. HGF/SF and K1K1 labeling for *in vivo* studies.
6. Develop a 3D microfluidic culture system (liver-on-a-chip) able to recapitulate NASH essential features.
7. Test and compare HGF/SF and K1K1 efficacy using the 3D microfluidic culture system.

Materials and Methods

Materials

Plastic and glassware

Plasticware was purchased from the following companies: Falcon, Gilson, Corning and Eppendorf.

Other general items

- SnakeSkin™ Dialysis Tubing, 10K MWCO - (Thermo Fisher)
- Litmus paper – (Merck)
- Centrifugal filter units - (Millipore)
- Centrifugal concentrator MWCO 3 kDa and 10 kDa - (Vivaspin)

Chemicals

Most of the chemicals were purchased from Sigma-Aldrich, Fluka, Merck and Thermo Fisher Scientific.

Solutions:

- PBS - 137 mM NaCl, 27 mM KCl, 8.3 mM Na_2HPO_4 *$2H_2O$, 1.76 mM KH_2PO_4 in 1 L of H_2O, pH 7.4
- 1 kb ladder - (New England Biolab Inc.)
- DNA elution buffer - 10 mM Tris-HCl, pH 8.5
- TAE - 40 mM Tris, 1.3 mM EDTA, 1.14 ml 100% acetic acid in 1 L of H_2O
- DNA loading dye – 5 mg/ml bromophenol blue, 50 mM Tris pH 7.6, 30% glycerol, 16% β-mercaptoethanol
- Precision Plus Protein Dual Color Standards - (Bio-Rad)
- Sodium Dodecyl Sulphate - Polyacrylamide Gel Electrophoresis (SDS-PAGE) loading dye - 225 mM Tris pH 6.8, 6% SDS, 30% glycerol, 0.5 mg/ml bromophenol blue, 16% β-mercaptoethanol
- SDS-PAGE buffer - 25 mM Tris, 192 mM glycine, 1 g/l SDS in 1 L of H_2O
- Transfer buffer - 25 mM Tris, 192 mM glycine, 1 g SDS, 20% methanol, in 1 L of H2O.
- TBT - 20 mM Tris, 137 mM NaCl, 0.5% Tween 20 in 1 L of H_2O, pH 7.4
- Coomassie stain - 1 g Coomassie blue, 10% acetic acid, 50% methanol, 40% H_2O

- Coomassie destain - 10% acetic acid, 50% methanol, 40% H_2O
- Modified RIPA buffer - 50 mM HEPES, 150 mM NaCl, 1.5 mM $MgCl_2$, 1 g/L Triton X-100, 10 g/L glycerol, 1 mM EDTA, 50 mM Na_3VO_4, 100 mM NaF, 1:100 phosphatase inhibitor cocktail 2 - (Sigma Aldrich)

FPLC columns

- HiTrap® Heparin HP, 5 ml - (GE Healthcare)
- HisTrap® HP, 1 ml, and 5 ml - (GE Healthcare)
- Resource™ S, 6 ml - (GE Healthcare)
- Superdex® 75 10/300 GL - (GE Healthcare)
- Superdex® 200 10/300 GL - (GE Healthcare)
- HiLoad® 26/60 Superdex® 200 pg - (GE Healthcare)
- HiLoad® 26/60 Superdex® 75 pg - (GE Healthcare)
- HiLoad® 16/60 Superdex® 200 pg - (GE Healthcare)
- HiLoad® 16/60 Superdex® 75 pg - (GE Healthcare)

Plamids

- pET45b (+) - (Invitrogen)
- pPIC9K - (Invitrogen)
- pMYTH - (property of our laboratory)

Enzymes

Restriction enzymes and their buffers were purchased from New England Biolab Inc. (NEB).

Antibodies

Table 1 List of the antibodies used for the experiments.

Name	Antigen	Reactivity	Source	Dilution	Firm
LIF 40-41	MET ECD	H	Mouse		GFG
LIF 39-58	MET ECD	H	Mouse	1 µg/ml	GFG
Met (D1C2) XP® Rabbit mAb #8198	MET C-terminus	H	Rabbit	1:100- 1:1000	Cell Signaling
1W53	HGF/SF	H	Goat	1:1000	GFG
HGFα (H-10): sc-374422 mAb	HGF/SF	H, M, R, others	Mouse	1:10	Santa Cruz Biotechnology
F2B3 pAb	HGF/SF	M,H	Rabbit		GFG
MSH2.B2 pAb	HGF/SF	M,H	Rabbit	20 µg/ml	GFG
MSH2.B6 pAb	HGF/SF	M,H	Rabbit	50 µg/ml	GFG
F1B3F pAb	HGF/SF	M,H	Rabbit		GFG
F2B3B run IV pAb	HGF/SF	M,H	Rabbit		GFG
F2B3B/C run VI pAb	HGF/SF	M,H	Rabbit		GFG
F2B3C run VII and VIII pAb	HGF/SF	M,H	Rabbit		GFG
F2B3E run IX and X pAb	HGF/SF	M,H	Rabbit		GFG
F2B3E run XI pAb	HGF/SF	M,H	Rabbit		GFG
F2B3EF run XII and XIII pAb	HGF/SF	M,H	Rabbit		GFG
F2B3EG run XIV and XV pAb	HGF/SF	M,H	Rabbit		GFG
EGH2/4C12.1 mAb	HGF/SF	M,H	Mouse	50 µg/ml	GFG
Phospho-Met (Tyr1349) Antibody #3121	p-MET	H, M, R	Rabbit	1:1000	Cell Signaling
Phospho-Met (Tyr1234/1235) (D26) XP® Rabbit mAb #3077	p-MET	H, M, R	Rabbit	1:1000	Cell Signaling
Phospho-Akt (Ser473) Antibody #9271	p-AKT	H, M, R, others	Rabbit	1:1000	Cell Signaling
Phospho-p44/42 MAPK (Erk1/2) (Thr202/Tyr204) (E10) Mouse mAb #9106	p-ERK	H, M, R, others	Mouse	1:5000	Cell Signaling
Akt Antibody #9272	AKT	H, M, R, others	Rabbit	1:1000	Cell Signaling
Erk V114A	ERK	H, M	Rabbit	1:5000	Promega
GAPDH antibody GTX100118	GAPDH	H, M, R, others	Rabbit	1:5000	GeneTex
Alexa Fluor® 647 anti-Cytokeratin (pan reactive)	Cytockeratins	H	Mouse	1:100	Biolegend
Alexa Fluor® 488 anti-Vimentin	Vimentin	H	Mouse	1:100	Biolegend
Brilliant Violet 421™ anti-human CD68	CD68	H	Mouse	1:50	Biolegend
Alpha-Smooth Muscle Actin Monoclonal Antibody (1A4), Alexa Fluor 488	α-SMA	H,M,R	Mouse	1:100	Invitrogen
Cleaved Caspase-3 (Asp175) Antibody (Alexa Fluor® 488 Conjugate) #9669	Caspase-3	H,M,R, others	Rabbit	1:50	Cell Signaling
Goat Anti-Rabbit Immunoglobulins/HRP P0448		Rb	Goat	1:1000	Agilent Technologies
Rabbit Anti-Mouse Immunoglobulins/HRP P0260		M	Rabbit	1:1000	Agilent Technologies
Rabbit Anti-Goat Immunoglobulins/HRP P0449		G	Rabbit	1:1000	Agilent Technologies

(Meaning of some abbreviations in table: GFG = Growth Factor Group, ECD = extracellular domain)

Proteins and drugs

- HGF/SF was stored flash-frozen in 50 mM MES, 750 mM NaCl, pH 6.
- K1K1 was stored flash-frozen in 25 mM Tris, 250 mM NaCl, pH 7.4.
- 1K1 was stored flash-frozen in 50 mM Tris, 250 mM NaCl, pH 7.4.
- NK1 was stored flash-frozen in 50 mM Tris, 250 mM NaCl, pH 7.4.
- TAK-242 liposomes.
- SR1078 liposomes.

Reagents for microfluidic devices preparation

- 184 Silicone Elastomer Kit - (Dow Chemical)
- Cultrex Poly-L-Lysine - (R&D Systems)
- Glutaraldehyde Solution - (Sigma-Aldrich)
- 3D Cell Culture Chips - (AIM Biotech)

Kits

- Pierce™ BCA Protein Assay Kit - (Thermo Fisher Scientific)
- ZR Plasmid Miniprep Classic - (Zymo Research)
- QIAGEN® Plasmid Maxi Kit - (Qiagen)
- Pierce™ ECL Western Blotting Substrate - (Thermo Fisher Scientific)
- Alexa Fluor™ 488 Microscale Protein Labeling Kit - (Thermo Fisher Scientific)
- LIVE/DEAD™ Viability/Cytotoxicity Kit, for mammalian cells - (Thermo Fisher Scientific)
- HCS LipidTOX™ Deep Red Neutral Lipid Stain, for cellular imaging - (Thermo Fisher Scientific)
- Human TNFα ELISA Kit - (Invitrogen)
- Human TGF beta 1 ELISA Kit - (Abcam)

Cells

- BL21 (DE3) - *Escherichia coli* strain - (New England Biolabs)
- DH5α - *Escherichia coli* strain - (New England Biolabs)
- GS115 - *Pichia Pastoris* strain - (Invitrogen)
- CHO lec 3.2.8.1 - Chinese hamster ovary cell line transfected with expression vector pA71d containing MET567 cDNA - (ICRF, UK)
- MDCK - Madine-Darby Canine Kidney cell line - (ICRF, UK)
- HepG2 - human liver cancer cell line - (ATCC)
- AML12 - alpha mouse liver 12 cell line - (ATCC)
- RFP-HUVECs - RFP Expressing Human Umbilical Vein Endothelial Cells - (Angio Proteomie)
- U937- pro-monocytic, human myeloid leukemia cell line - (ATCC)
- Hepatocyte cells (HCs) - (Zen Bio Inc.)
- Kupffer cells (KCs) - (Zen Bio Inc.)
- Liver sinusoidal endothelial cells (LSECs) - (Zen Bio Inc.)
- Hepatocyte stellate cells (HSCs) - (Zen Bio Inc.)

Media for cell cultures

- LB - Luria Bertani medium - 10 g/L bacto tryptone, 10 g/l yeast extract, 5 g/l NaCl, pH 7.4.
- YPD - yeast extract peptone dextrose medium - 1% yeast extract, 2% peptone, 2% glucose.
- BMGY - buffered methanol complex medium - 10g/l yeast extract, 20g/l peptone, 0.1 M phosphatase, 13.4 g/l yeast nitrogen base, 0.4 mg/l *d*-biotin, 1% glycerol.
- BMMY - buffered methanol complex medium - 10g/l yeast extract, 20g/l peptone, 0.1 M phosphatase, 13.4 g/l yeast nitrogen base, 0.4 mg/l *d*-biotin, 0.5% methanol.
- MEM α - Minimum Essential Medium - (Thermo Fisher Scientific).
- EMEM - Eagle's Minimum Essential Medium - (ATCC).
- DMEM - Dulbecco's Modified Eagle Medium - (Thermo Fisher Scientific).
- EBM-2 - Endothelial Cell Growth Basal Medium-2 - (Lonza).
- DMEM/F-12 - Dulbecco's Modified Eagle Medium/Nutrient Mixture F-12 - (Thermo Fisher Scientific).
- RPMI-1640 - (Thermo Fisher Scientific).
- Hepatocyte plating medium (HM-1) - (Zen Bio Inc.).
- Hepatocyte maintenance medium (HM-2) - (Zen Bio Inc.).
- Kupffer cells plating medium (KC-1) - (Zen Bio Inc.).
- Kupffer cells maintenance medium (KC-2) - (Zen Bio Inc.).
- Endothelial cell growth medium - (Zen Bio Inc.).

Reagents for cell cultures

- Fetal Bovine Serum (FBS) - (Gibco)
- Corning® Fetal Bovine Serum - (Corning)
- Penicillin-Streptomycin (Pen/Strep) (100X) - (Lonza)
- Penicillin-Streptomycin-Glutamine (100X) - (Thermo Fisher Scientific)
- Trypsin 10X - (Lonza)
- 0.05% Trypsin-EDTA - (Thermo Fisher Scientific)
- DPBS - Dulbecco's Phosphate Buffered Saline - (Lonza)
- L- Glutamine - (Euroclone)
- Dexametasone - (Stemcell technologies)
- Insulin, transferrin, sodium selenite supplements (ITS) 1000X - (Boehringer Mannheim)
- EBM-2 medium supplements - (Lonza)
- Recovery™ Cell Culture Freezing Medium - (Thermo Fisher Scientific)
- Collagen I, Rat Tail, 100 mg - (Corning)
- NaOH 1N
- PBS 10X - (VWR)
- Lipopolysaccharides from Escherichia coli O111:B4 - (Sigma-Aldrich)
- Sodium palmitate ≥98.5% - (Sigma-Aldrich)
- Sodium oleate ≥99% - (Sigma-Aldrich)
- Human M-CSF - (Peprotech)
- Human IL-4 - (Peprotech)
- Fibronectin Human Plasma - (Sigma-Aldrich)
- Hoechst solution - (Invitrogen)

Patient samples

In collaboration with the Unit of Pathology of "Maggiore della Carità" Hospital in Novara, a study on 34 liver biopsies of patients with steatosis or NASH diagnosis has been set up. Six biopsies of normal liver were included in the study and two samples of colorectal adenocarcinoma were also used as positive controls.

The NASH clinical research network (CRN) system was selected for case classification and a composite grade, the NAFLD activity score (NAS) was used as an indication of the severity of the disease. NAS is the unweight sum of steatosis (0-3), lobular inflammation (0-3), and hepatocellular ballooning scores (0-2) (**Fig. 7**). Biopsies with NAS ≥5 correlate with a diagnosis of NASH, while biopsies with NAS less than 3 were diagnosed as "not NASH" [60]. Fibrosis was considered separate as the representative for the stage of NAFLD (0-4) (**Fig. 8**) [60].

All the samples were formalin-fixed paraffin-embedded (FFPE) tissues and only those patients with adequate biopsy tissue and available retrospective clinical data were included in the study.

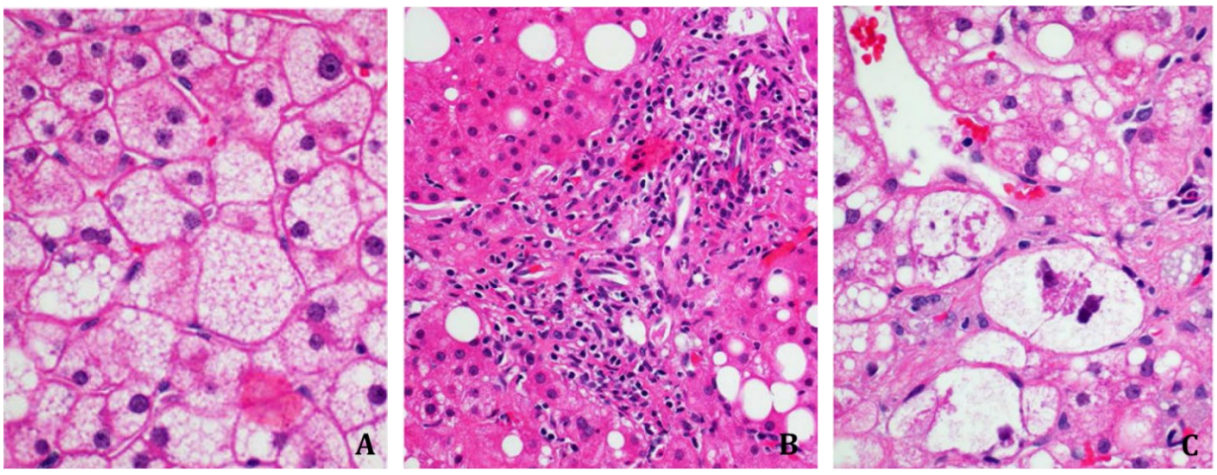

Fig. 7 Representative haematoxylin-eosin staining images of livers with NASH showing microvescicular steatosis (magnification 600X) (**A**), mild portal inflammation (magnification 400X) (**B**), and ballooned hepatocytes with large Mallory-Denk body cytoplasmic inclusions (magnification 600X) (**C**) [60].

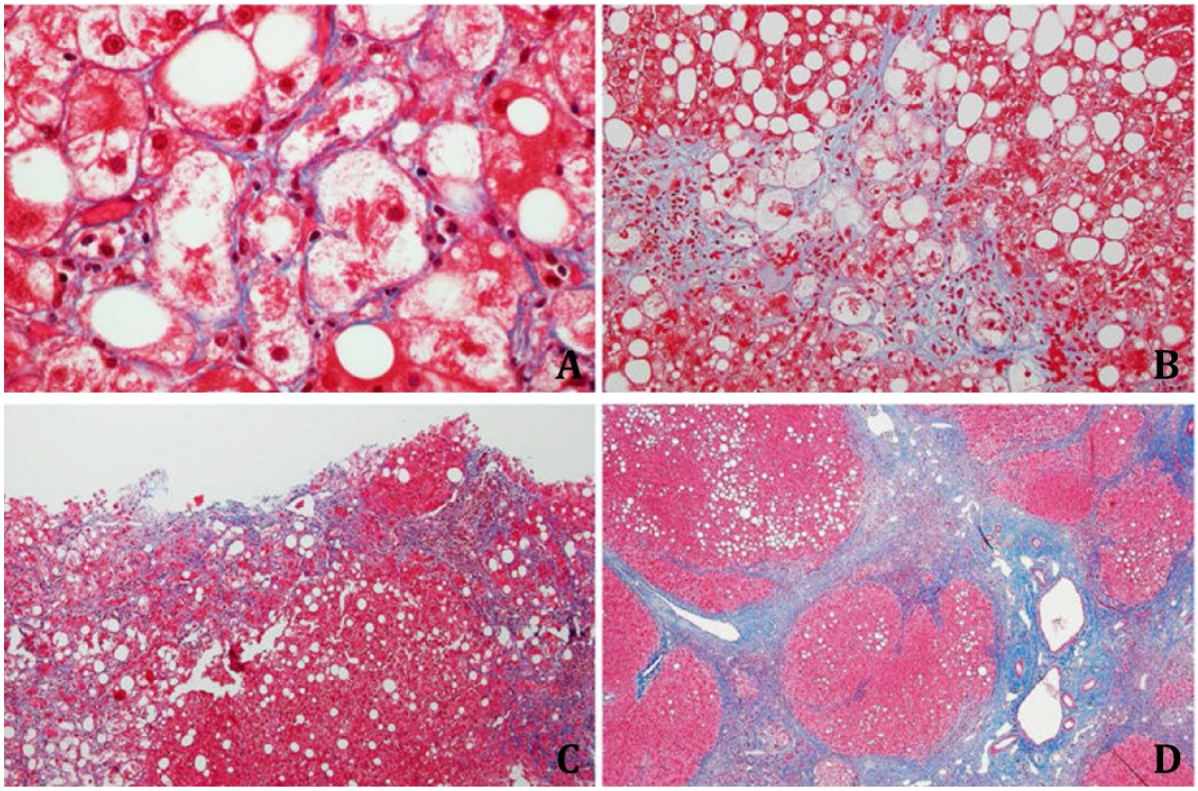

Fig. 8 Representative Masson's trichrome staining images showing fibrosis progression in NASH. Early perisinusoidal fibrosis with delicate collagen strands between ballooned hepatocytes (magnification 600X) (**A**), advanced perisinusoidal fibrosis (magnification 200X) (**B**), bridging fibrosis with extensive networks of perisinusoidal fibrosis nearly encircling a regenerative nodule (magnification 100X) (**C**), and established cirrhosis (magnification 40X) (**D**) [60].

Programs and tools

- ProtParam tool (ExPASy - SIB Bioinformatics Resource Portal)
- SnapGene
- ImageJ
- NIS elements software
- GraphPad Prism 9

Methods

K1K1 expression and purification

Bacterial transformation

Production of K1K1 recombinant protein was performed in the *E. Coli* competent strain BL21(DE3). The pET45b (+) expression vector was used for expression of K1K1, the sequences are given in the appendix section (**Fig. 46**). cDNA was used and the transformation protocol was performed as follows:

- Thaw one BL21(DE3) vial on ice.
- Mix 50 µl of competent cells with 2 µl of expression vector.
- Incubate on ice for 30 min.
- Heat shock at 42 °C for 30 sec.
- Add 950 µl of LB medium at room temperature.
- Incubate at 37 °C for 60 min at 250 rpm.
- Warm LB-agar selective plate during the incubation.
- Use 100 µl of culture, plate and incubate at 37 °C overnight.

The same transformation protocol was applied for the *E. Coli* DH5α competent strain, for the purpose of DNA propagation.

DNA extraction

Inoculation of 5 ml of LB + ampicillin medium was performed with DH5α containing the plasmid. The culture was then incubated at 37 °C overnight at 250 rpm. The culture was then centrifuged, and plasmid DNA was recovered following ZR Plasmid Miniprep kit protocol.

Plasmid digestion, agarose gel and sequencing

To verify the presence of K1K1 insert, 1 µg of plasmid DNA was digested at 37 °C for 2 hours. The mix had a total volume of 50 µl, 1 µl of each restriction enzyme (NcoI HF and NotI HF) was used together with 5 µl of CutSmart® Buffer.

For the analysis of DNA fragments a 1.5% TBE agarose gel and 0.5% ethidium bromide was prepared. TBE was also used as a buffer to fill a midi agarose gel unit (EH100, Engineering & Design Plastics Ltd, UK). DNA samples were mixed with DNA loading buffer and 1 kb ladder was used for molecular weight estimation.

Plasmid DNA extracted from the colonies was then sent to confirm the K1K1 nucleotide sequence by Sanger sequencing.

Protein expression

The protocol was performed as follows:

- Inoculate 5 ml of LB plus ampicillin medium with a BL21 (DE3) colony containing the plasmid.
- Incubate at 37 °C overnight, 250 rpm.
- Pour the inoculum in 500 ml of fresh LB plus ampicillin medium.
- Incubate at 30 °C, 250 rpm until OD_{600} is between 0.6 and 0.8.
- Lower the culture temperature to 18 °C for few minutes.
- Start induction by adding 0.4 mM IPTG.
- Incubate at 18 °C for 24 hours, 250 rpm.

Harvesting from non-classical inclusion bodies

The protocol was performed as follows:

- Harvest bacterial cell by centrifugation at 10.000 x g for 30 min at 4 °C.
- Discard the supernatant.
- Store the pellets at -80 °C until ready for processing.
- Resuspend the pellet of 500 ml culture in 25 ml of 50 mM Tris, 500 mM NaCl, pH 8.5 buffer with added lysozyme, benzonase and EDTA-protease inhibitor.
- Incubate rotating for 30 min at 4 °C.
- Place the tube in melting ice and water before sonication.
- Sonicate with Fisherbrand™ Model 705 Sonic Dismembrator (Thermo Fisher), maximum energy for 10 cycles, 30 sec ON followed by 1 min OFF.
- Centrifuge at 10.000 x g for 10 min at 4 °C.
- Discard the supernatant and resuspend the pellet in 25 ml 50 mM Tris, 500 mM NaCl, pH 8.5 buffer with added 0.4% Triton X-100.
- Incubate rotating for 30 min at 4 °C.
- Centrifuge at 10.000 x g for 10 min at 4 °C.
- Discard the supernatant and resuspend the pellet in 25 ml 50 mM Tris, 500 mM NaCl, pH 8.5 buffer with added 0.025% NP40.
- Incubate rotating for 30 min at 4 °C.
- Centrifuge at 10.000 x g for 10 min at 4 °C.

- Discard the supernatant and resuspend the pellet in 25 ml 50 mM Tris, 500 mM NaCl, pH 8.5.
- Incubate rotating for 30 min at 4 °C.
- Centrifuge at 10.000 x g for 10 min at 4 °C.
- Discard the supernatant and resuspend the pellet in 20 ml 50 mM Tris, 500 mM NaCl, 2M L-arginine, 0.5 mM oxidize glutathione (GSSG), 5 mM reduced glutathione (GSH), pH 8.5.
- Incubate rotating for 3 days at 4 °C.
- Centrifuge at 20.000 x g for 30 min at 4 °C and keep the supernatant.
- Repeat centrifugation using new tubes until there is no pellet left.
- Dilute 20 ml supernatant into 2 L of 50 mM Tris, 100 mM NaCl, pH 7.4.
- Check pH again and adjust to pH 7.4 if necessary.
- Filter the solution.
- Start purification on GE Healthcare's AKTA FPLC Systems.

Purification

A HiTrap® Heparin HP, 5 ml column was used for the first purification step. The column was equilibrated with buffer A (25 mM Tris, 150 mM NaCl, pH 7.4). The filtered protein solution was applied on the column at a flow rate of 1.5 ml/min overnight. After flowing all the filtered extract, an elution protocol was created. Bound proteins were eluted at 5 ml/min with a gradient from 0% to 100% of buffer B (25 mM Tris, 1 M NaCl, pH 7.4) over 20 column volumes. Additional 5 column volumes were used with a 100% concentration of buffer B. Five ml fractions were collected.

The proteins fractions corresponding to the peak were loaded on a polyacrylamide gel, then those of interest were pooled together, and the protein concentration was determined using a BCA assay or 280 nm absorbance using a POLARstar Omega Plate Reader (BMG LABTECH). A centrifugal concentrator (MWCO 3 kDa) was then used to reduce the volume of the sample.

The second step of purification involved size exclusion chromatography (SEC). Based on the pooled sample size, one of the HiLoad columns given in the material section was used. The column was equilibrated with buffer A (25 mM Tris, 250 mM NaCl, pH 7.4) and the pooled and concentrated fractions from affinity chromatography were loaded with a 2 ml or 5 ml loop on the chosen column. Five ml fractions were collected.

The proteins fractions corresponding to the peak were loaded on a polyacrylamide gel, then those of interest were pooled together, and the protein concentration was

determined. A centrifugal concentrator (MWCO 3 kDa) was then used to reduce the volume of the sample and K1K1 aliquots were filtered using centrifugal filters and flash frozen for storage at – 80 °C.

1K1 expression and purification

Protein expression

The protocol was performed as follows:

- Thaw a glycerol stock containing GS115 *P. pastoris* cells containing pPIC9K plasmid with 1K1 insert (appendix section, **Fig. 47**).
- Use a loop to spread the cells on a YPD plate containing G418.
- Incubate the plate for 2-3 days at 30 °C until colonies develop.
- Inoculate 5 ml YPD plus ampicillin culture with one of the colonies.
- Incubate for 3 hours at 30 °C, 250 rpm.
- Pour the inoculum in 1 l of fresh BMGY medium.
- Incubate overnight at 30 °C, 250 rpm.
- Control OD_{600} in the morning.
- Centrifuge at 3000 x g for 5 min at 4 °C.
- Resuspend the pellet in few ml of BMMY
- Use the pellet to inoculate 6 l of BMMY medium at initial OD_{600} of 1.
- Incubate overnight at 22 °C, 250 rpm.
- Add 5 ml of methanol for each liter of BMMY after 24 hours.
- Add 5 ml of methanol for each liter of BMMY after 48 hours.
- Centrifuge at 5000 x g for 30 min at 4 °C.
- Collect the medium and filter it.

Protein purification

A final volume of 6 l of medium was collected, concentrated, and dialysed at 4 °C using a SARTOFLOW® machine (Sartorius). The composition of dialysis buffer was PBS at pH 7.4. A 5 ml HiTrap® Heparin HP column was used for the first purification step. The column was equilibrated with buffer A (PBS). The filtered protein solution was applied on the column at a flow rate of 2 ml/min overnight. Bound proteins were eluted at 5 ml/min with a gradient from 0% to 50% of buffer B (PBS, 1.85 M NaCl, pH 7.4) over 25 column volumes and from 50% to 100% over 5 column volumes. Additional 5 column volumes were used with 100% concentration of buffer B. Five milliliter fractions were collected. The proteins fractions corresponding to the peak were loaded on a polyacrylamide gel, then they were pooled together, and protein concentration was determined using a BCA assay or 280 nm absorbance using a POLARstar Omega Plate Reader. A centrifugal concentrator (MWCO 3 kDa) was then used to reduce the volume of the sample.

The second step of purification involved SEC and a HiLoad® 26/60 Superdex® 75 pg column was used. The column was equilibrated with buffer A (50 mM Tris, 250 mM NaCl, pH 7.4) and the concentrated fractions from affinity chromatography were loaded with a 10 ml loop. A flow rate of 1 ml/min was used and 5 ml fractions were collected. The proteins fractions corresponding to the peak were loaded on a polyacrylamide gel, then those of interest were pooled together, and the protein concentration was determined. A centrifugal concentrator (MWCO 3 kDa) was then used to reduce the volume of the sample and 1K1 aliquots were filtered using centrifugal filters and flash frozen for storage at – 80 °C.

MET567 expression and purification

Protein expression

CHO lec 3.2.8.1 (named EGT34/A60.95) stably transfected with plasmid pMYTH containing MET567 coding sequence (a truncated form of the MET ectodomain, with the SEMA and PSI domains as showed in the appendix section in **Fig. 48**) were used for expressing the receptor construct. The protein was secreted in the medium that was collected, centrifuged at 1000 x g for 20 min at 4 °C. The supernatant was then stored at 4 °C in presence of sodium azide.

Protein purification

Medium was collected for several weeks to a final volume of 30 l which was concentrated and dialysed at 4 °C overnight using a SARTOFLOW® machine. The composition of dialysis buffer was PBS, 10 mM imidazole, 350 mM NaCl pH 7.4.

A 1 ml HisTrap® HP column was used for the first purification step. The column was equilibrated with buffer A (dialysis buffer). After filtration, the protein solution was applied on the column at a flow rate of 1 ml/min. An elution protocol was then created, bound proteins were eluted at 1 ml/min with a gradient from 0% to 100% of buffer B (PBS, 500 mM imidazole, 350 mM NaCl, pH 7.4) over 20 column volumes. Additional 10 column volumes were used of 100% buffer B. One ml fractions were collected. The proteins fractions corresponding to the peaks were loaded on a polyacrylamide gel, then they were pooled together, and protein concentration was determined using a BCA assay or 280 nm absorbance read on a POLARstar Omega Plate Reader.

A second dialysis step was necessary to remove contaminant band with an ion exchange chromatography step. SnakeSkin™ Dialysis Tubing (MWCO 10 kDa) was used to dialyse into 50 mM MES, 100 NaCl mM, pH 5.8. Dialysis was performed at 4 °C overnight and a 6 ml Resource™ S column was used. The column was first equilibrated with buffer A (dialysis buffer) and after a short centrifugation and filtration, the protein solution was applied on the column at a flow rate of 1 ml/min. Bound proteins were eluted at 1 ml/min with a gradient from 0% to 100% of buffer B (50 mM MES, 500 mM NaCl, pH 5.8) over 50 column volumes. Additional 5 column volumes were used with a 100% concentration of buffer B. One milliliter fractions were collected.

The proteins fractions corresponding to the peak were loaded on a polyacrylamide gel, then those of interest were pooled together, and the protein concentration was determined. A centrifugal concentrator (MWCO 10 kDa) was then used to reduce the volume of the sample and MET567 aliquots were filtered using centrifugal filters and flash frozen for storage at – 80 °C.

SDS-PAGE

SDS-PAGE was used to separate proteins based on their size. Proteins samples were quantified, reducing loading dye was added and samples were boiled for 5 minutes. One mm thick polyacrylamide gels were used, the percentage was chosen according to the molecular weight of the proteins of interest, and the samples were loaded together with Precision Plus Protein Dual Color Standards for molecular weight estimation.

Coomassie staining

After SDS-PAGE, the gel was removed from the system and Coomassie stain was used to allow visualization of protein bands. After a few hours of incubation, the gel was rinsed with water and immerged in destaining solution to remove the excess of Coomassie not bound to the proteins.

Protein incubation for stability study

Purified HGF/SF, 1K1, and K1K1 were first quantified with BCA assay then diluted in PBS to a final concentration of 10 μM and incubated at 37 °C for three weeks. Samples were collected each week, flash frozen in liquid nitrogen and stored at -80 °C till the end of the experiment. LoBind tubes were used to minimize sample-to-surface binding.

Thermal shift assay

A Tycho NT.6 system (NanoTemper Technologies) was used to test and compare the relative quality and stability of protein samples. The unfolding of a protein causes changes in the fluorescence emission properties of its aromatic amino acid residues (tryptophan and tyrosine mainly). Tycho NT.6 follows proteins unfolding process by measuring samples fluorescence intensity (brightness) at 330 nm and 350 nm during thermal unfolding with a 30 °C/min ramp from 35 to 95 °C.

The brightness signals are displayed as a ratio (350 nm/330 nm) and plotted against the temperature, and the resulting curves are known as unfolding profiles. The curves are analysed for inflections points also named inflection temperatures (Ti) that represent unfolding events detected in the sample (**Fig. 9**).

The brightness ratio (350 nm/330 nm) is used to set the initial ratio at 35°C and the Δ ratio as showed in **Fig. 9**.

The brightness values can be also used for concentration assessment of the specimens if the samples contain the same protein.

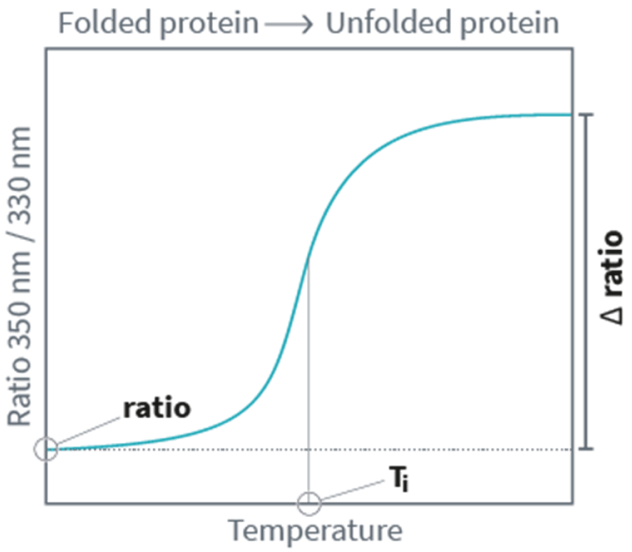

Fig. 9 Representative unfolding profile showing initial ratio, Δ ratio and Ti.

Scatter assay

MDCK cells were cultured in DMEM+5% FCS+ Pen-Strep and plated at 1000 cells/well inside 96 well plate 16-24 h before the addition of serial dilutions of the proteins to be tested. After overnight incubation, the medium was removed, the cells were fixed in 4% paraformaldehyde and then stained with Coomassie stain. Representative images were collected using an inverted microscope (Nikon Instruments Inc, USA).

Immunohistochemistry (IHC)

Different protocols were used to test a panel of anti-HGF/SF and anti-MET antibodies on paraffin embedded patient liver material, and they will be later described in detail in the result section. All these protocols can be divided in completely automated or partially automated. With the first one, 2 µm thick sections were cut and baked for 20 minutes at 60 °C. Then the sections were loaded into a BenchMark ULTRA IHC/ISH system (Roche) and an IHC protocol was created with first a deparaffinization step, an antigen retrieval with Cc1 buffer (Roche), incubation with primary antibody followed by incubation with the secondary, and subsequent 3'3-diaminobenzidine tetrahydrochloride (DAB) staining. The slides were counterstained with haematoxylin and the coverslips were mounted.

The partially automated protocols started with the cutting of 2 µm thick sections, baked for 20 minutes at 60 °C. Then the sections were deparaffinised and rehydrated, and antigen retrieval was performed in heated Tris-EDTA pH 9 buffer for 15 min at 650 W in a microwave oven. After buffer cooling, sections were incubated in a 10% H_2O_2 solution for 10 minutes. Finally, the slides were loaded into a BenchMark ULTRA IHC/ISH system and an IHC protocol was created, with an incubation with primary antibody followed by incubation with the secondary and DAB staining. The slides were counterstained with haematoxylin and the coverslips were mounted.

The Ventana DP 200 slide scanner (Roche) was used to acquire all the images.

ELISA

The protocol was performed as follows:

- Coat 96 well plates with 100 µl/well 50 nM HGF/SF in PBS 1X.
- Seal the plate and store it at 4 °C overnight.
- Wash the plate 3 times with PBS + 0.1% Tween 20.
- Incubate with 200 µl/well PBS + 0.1% Tween 20 + 1% BSA for 1 hour.
- Wash the plate 3 times with PBS + 0.1% Tween 20.
- Incubate with 50 µl/well anti-HGF/SF primary antibodies for 1 hour at room temperature.
- Wash the plate 3 times with PBS + 0.1% Tween 20.
- Incubate with 100 µl/well secondary antibody for 1 hour at room temperature.
- Wash the plate 3 times with PBS + 0.1% Tween 20.
- Add 100 µl/well Sure blue TMB.
- Incubate for 2 minutes at room temperature.
- Add 50 µl/well 0.5 M H_2SO_4 to stop the reaction and read OD_{450}.

Cell lysis protocol

Different cell lines were used for these experiments. The cells were seeded in the evening with a 50% confluence in 6 well plates. The day after the medium was removed and cells were first starved for 3 hours and later stimulated for 10 minutes with growth factors. After stimulation, cells were washed in cold PBS and placed on an ice-cold metal plate to keep the temperature low. Two hundred microliters of modified RIPA buffer were added to each well and the cells were immediately scraped. Cells lysates were collected in Eppendorf tubes, flash frozen in nitrogen and stored at -80 °C.

Before western blot, cell lysates were centrifuged at 10.000 x g for 20 min at 4 °C. Total protein concentration was measured with BCA assay. Twelve percent 1mm polyacrylamide thick gels were prepared, and 40 µg of total protein lysate was loaded in each well. SDS-PAGE was performed in reducing conditions. Slightly different protocols were used for each cell line, and they will be later described in detail in the result section.

Western blot

Immediately after SDS-PAGE, proteins were transferred and immobilized on a nitrocellulose membrane. A vertical blotting device was used to transfer the proteins (Cambridge Electrophoresis Ltd.). A fixed current of 220 mA and maximum voltage of 150 V was applied for 2 hours. After transfer, the membrane was blocked with TBT + 5% BSA or with PBS + 0.2% Tween 20 + 5% milk for 1 hour. After the blocking step, the membrane was incubated for a few hours at room temperature or overnight with the primary antibody diluted in blocking buffer. The membrane was then washed 3 times for 10 minutes with PBS + 0.2% Tween 20 or with TBT followed by one hour incubation with HRP-conjugated secondary antibody diluted in blocking buffer.

The membrane was washed again 3 times for 10 minutes with PBS + 0.2% Tween 20 or with TBT and ECL chemiluminescent detection reagent was used to detect the bands. Images were collected with Azure c600 Imager (Azure Biosystems). Slightly different protocols were used for each antibody, and they will be described in detail in the result section.

Data analysis

Western blot bands intensities of the proteins of interest were quantified with ImageJ software. The bands intensities of a loading-control protein, GAPDH, were also quantified. Loading-control proteins are proteins that are presumably expressed at a constant level regardless of the treatment applied to the cells or organisms. Therefore, western blot bands intensities of GAPDH were used to normalize the bands intensities of all the proteins of interest.

The bands intensities of the proteins of interest and of GAPDH were analyzed, the values were shown in the Results window of ImageJ (Area and Percent) and moved to a spreadsheet. There, in a new column next to the percent column, the percent value of each sample was divided by the percent value of the standard (the non-treated sample).

The resulting column of values was a measure of the relative density of each peak, compared to the standard (the non-treated sample), which had a relative density of 1. This procedure was applied both for the proteins of interest and for the loading-control protein, GAPDH. Then it was necessary to divide the relative density values for the proteins of interest by the relative density of the corresponding loading-control protein (GAPDH) for each lane. This second step was performed based on the assumption that the proportional differences in the relative densities of the loading-control bands represent the proportional differences in amounts of total protein that were loaded on the gel. The values obtained after this second step of analysis were represented graphically.

HGF/SF and K1K1 labeling

Alexa Fluor ® 488 Microscale Protein Labeling Kit was used for protein labeling. Before using this kit, proteins were concentrated or diluted to 1 mg/ml concentration and dialysis in PBS was performed overnight at 4 °C.

After dialysis, the labeling protocol was applied exactly as indicated on the datasheet or with a deletion of one step involving the addiction of 1 M sodium bicarbonate to the proteins of interest.

Preparation of the microfluidic NASH-on-a-chip model

Standard photolithography or resin 3D printing were used to prepare the five-channel microfluidic devices. Three different models were created, all of them consisting of three hydrogel channels surrounded by inlet and outlet channels. A poly-dimethyl-siloxane (PDMS) mixture with a curing agent at a ratio of 10:1 was degassed to remove bubbles and poured inside selected molds. Degassing was repeated a second time before curing the devices at 65 °C overnight. After this step, PDMS devices were removed from the molds and biopsy punches were used to create the holes for inlets and outlets channels (1 mm for the middle channels and 4 mm for the fluidic channels). The punched devices were then bonded with cover glasses (25 × 25 mm) by oxygen plasma treatment for 2 min. Poly-L-lysine (0.1 mg/mL) was applied overnight followed by glutaraldehyde (1%) for another 1.5 h to allow firm attachment of the hydrogel to the glass substrate. The devices were washed four times with deionized water and incubated again at 65 °C for at least 24 hours. Finally, they were sprayed with 70% ethanol and exposed to UV light for 30 minutes to ensure complete sterilization.

Construction of liver on a chip with cell lines

Three different models were used, all of them were five-channel microfluidic devices. Standard photolithography was used to prepare model 1 while for models 2 and 3 resin 3D printing was used. The devices also differed for the width of the channels, as shown in **Fig. 10.**

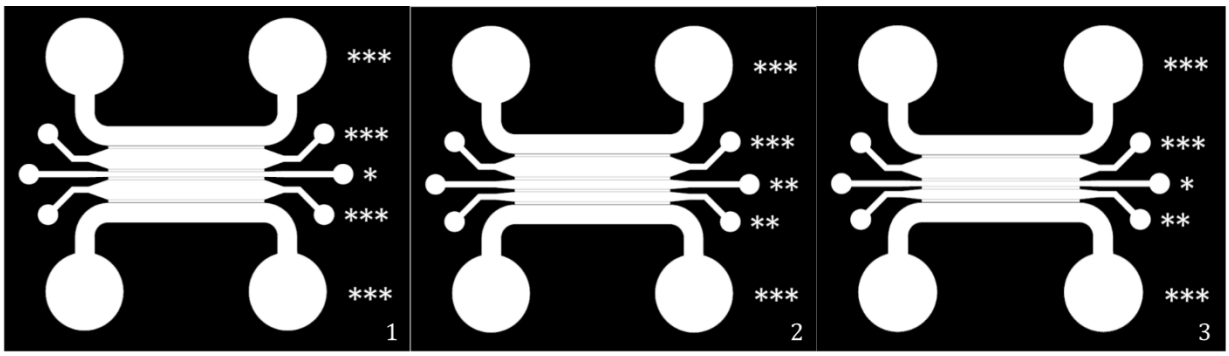

Fig. 10 Schematic design of the microfluidic NASH-on-a-chip models.

* 250 μm, ** 500 μm, *** 1000 μm

Model 1

First, three different mixes of rat tail collagen type I were prepared (2.5 mg/ml) in ice. The following components were used:

1. PBS 10X = Final volume/10
2. Rat tail collagen type I = Final volume x 2.5 mg/ml / collagen stock concentration
3. NaOH 1N = Collagen volume x 0.0023
4. Milli Q water = Final volume – (1+2+3)

Collagen was the last component added and the final volume for each mix was decided according to the number of devices used for the experiment (considering 10 to 15 microliters of mix were needed to fill every channel).

For the first experiment with model 1, cells concentrations were the following:

- HepG2 (1.25×10^6 cells/ml)
- Hepatocyte stellate cells (1.25×10^5 cells/ml)
- U937 (3.75×10^5 cells/ml)

For the second experiment concentrations were changed:

- HepG2 (3×10^6 cells/ml)
- Hepatocyte stellate cells (3×10^5 cells/ml)
- U937 (1.5×10^6 cells/ml)

Cells were harvested, centrifuged for 5 min at 300 x g, the pellets were resuspended in 1 ml of fresh medium and counting was performed manually with a hemocytometer. The cell suspension volume needed for each cell type was calculated, the suspension was centrifuged again for 5 min at 300 x g, all the medium was removed with a pipette, and the pellets were stored in ice for few minutes. Once all the pellets were ready, the pH of all the mixes was tested with litmus paper before adding the cells. If the pH was closed to 7, the mixes were added to the cell pellets and stored in ice. The pH was tested a second time before proceeding with the seeding.

The previously sterilized devices were moved inside Petri plates together with another small Petri plate filled with water to keep humidity constant. A pipette was used to inject HepG2 and U937 inside the respective channels, leaving the middle one empty. The chips were then incubated in the cell incubator for 30 minutes until the collagen formed a gel and subsequently stellate cells were injected and the incubation was repeated. After this second incubation, cell medium was added to both inlet and outlet channels. The first time the media was an equal mixture of EMEM: DMEM/F12: RPMI-1640 with the addiction of 10% FBS and Pen-Strep. The second time only EMEM with the addiction of 10% FBS and Pen-Strep was used.

After adding the medium to both channels, the devices were incubated for 90 minutes, then RFP-HUVEC cells were harvested, centrifuged for 5 min at 300 x g, the pellets were resuspended in 1 ml of fresh medium and counting was performed manually with a hemocytometer. A density of 2 × 10^6 cells/ml was used for both the experiments. Finally, the medium was removed from both inlet and outlet channels and RFP-HUVEC suspension was flowed through the inlet channel. The chips were then incubated in the cell incubator for 90 minutes and RFP-HUVEC medium EBM-2 plus supplements was used to fill the inlet channel while the outlet was filled the first time with an equal mixture of EMEM: DMEM/F12: RPMI-1640 with the addiction of 10% FBS and Pen-Strep. The second time only EMEM with the addiction of 10% FBS and Pen-Strep was used. After other 90 minutes of incubations, the Petri plates with the devices were moved to a tilting platform placed inside cell incubator. The devices were monitored daily, and the medium was changed every two days. Images were collected using brightfield microscopy.

Models 2 and 3

Models 2 and 3 were also tested and the following cells concentrations were used:

- HepG2 (3 × 10^6 cells/ml)
- Hepatocyte stellate cells (3 × 10^5 cells/ml)
- U937 (1.5 × 10^6 cells/ml)

Cells were harvested, centrifuged for 5 min at 300 x g, the pellets were resuspended in 1 ml of fresh medium and counting was performed manually with a hemocytometer. The cell suspension volume needed for each cell type was calculated, the suspension was centrifuged again for 5 min at 300 x g, all the medium was removed with a pipette, and the pellets were stored in ice for few minutes. Once all the pellets were ready, the pH of all the mixes was tested with litmus paper before adding the cells. If the pH was closed to 7, the mixes were added to the cell pellets and stored in ice. The pH was tested a second time before proceeding with the seeding.

The previously sterilized devices were moved inside Petri plates together with another small Petri plate filled with water to keep humidity constant. A pipette was used to inject HepG2 and U937 inside the respective channels, leaving the middle one empty. The chips were then incubated in the cell incubator for 30 minutes until the collagen formed a gel and subsequently stellate cells were injected and the incubation was repeated. After this second incubation, EMEM with the addiction of 10% FBS and Pen-Strep was added to both inlet and outlet channels.

After adding the medium to both channels, the devices were incubated for 90 minutes, then RFP-HUVEC cells were harvested, centrifuged for 5 min at 300 x g, the pellets were resuspended in 1 ml of fresh medium and counting was performed manually with a hemocytometer. A density of 2×10^6 cells/ml was used for both the experiments.
Finally, the medium was removed from both inlet and outlet channels and RFP-HUVEC suspension was flowed through the inlet channel. The chips were then incubated in the cell incubator for 90 minutes and RFP-HUVEC medium EBM-2 plus supplements was used to fill the inlet channel while the outlet was filled with EMEM plus 10% FBS and Pen-Strep. After other 90 minutes of incubations, the Petri plates with the devices were moved to a tilting platform placed inside cell incubator. The chips were monitored daily, and the medium was changed every two days. Images were collected using brightfield microscopy.

Construction of liver on a chip with primary cells

Two different models were used, and slightly different protocols were applied.
For the first experiment 120 five-channel microfluidic devices were prepared, model 3 was chose.
First, we prepared 3 different mixes of rat tail collagen type I (2.5 mg/ml) in ice with the same formula described in the previous chapter.
Cells concentrations were the following:

- Hepatocyte cells (HCs) (3×10^6 cells/ml)
- Hepatocyte stellate cells (HSCs) (3×10^5 cells/ml)
- Kupffer cells (KCs) (1×10^6 cells/ml)

HSCs were harvested as described in the previous chapter while for HCs and KCs a different procedure was followed. HCs vial was thaw and the cells were centrifuged at 100 x g, at 4 °C for 10 min. Then the pellet was resuspended in a small volume of cold plating medium HM-1 and cells were centrifuged again at 100 x g, at 4 °C for 10 min. The medium was removed, and collagen mix was added to cell pellet.
KCs vial was thaw, 9 ml of cold plating medium KC-1 was added, and the cells were centrifuged at 500 x g, at 4 °C for 5 min. The medium was removed, and collagen mix was added to cell pellet.
HCs and KCs were injected inside the respective channels, leaving the middle one empty. The devices were then incubated in the cell incubator for 30 minutes until the collagen formed a gel and subsequently HSCs were also injected, and the incubation was repeated. After this second incubation, the devices were conditioned by a mixture of HM-1: HSC

medium: KC- 1 at their corresponding cell ratio (10:1:3). After 4 hours the media was removed, and a new combination of media was used: HM-2: HSC medium: KC- 2 at their corresponding cell ratio (10:1:3). The Petri plates with the devices were moved to a tilting platform in the cell incubator.

After two days, the medium was removed from the inlet channel, 15 µl of fibronectin (0.05 mg/ml) were added, and the devices were then incubated in the cell incubator for 30 minutes. The medium of the outlet channel was also removed after the incubation, and a new combination of media was used: HM-2: KC- 2 (10:3) to fill both channels.

On day five, due to the slow growth of LSECs, both RFP-HUVEC and LSECs were used to fill the inlet channel. The cells were mixed and resuspended in LSEC-growth media at a density of 2×10^6 cells/ml. The media was removed from the reservoir of both channels and then 50 µl of LSECs suspension was flowed through the inlet channel. The devices were moved again onto a tilting platform in the cell incubator for 1 hour. After this step, a combination of media was used to fill the outlet channel: HM-2: KC- 2 (10:3). The inlet channel with endothelial cells was filled with EBM-2 plus supplements.

The Petri plates with the devices were then moved again to a tilting platform, the devices were monitored daily, and the medium was changed and collected for storage at -80 °C every two days. Images were collected using brightfield microscopy.

For the second experiment, 41 3D Cell Culture Chips (Aim Biotech) were used, they were already sterile and ready for cell seeding. First, a single rat tail collagen type I (2.5 mg/ml) mix was prepared in ice, following the same calculation used for the experiment with cell lines.

Cells concentrations were the following:

- HCs (5×10^5 cells/ml)
- HSCs (5×10^4 cells/ml)
- KCs (15×10^4 cells/ml)

The harvesting procedures for these three cell types were the same described before but this time the pellets were all mixed with collagen in the same Eppendorf.

After the injection of the mix, the chips were incubated in the cell incubator for 30 minutes until the collagen formed a gel and subsequently the inlet channel was filled with 15 µl of fibronectin (0.05 mg/ml). The devices were then incubated again in the cell incubator for 30 minutes. After this second incubation, the chips were conditioned by a mixture of HM-1: KC- 1 medium (10:3). After 4 hours, the mixture was removed, and a new combination

of media was used: HM-2: KC- 2 (10:3). The Petri plates with the devices were then moved to a tilting platform in the cell incubator.

The day after the seeding, HUVECs cells were used to fill the inlet channel. The cells were resuspended in EBM-2 plus supplements media at a density of 2×10^6 cells/ml. The media was removed from the reservoir of both channels and then 50 µl of cell suspension was flowed through the inlet channel and the devices were incubated for 30 minutes. After this step, a combination of media was used to fill the outlet channel: HM-2: KC- 2 (10:3). The inlet channel with endothelial cells was filled with EBM-2 plus supplements: HM-2: KC-2 mix (1:1).

The Petri plates with the devices were then moved again to a tilting platform, the chips were monitored daily, and the medium was changed and collected for storage at -80 °C every two days. Images were collected using brightfield microscopy.

NASH induction and drugs application

The 120 five-channel microfluidic devices underwent contamination immediately after NASH induction. Here is described the procedure followed using the 41 commercial three-channel microfluidic devices. After this episode of contamination, all the media were filtered and pen-strep was added.

After 24 hours the HUVECs cells were well attached and spread onto the channel surface and the devices were treated with various disease triggers and treatments.

The following groups were created:

1. Control
2. NASH
3. NASH + 0.1 µM K1K1
4. NASH + 0.01 µM K1K1
5. NASH + 0.1 µM HGF/SF
6. NASH + 0.1 µM K1K1 + 30 µM TAK-242
7. NASH + M-CSF/IL4
8. NASH + 30 µM TAK-242
9. NASH + 30 µM SR1078

For the control group HM-2: KC- 2 (10:3) media was used to fill the outlet channel while for the inlet channel with endothelial cell EBM-2 plus supplements: HM-2: KC-2 mix (1:1) media was used. EBM-2 plus supplements: HM-2: KC-2 mix (1:1) media was used to fill the outlet channels of all the groups. For the 9 groups where NASH was induced, a special media was created, and drugs were added freshly every 2 days. NASH media was used to fill the inlet channels, its composition was:

- EBM-2 plus supplements: HM-2: KC-2 mix (1:1) media
- Sodium oleate (0.66 mM)
- Sodium palmitate (0.33 mM)
- LPS (10 μg/ml)
- BSA 1%

All the devices were moved on a tilting platform and incubated at 37 °C. Media was refreshed every 2 days and collected for storage at -80 °C till day 9 after NASH induction. Images were collected using brightfield and fluorescence microscopy.

Immunofluorescence staining

Immunofluorescence protocol was performed as follows:

- Remove the medium from the channels and quickly wash with DPBS.
- Fix with 4% paraformaldehyde at room temperature for 15 min.
- Wash 3 times for 10 minutes with PBS.
- Permeabilize with 0.2% Triton X-100 at room temperature for 10 min.
- Wash 3 times for 10 minutes with PBS + 0.25% Tween 20.
- Incubate with BSA (10%w/v) for at least 2 hours.
- Incubate with primary antibodies diluted in PBS + 0.25% Tween 20 overnight at 4°C.
- Wash 3 times for 10 minutes with PBS + 0.25% Tween 20.
- Incubate with Hoechst solution diluted 1:500 in PBS for 30 min at room temperature.
- Wash 3 times for 10 minutes with PBS + 0.25% Tween 20.
- Collect immunofluorescence images of stained cells with fluorescence microscope and analyze with ImageJ software.

Live/dead assay

LIVE/DEAD/Viability/Cytotoxicity kit is a two-color fluorescence cell viability assay, based on the simultaneous detection of live and dead cells with two probes, calcein AM and ethidium homodimer (EthD-1). Two parameters of cell viability were assessed: intracellular esterase activity and plasma membrane integrity.

Calcein AM/ EthD-1 were diluted in DPBS to a final concentration of 2 μM and 4 μM. The liver cells on chip were then incubated with the mix for 30 min at 37 °C avoiding light exposition.

A fluorescence microscope was used to identify and take photos of viable cells (green fluorescence) and dead cells (red fluorescent nuclei) which were analyzed with ImageJ software to quantify red and green fluorescence intensities.

Neutral lipid staining

HCS LipidTOX® red neutral lipid stain was diluted 1:500 in PBS and applied on chips for 1h at 37 °C. Fluorescence microscope was used to take pictures of stained oil globules within hepatocytes. ImageJ software analysis was performed to quantify red fluorescence intensity.

Commercial ELISA

Media effluents were collected from both inlet and outlet channels every 2 days starting from NASH induction. The samples were stored at -80 °C until analysis. Before using commercial kits, the samples were centrifuged at 500 x g for 10 min at 4 °C, aliquots were prepared and if not used they were stored again at -80 °C. ELISA kits were used to quantify TNFα and TGF β.

Results

Large scale recombinant proteins production

K1K1

pET45b (+) plasmid containing K1K1 was used to transform *Escherichia coli* strain BL21(DE3) for protein expression. After induction with IPTG, the cells were grown for 24 hours at 18 °C. The cells were harvested by centrifugation and the pellets were frozen at -80 °C. The protein was then extracted following a protocol for non-classical inclusion bodies extraction and an L-arginine-containing buffer was used to solubilize and to refold the molecules in the final step before purification.

After 3 days in an L-arginine-containing buffer, the protein sample was diluted, filtered, and loaded on a 5 ml HiTrap® Heparin HP column for an affinity chromatography step. Both ÄKTA Purifier FPLC and ÄKTA Pure FPLC systems were used. The fractions underneath the peak were loaded on a 20% polyacrylamide gel under reducing conditions and Coomassie Blue was used to stain proteins to confirm the presence of K1K1 (**Fig. 11**).

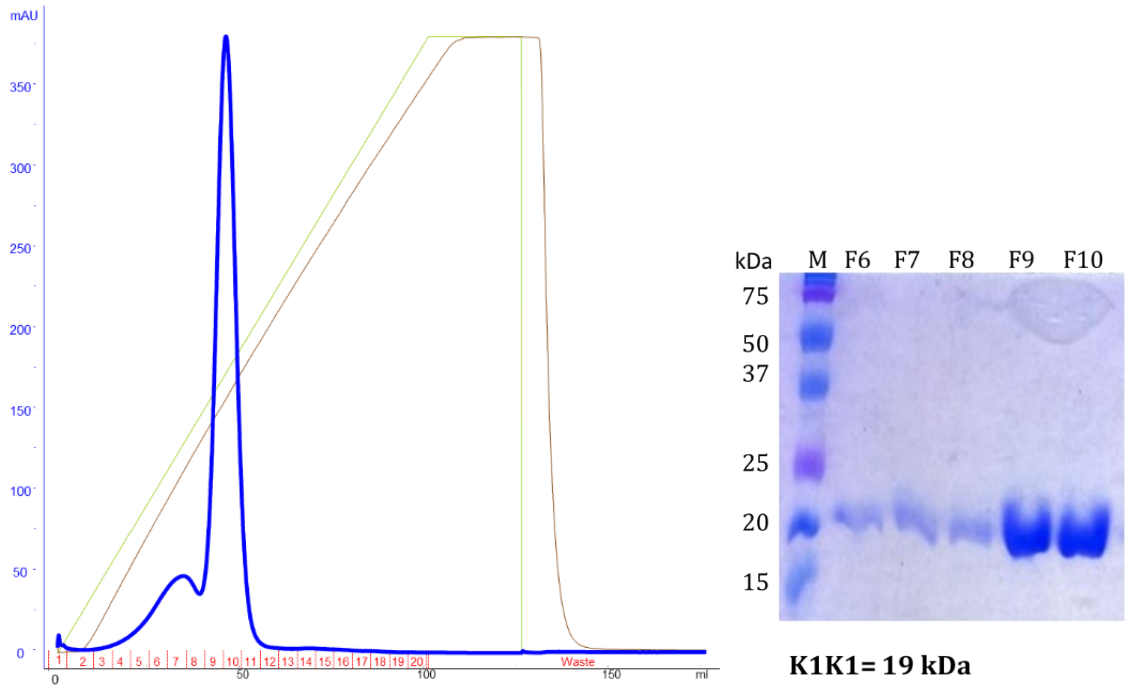

Fig. 11 K1K1 purification on a 5 ml HiTrap® Heparin HP column (**left**), K1K1 fractions separated on a 20% polyacrylamide gel stained with Coomassie Blue (**right**).

After this first purification, different fractions from many batches were pooled together, and concentrated. The protein was later quantified, and SEC was performed on a HiLoad® 26/60 Superdex® 200 pg column (**Fig. 12**).

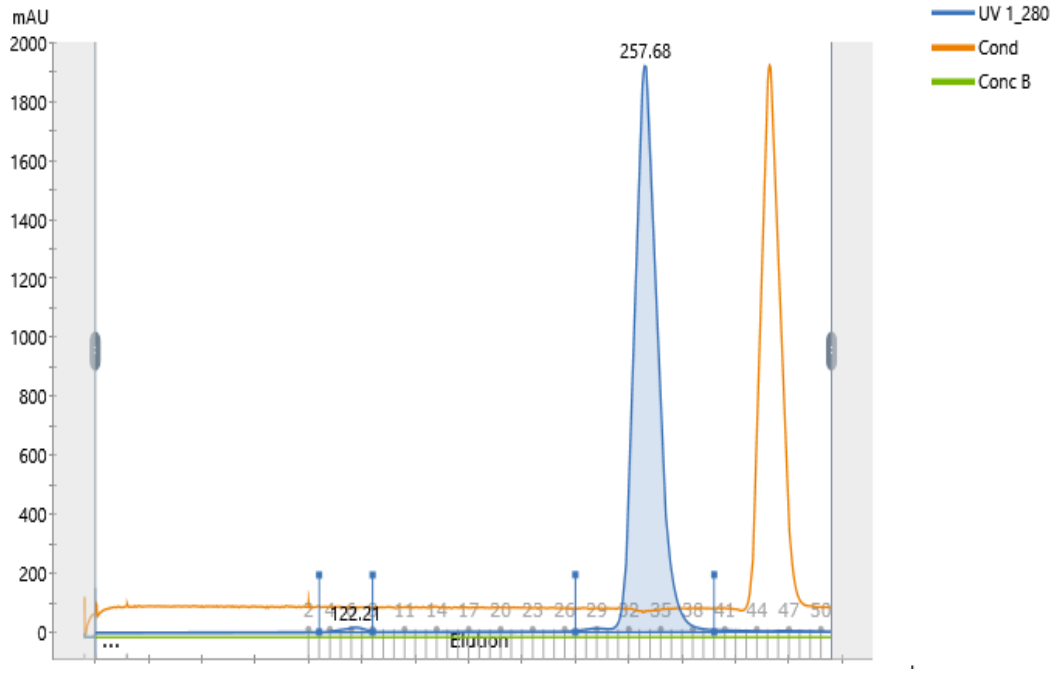

Fig. 12 K1K1 purification on a HiLoad® 26/60 Superdex® 200 pg column.

The fractions underneath the peak were loaded again on a 20% polyacrylamide gel under reducing conditions and Coomassie Blue was used to stain proteins. The chosen fractions were pooled together, concentrated, quantified and flash frozen in nitrogen for storage at -80 °C.

1K1

GS115 *P. pastoris* cells transformed with pPIC9K plasmid with the 1K1 insert were used for protein production. After one week, the protein secreted in the medium was collected, concentrated and, as a final step, dialysis was performed to change protein buffer. The protein sample was filtered and loaded on a 5 ml HiTrap® Heparin HP column for an affinity chromatography step. Both ÄKTA Purifier FPLC and ÄKTA Pure FPLC systems were used. The fractions underneath the peak were loaded on a 20% polyacrylamide gel under reducing conditions and Coomassie Blue was used to stain proteins to confirm the presence of 1K1 (**Fig. 13**).

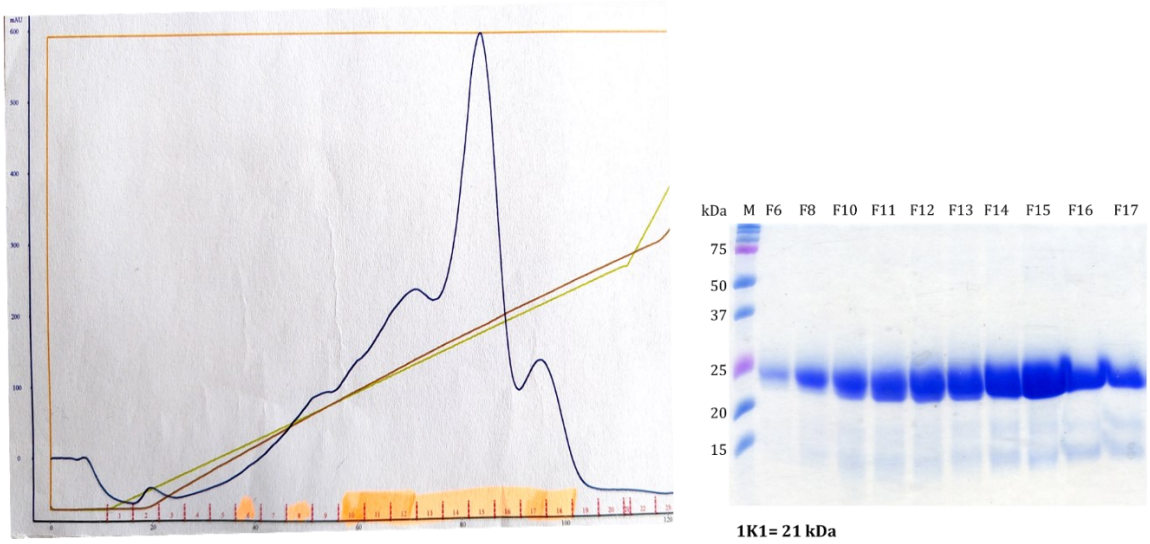

Fig. 13 1K1 purification on a 5 ml HiTrap® Heparin HP column (**left**), 1K1 fractions separated on a 20% polyacrylamide gel stained with Coomassie Blue (**right**).

After this first purification, different fractions were pooled together, and concentrated. The protein was later quantified, and SEC was performed on a HiLoad® 26/60 Superdex® 75 pg column. The fractions underneath the peak were loaded again on a 20% polyacrylamide gel under reducing conditions and Coomassie Blue was used to stain proteins (**Fig. 14**)

The chosen fractions were pooled together, concentrated, quantified and flash frozen in nitrogen for storage at -80 °C.

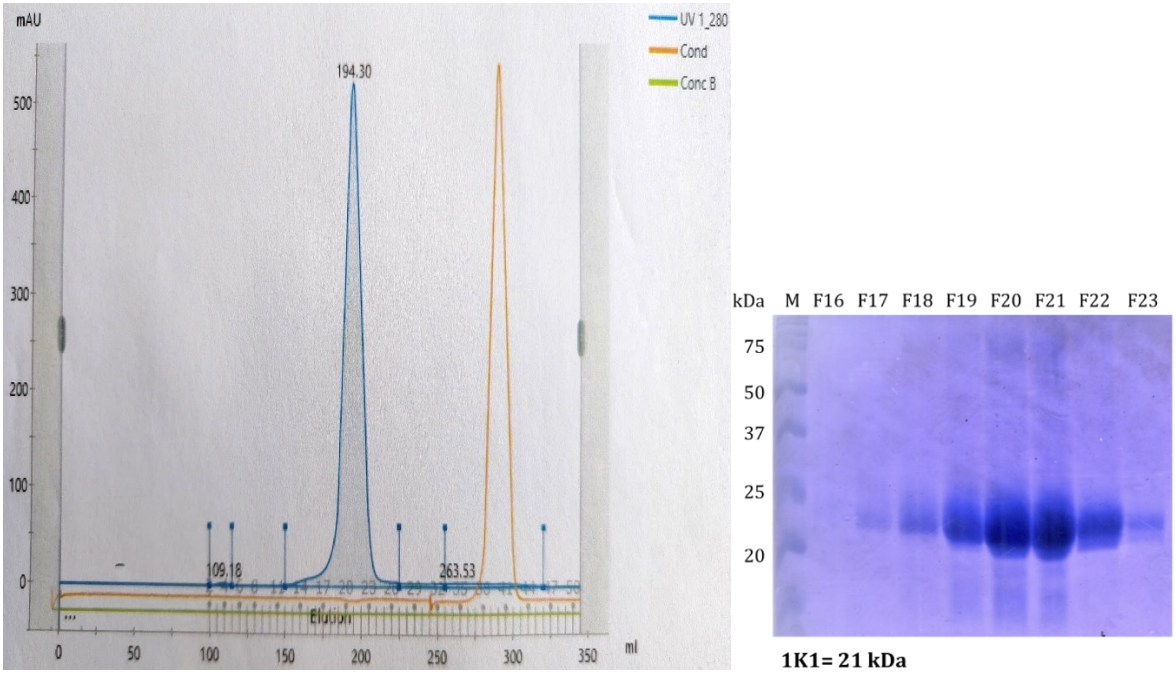

Fig. 14 1K1 purification on a HiLoad® 26/60 Superdex® 75 pg column (**left**), 1K1 fractions separated on a 20% polyacrylamide gel stained with Coomassie Blue (**right**).

MET567

CHO lec 3.2.8.1 cells were previously stably transfected with plasmid pA71d containing MET567 insert. The protein was secreted in the medium that was collected from roller bottles, filtered, and concentrated. As a final step, dialysis was performed to change protein buffer. The protein solution was loaded on a 1 ml HisTrap® column for an affinity chromatography step. The fractions underneath the peak were then loaded on a 12% polyacrylamide gel under reducing conditions and Coomassie Blue was used to confirm the presence of the protein (**Fig. 15**).

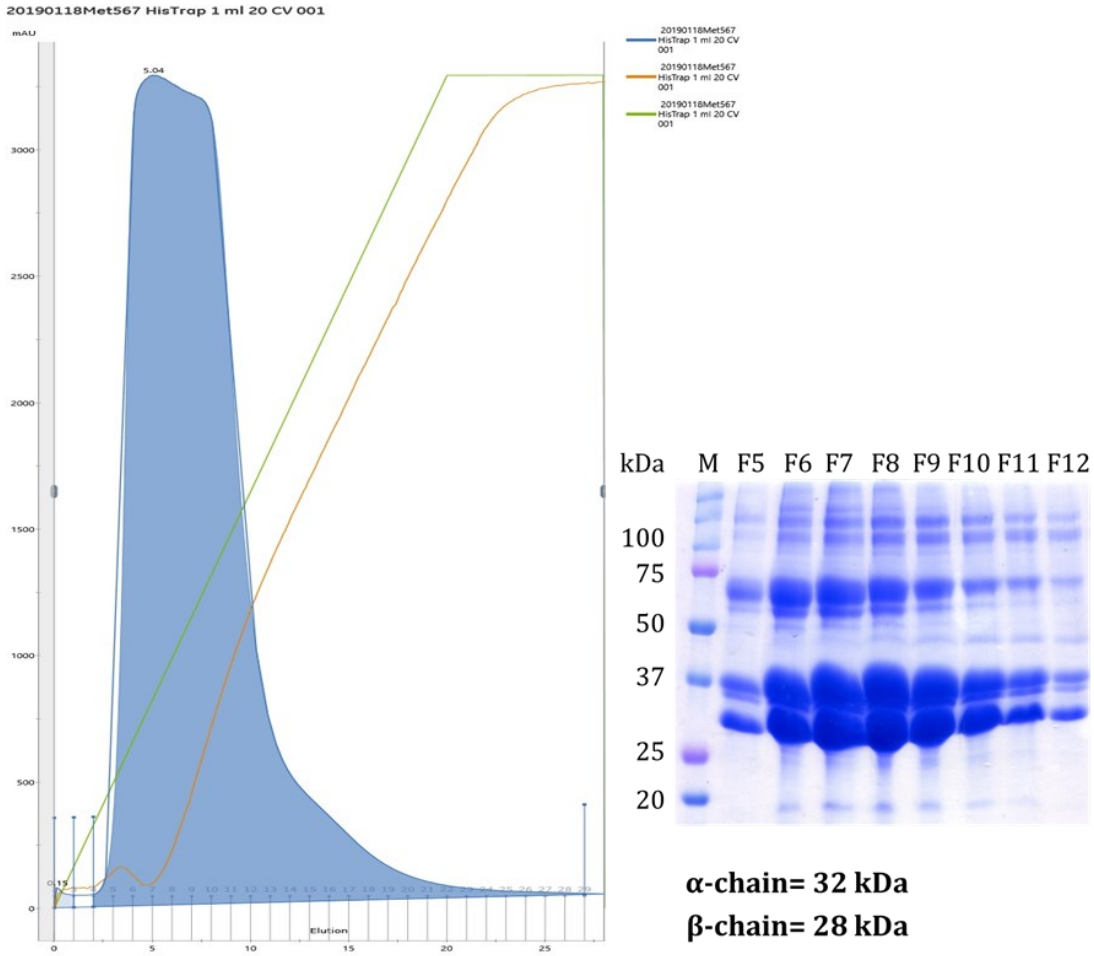

Fig. 15 MET567 purification on a 1 ml HisTrap® HP column (**left**), MET567 fractions separated on a 12% polyacrylamide gel stained with Coomassie blue (**right**).

After the first step of purification by affinity chromatography, a second step was required to remove contaminant protein visible on gel as bands with higher molecular weight. A 6 ml cation exchange Resource™ S column was used for this purpose (**Fig. 16**).

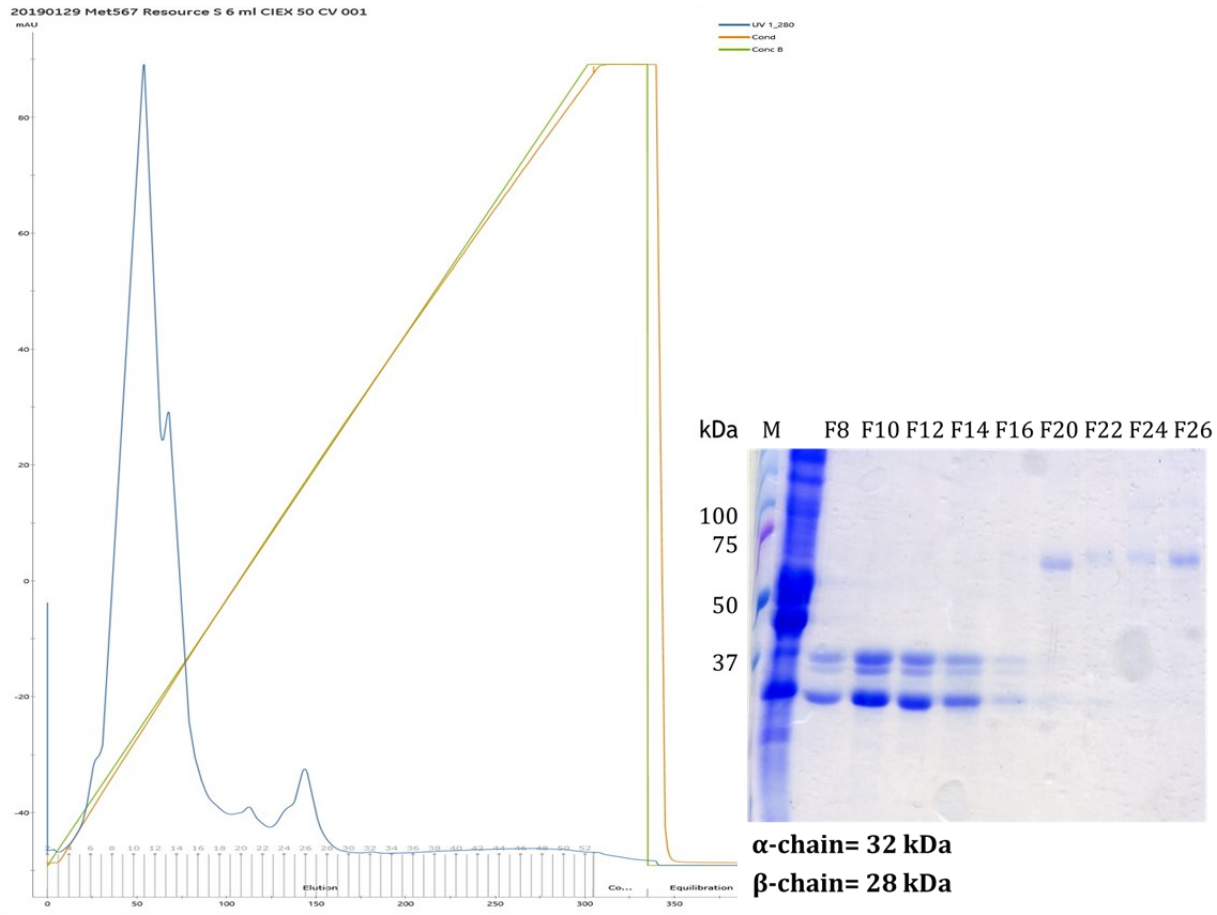

Fig. 16 MET567 purification on a 6 ml Resource™ S column (**left**), MET567 fractions separated on a 12% polyacrylamide gel stained with Coomassie blue (**right**).

With this second step of purification, pure protein was obtained. Subsequently, the fractions containing MET567 were pooled together, concentrated, quantified and flash frozen in nitrogen for storage at -80 °C.

Comparison of HGF/SF, K1K1 and 1K1 protein stability

Ten micromolar (10^{-5} M) concentrated HGF/SF, 1K1 and K1K1 were incubated at 37 °C for 3 weeks. Samples were collected weekly and at the end of the experiment, 3.5 µg of each protein sample were loaded on a 12% SDS-PAGE gel under reducing conditions (**Fig. 17**).

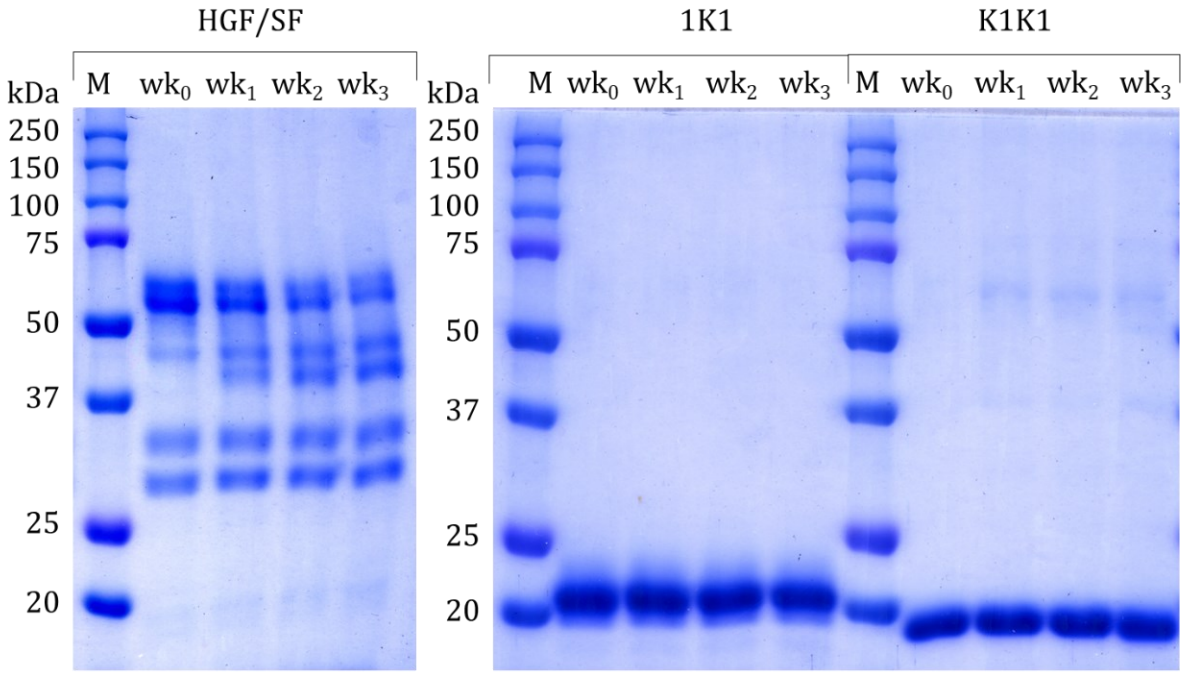

Fig. 17 Coomassie stained gels of HGF/SF (**left**) and K1K1 and 1K1 samples (**right**).

K1K1 and 1K1 bands were still visible and well defined after 3 weeks of incubation at 37 °C while the HGF/SF bands, in particular the α-chain, seemed to fade after 2 to 3 weeks. This first impression was further confirmed with a western blot performed on HGF/SF samples. For this, one microgram of each HGF/SF sample was loaded on a 12% SDS-PAGE gel under reducing conditions and the procedure described in method section was followed. The membrane was incubated overnight with a goat polyclonal anti-HGF/SF Ab (GFG 1W53, 1:1000) followed by a 1-hour incubation with HRP-conjugated rabbit anti-goat Ab (Agilent Technologies, 1:1000) (**Fig. 18**).

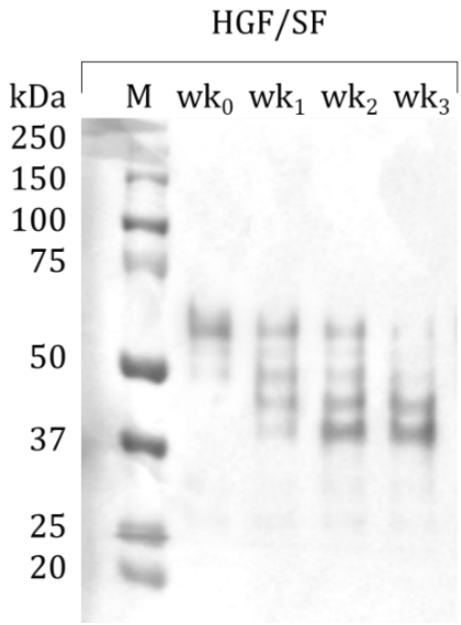

Fig. 18 Western blot of HGF/SF samples.

The stability of HGF/SF, 1K1 and K1K1 samples diluted in PBS was then analyzed using a thermal shift assay. Tycho NT.6 was used to measure changes in brightness of aromatic amino acid residues at 330 nm and 350 nm during thermal unfolding. The brightness signals were reported as 350 nm/330 nm ratio and used to calculate the inflection temperature (Ti).

Loss or shift of Ti or decrease in Δ ratio are signals of increased destabilization and unfolding but here, no observable shift of the Ti or decrease in Δ ratio was reported for the 3 proteins over time (**Fig. 19**). As for the Ti and the Δ ratio, brightness values were also stable for all the proteins during the 3 weeks of incubation as shown in **Table 2**.

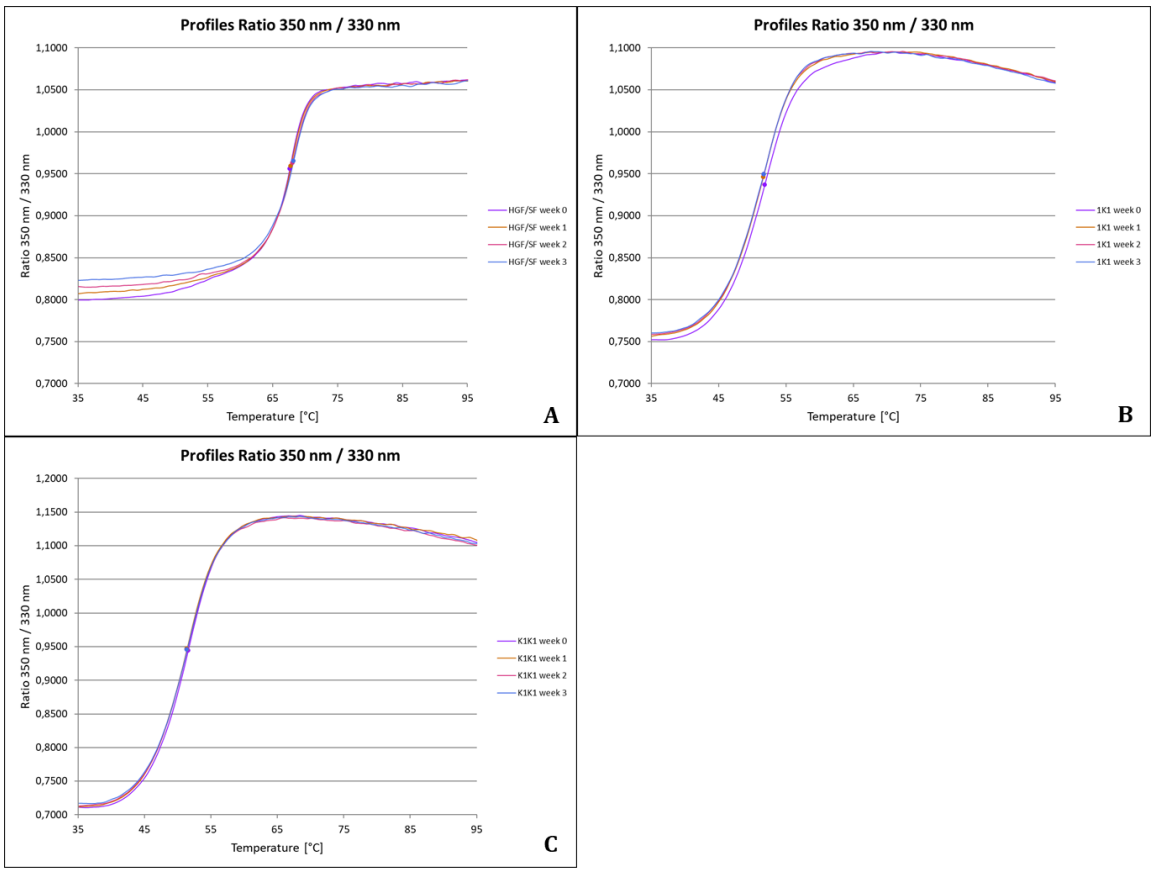

Fig. 19 Thermal unfolding profiles of HGF/SF, 1K1 and K1K1 (**A-C**).

Table 2 Ti, initial ratio, Δ ratio and sample brightness of HGF/SF, 1K1 and K1K1 samples.

Capillary label	Ti	Initial Ratio	Δ Ratio	Sample Brightness
HGF/SF week 0	67.6	0.7991	0.2641	487.7
HGF/SF week 1	67.8	0.8083	0.2537	492.9
HGF/SF week 2	68.1	0.8150	0.2469	497.4
HGF/SF week 3	68.2	0.8234	0.2384	499.4
1K1 week 0	51.9	0.7475	0.3098	40.2
1K1 week 1	51.6	0.7530	0.3047	39.7
1K1 week 2	51.7	0.7546	0.3064	38.4
1K1 week 3	51.7	0.7559	0.2991	38.1
K1K1 week 0	51.6	0.7094	0.3942	67.9
K1K1 week 1	51.4	0.7117	0.3979	66.0
K1K1 week 2	51.4	0.7131	0.3858	65.6
K1K1 week 3	51.4	0.7150	0.3864	65.6

After testing protein stability with two different methods, protein biological activity was also evaluated with MDCK scatter assay, performed as described in the methods section. The untreated cells shown a typical epithelial appearance and grow in tight colonies while the ones treated with HGF/SF, 1K1, or K1K1 showed scattering and a morphological change. There was no evident loss of activity for all the proteins during the 3 weeks of incubation. HGF/SF was active down to a concentration of 3 x 10^{-12} M while K1K1 was able to induce colony scattering as low as 10^{-12} M. In the end, 1K1 was less active than HGF/SF and K1K1 and the treatment with this protein was able to induce scattering only down to a concentration of 3 x 10^{-11} M (**Fig. 20**).

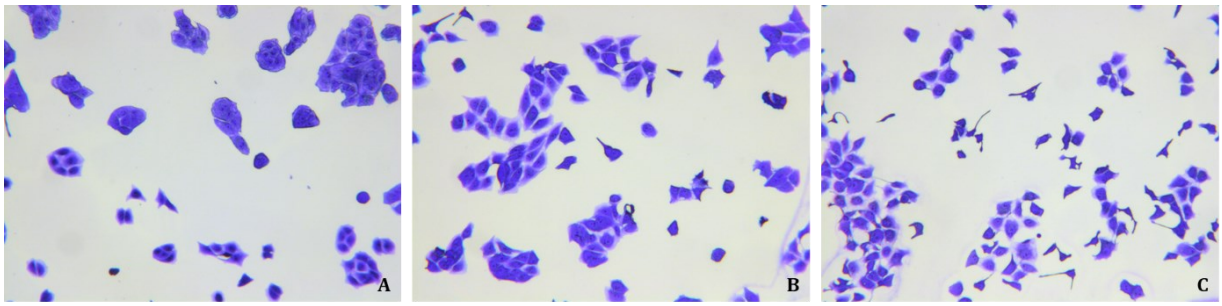

Fig. 20 Representative images of MDCK colonies after overnight incubation with medium only (**A**), 10^{-12} M K1K1 (**B**), 10^{-11} M K1K1 (**C**).

Assessment of MET and HGF/SF protein expression with IHC in FFPE liver samples of patients with steatosis or NASH

Patients

In collaboration with the Unit of Pathology of "Maggiore della Carità" Hospital in Novara, a study on 34 liver biopsies (cases) from 34 patients with steatosis or NASH diagnosis has been set up. Six biopsies of normal liver (controls) from 6 patients were also included. The NASH clinical research network (CRN) system was selected for case classification and a composite grade, the NAFLD activity score (NAS) was used as an indication of the severity of the disease. NAS is the unweight sum of steatosis (0-3), lobular inflammation (0-3), and hepatocellular ballooning scores (0-2). Biopsies with NAS ≥5 correlate with a diagnosis of NASH, while biopsies with NAS less than 3 were diagnosed as "not NASH" [60]. Fibrosis was considered separate as the representative for the stage of NAFLD (0-4) [60].

The sample (controls and cases) showed an almost similar distribution between males and females (47.5% vs 52.5%). There was no statistically significant difference in the distribution of the sex variable by group (Fisher's exact test = 0.071) although in the control group, approximately 83% of subjects were male compared to the 42% of the subjects in the case group (**Table 3**).

Table 3 Frequency distribution of sex in cases and controls.

	Controls	Cases	Total
Male	5	14	19
	83.33	41.18	47.50
Female	1	20	21
	16.67	58.82	52.50
Total	6	34	40
	100.00	100.00	100.00

There was a significant difference of the NAS between cases and controls (Fisher's exact test <0.0001). In cases, grades 4 and 5 were predominant, while grade 0 was present only among the controls (**Table 4**).

Table 4 Frequency distribution of grade in cases and controls.

Grade	Controls	Cases	Total
0	6	0	6
	100.00	0.00	15.00
1	0	4	4
	0.00	11.76	10.00
2	0	5	5
	0.00	14.71	12.50
3	0	5	5
	0.00	14.71	12.50
4	0	8	8
	0.00	23.53	20.00
5	0	10	10
	0.00	29.41	25.00
6	0	1	1
	0.00	2.94	2.50
7	0	1	1
	0.00	2.94	2.50
Total	6	34	40
	100.00	100.00	100.00

There was a significant difference (Fisher's exact test = 0.033) in disease staging between case and control groups, as expected. Within the cases, it was observed that stages 1 and 3, but also 0, were equally frequent, followed by stage 4 while stage 2 was poorly represented (**Table 5**).

Table 5 Frequency distribution of stage in cases and controls.

Stage	Controls	Cases	Total
0	6	9	15
	100.00	26.47	37.50
1	0	9	9
	0.00	26.47	22.50
2	0	2	2
	0.00	5.88	5.00
3	0	9	9
	0.00	26.47	22.50
4	0	5	5
	0.00	14.71	12.50
Total	6	34	40
	100.00	100.00	100.00

Steatosis score was considered and as expected, there was a different frequency distribution between cases and controls (Fisher's exact test <0.0001). Approximately 70% of cases had a ≥2 steatosis score, 35% of cases had a steatosis score = 2, followed by equal distribution of scores 1 and 3. The subjects with score 0 were all controls (**Table 6**). Representative haematoxylin-eosin staining of a normal liver and of a liver with high steatosis score are shown in **Fig. 21.**

Table 6 Frequency distribution of steatosis in cases and controls.

Steatosis	Controls	Cases	Total
0	6	0	6
	100.00	0.00	15.00
1	0	10	10
	0.00	29.41	25.00
2	0	14	14
	0.00	41.18	35.00
3	0	10	10
	0.00	29.41	25.00
Total	6	34	40
	100.00	100.00	100.00

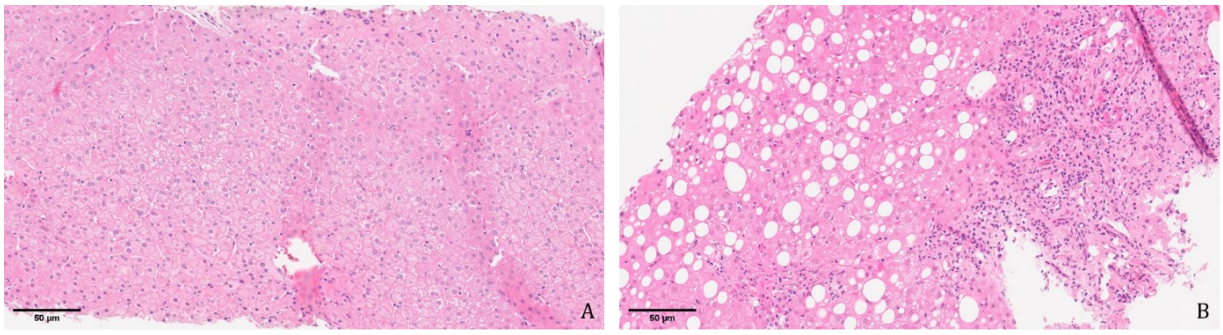

Fig. 21 Representative haematoxylin-eosin staining of a normal liver (**A**), and of a liver with steatosis score = 3 (**B**) (magnification 200X).

Almost all cases have an absent or mild level of hepatocellular ballooning, and all the controls were negative as expected (**Table 7**). The difference between the two groups was significant (Fisher's exact test = 0.031).

Table 7 Frequency distribution of hepatocellular ballooning in cases and controls.

Ballooning	Controls	Cases	Total
0	6	12	18
	100.00	35.29	45.00
1	0	19	19
	0.00	55.88	47.50
2	0	2	2
	0.00	5.88	5.00
3	0	1	1
	0.00	2.94	2.50
Total	6	34	40
	100.00	100.00	100.00

MET detection

Different protocols were used to test a panel of anti-MET antibodies, their characteristics are reported in **Table 8.**

Table 8 List of anti-MET antibodies used for IHC.

Name	Antigen	Reactivity	Source	Dilution	Firm
LIF 40-41	MET ECD	H	Mouse		GFG
LIF 39-58	MET ECD	H	Mouse	1 µg/ml	GFG
Met (D1C2) XP® Rabbit mAb #8198	MET C-terminus	H	Rabbit	1:100	Cell Signaling

(Meaning of some abbreviations in table: GFG = Growth Factor Group, ECD = extracellular domain)

Completely automated protocols were used for all these antibodies. Colorectal adenocarcinoma samples were used before liver samples to test all the antibodies as colorectal adenocarcinoma have high MET expression (https://www.proteinatlas.org).

All the protocols used to test LIF 40-41 failed as the staining of colorectal adenocarcinoma samples were always negative. Different protocols were also used to test LIF 39-58, the staining was positive but non-specific and diffused.

After these two antibodies, Met (D1C2) XP® Rabbit mAb was also tested with positive results, 2 µm thick sections were cut and baked for 20 minutes at 60 °C. Then the sections were loaded on BenchMark ULTRA IHC/ISH system and an IHC protocol was created with a first deparaffinization step, 76 minutes of antigen retrieval with Cc1 buffer (Roche), 60 minutes of incubation with Met (D1C2) XP® Rabbit mAb (1:100) followed by incubation

with the secondary Ab and subsequent DAB staining. The slides were counterstained with haematoxylin for 24 minutes and the coverslips were mounted.
The staining was specific and as expected MET was highly expressed in cancer cells both in the membrane and in the cytoplasm with the membrane expression being higher compared to the cytoplasm one. MET expression was also detected at a lower level in non-neoplastic enterocytes membranes. (**Fig. 22**)

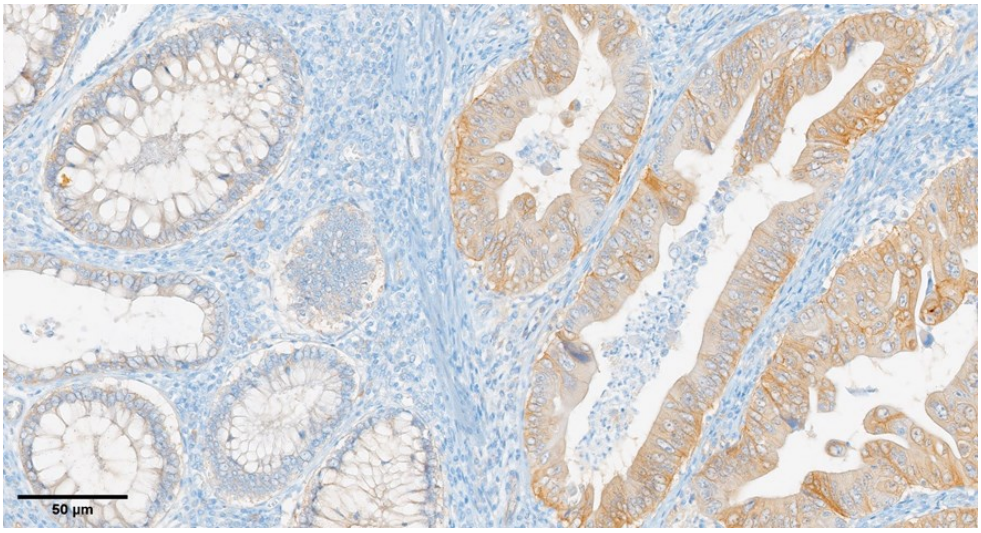

Fig. 22 Representative IHC staining for MET in colorectal adenocarcinoma (magnification 200X).

After protocol optimization with colorectal carcinoma samples, 5 biopsies of normal liver and 30 liver biopsies of patients with steatosis or NASH diagnosis were stained.
When present, a weak-moderate MET expression was detected in the membrane of the hepatocytes (**Fig. 23**).

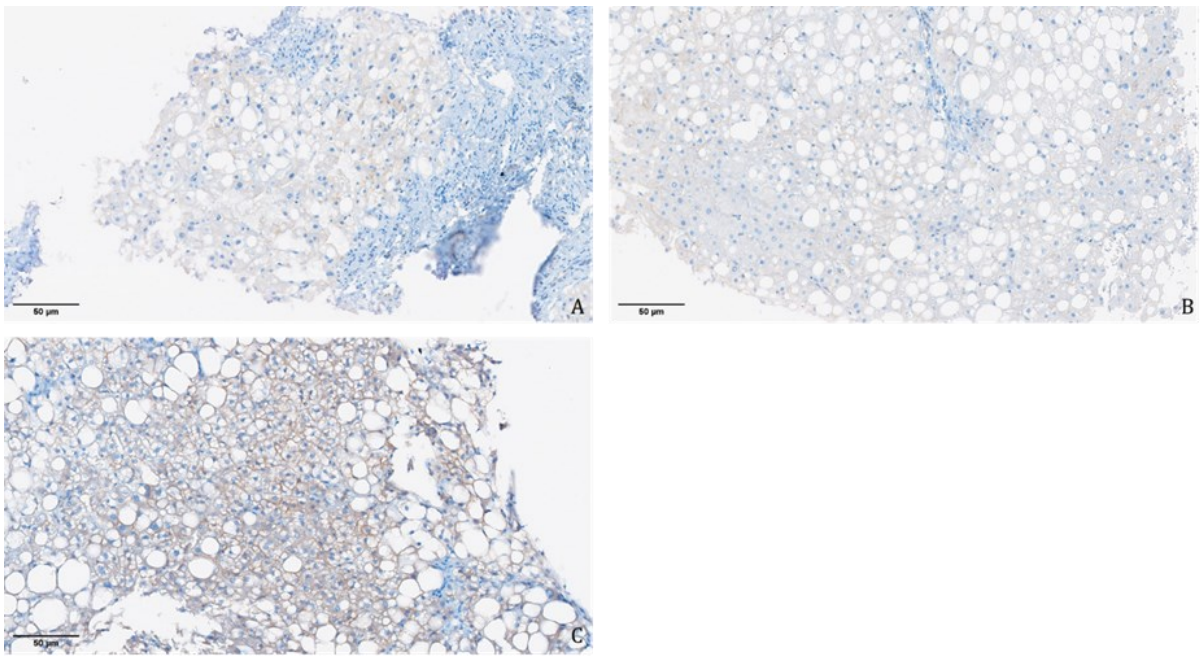

Fig. 23 Representative IHC staining for MET in liver with NAS = 2 (**A-B**), liver with NAS = 7 (**C**) (magnification 200X).

Haematoxylin-eosin stained slides and IHC slides were later examined by a pathologist who evaluated IHC staining using a semiquantitative system for both the staining intensity and the percentage of positive cells (i.e. staining extension). The staining intensity was scored as follows: no staining (score = 0), weak staining (score =1), moderate staining (score = 2) and intense staining (score = 3). The staining extent was scored as 0 (<1%), 1 (1-25%), 2 (26-50%), 3 (51-74%), and 4 (≥75%).

A statistical analysis was performed, with the variables of interest (MET intensity and MET extension) were scored as previously indicated or transformed into two new variables to minimize the degree of data dispersion, and to try to increase the precision of the estimates. Specifically, the two new variables were created as follows:

- MET intensity (MET-Int01) in which, based on the degree of intensity, code 1 was assigned in the presence of any positive staining of this protein, code 0 otherwise.
- MET extension (MET-Ext01) in which code 1 was assigned in the presence of staining in ≥1% of the cells, code 0 otherwise.

As can be seen from **Table 9**, although there were differences in the frequency distribution of staining intensity between cases and controls (100% of the controls were negative for MET staining while 60% of cases showed a mild or moderate degree of staining), there is no statistically significant difference between MET staining intensity

and membership to the two groups (Fisher's exact test = 0.088). In other words, case or control groups membership did not appear to be discriminated by MET staining intensity.

Table 9 Frequency distribution of MET staining intensity.

MET_INT	Controls	Cases	Total
NO STAINING	5	12	17
	100.00	40.00	48.57
WEAK STAINING	0	15	15
	0.00	50.00	42.86
MODERATE STAINING	0	3	3
	0.00	10.00	8.57
Total	5	30	35
	100.00	100.00	100.00

About 37% of subjects had a percentage of cells positive for MET staining between 1% and 25%. Eleven percent showed a percentage of stained cells between 26% and 50%, while only 3% of the sample had a percentage greater than 75% (**Table 10**). There was no statistically significant difference between MET staining extension and group membership (exact Fisher's test = 0.116). Specifically, 100% of the controls and 40% of the cases were negative for MET staining.

Table 10 Frequency distribution of MET staining extension**.**

MET_EXT	Controls	Cases	Total
0	5	12	17
	100.00	40.00	48.57
1	0	13	13
	0.00	43.33	37.14
2	0	4	4
	0.00	13.33	11.43
4	0	1	1
	0.00	3.33	2.86
Total	5	30	35
	100.00	100.00	100.00

Later, associations between MET expression and groups were examined using the new dichotomized expression variables, MET-Int01 and MET-Ext01(**Tables 11-12**). There was a possible association between MET intensity or MET extension and groups belonging (exact Fisher's test = 0.019) because there was a difference in the frequency of positivity between the cases and the controls, respectively equal to 60% and 0% (**Tables 11-12**). The result, however, must be read with caution given the low sample size and the low number of controls.

Table 11 Frequency distribution of MET staining intensity using dichotomized expression variables.

MET_INT	Controls	Cases	Total
Absent	5	12	17
	100.00	40.00	48.57
Present	0	18	18
	0.00	60.00	51.43
Total	5	30	35
	100.00	100.00	100.00

Table 12 Frequency distribution of MET staining extension using dichotomized expression variables.

MET_EXT	Controls	Cases	Total
Absent	5	12	17
	100.00	40.00	48.57
Present	0	18	18
	0.00	60.00	51.43
Total	5	30	35
	100.00	100.00	100.00

Finally, subjects were divided in subgroups according to disease severity (0 = no pathology; 1 = mild or borderline disease, NAS ≥1 and <5; 2 = severe disease, NAS ≥5) and the relation with MET staining intensity or extension was considered.

All the subjects with no pathology had absent MET staining. MET staining was instead present in 63% of the subjects with mild or borderline disease and in 54% of the subjects with severe disease (**Tables 13-14**).

There may be a difference in the intensity or extension of MET protein staining in relation to the severity of the disease, the significance was at the limit of acceptability (exact Fisher's test = 0.05) (**Tables 13-14**).

Table 13 Frequency distribution of MET staining intensity in subgroups organized according to disease severity.

MET_INT	0	1	2	Total
Absent	5	7	5	17
	100.00	36.84	45.45	48.57
Present	0	12	6	18
	0.00	63.16	54.55	51.43
Total	5	19	11	35
	100.00	100.00	100.00	100.00

Table 14 Frequency distribution of MET staining extension in subgroups organized according to disease severity.

MET_EXT	0	1	2	Total
Absent	5	7	5	17
	100.00	36.84	45.45	48.57
Present	0	12	6	18
	0.00	63.16	54.55	51.43
Total	5	19	11	35
	100.00	100.00	100.00	100.00

HGF/SF detection

Different protocols were used to test a panel of anti-HGF/SF antibodies, their characteristics are reported in **Table 15.**

Table 15 List of anti-HGF/SF antibodies used for IHC.

Name	Antigen	Reactivity	Source	Dilution	Firm
HGFα (H-10): sc-374422 mAb	HGF/SF	H, M, R, others	Mouse	20 µg/ml	Santa Cruz Biotechnology
F2B3 pAb	HGF/SF	M,H	Rabbit		GFG
MSH2.B2 pAb	HGF/SF	M,H	Rabbit	20 µg/ml	GFG
MSH2.B6 pAb	HGF/SF	M,H	Rabbit	50 µg/ml	GFG
F1B3F pAb	HGF/SF	M,H	Rabbit		GFG
F2B3B run IV pAb	HGF/SF	M,H	Rabbit		GFG
F2B3B/C run VI pAb	HGF/SF	M,H	Rabbit		GFG
F2B3C run VII and VIII pAb	HGF/SF	M,H	Rabbit		GFG
F2B3E run IX and X pAb	HGF/SF	M,H	Rabbit		GFG
F2B3E run XI pAb	HGF/SF	M,H	Rabbit		GFG
F2B3EF run XII and XIII pAb	HGF/SF	M,H	Rabbit		GFG
F2B3EG run XIV and XV pAb	HGF/SF	M,H	Rabbit		GFG
EGH2/4C12.1 mAb	HGF/SF	M,H	Mouse	50 µg/ml	GFG

Completely automated or partially automated protocols were used for all these antibodies. Colorectal adenocarcinoma samples were used before liver biopsies to test all the antibodies as these samples have high-medium HGF/SF expression (https://www.proteinatlas.org).

This time the commercial antibody was used immediately, with positive results.

The protocol used was partially automated and started with the cutting of 2 µm thick sections, baked for 20 minutes at 60 °C. Then the sections were deparaffinised and rehydrated, and antigen retrieval was performed in heated Tris-EDTA pH 9 buffer for 15 min at 650 W in a microwave oven. After buffer cooling, sections were incubated in a 10% H_2O_2 solution for 10 minutes. Finally, the slides were loaded on BenchMark ULTRA IHC/ISH system and an IHC protocol was created, with 60 minutes of incubation with anti-

HGFα Ab (H-10) (1:10) followed by incubation with the secondary Ab and DAB staining. The slides were counterstained with haematoxylin for 24 minutes and the coverslips were mounted.

The staining was specific, and HGF/SF was moderately expressed in cancer cells in the cytoplasm (**Fig. 24**).

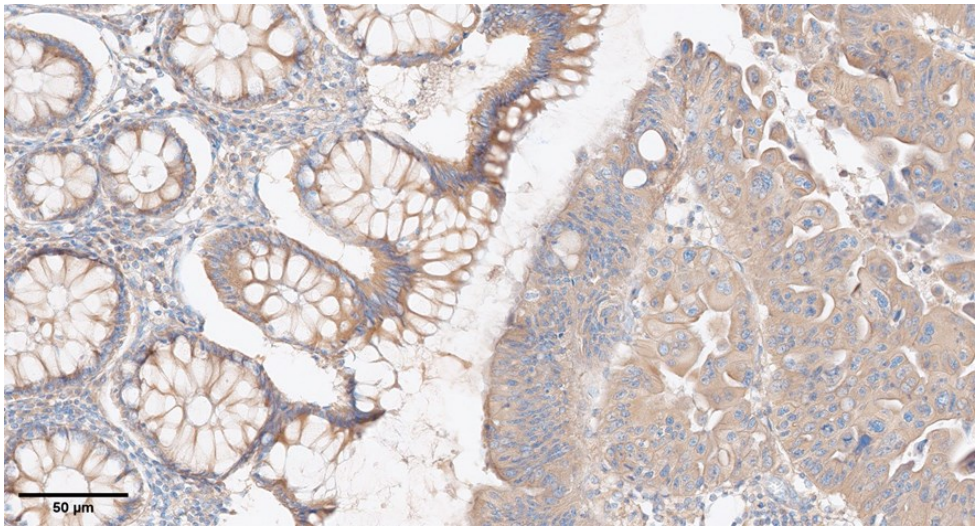

Fig. 24 Representative IHC staining for HGF/SF in colorectal adenocarcinoma (magnification 200X).

After protocol optimization with colorectal carcinoma samples, 5 biopsies of normal liver and 17 liver biopsies of patients with steatosis or NASH diagnosis were stained. When present, variable HGF/SF expression was detected in the cytoplasm of the hepatocytes while Kupffer cells, the ones that produce HGF/SF [61], were negative for the staining (**Fig. 25**).

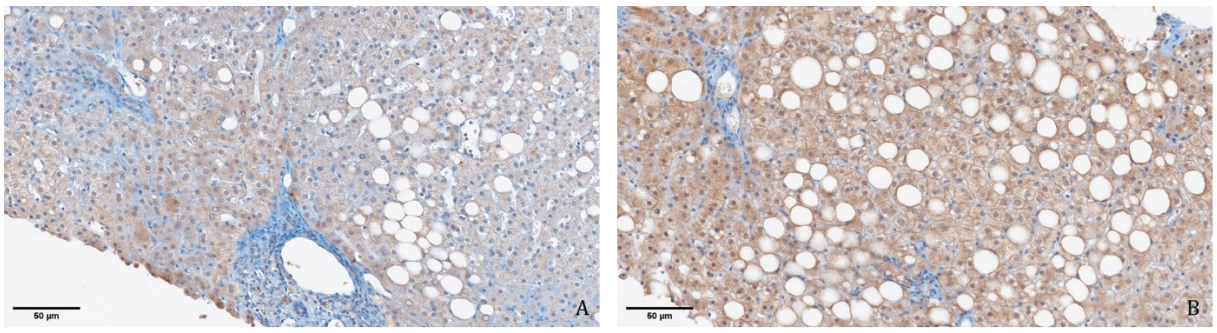

Fig. 25 Representative IHC staining for HGF/SF in liver with NAS = 2 (**A**), liver with NAS = 5 (**B**) (magnification 200X).

Haematoxylin-eosin stained slides and IHC slides were later examined by a pathologist who evaluated IHC staining using a semiquantitative system for both the staining intensity and the percentage of positive cells (i.e. staining extension). The staining intensity was scored as follows: no staining (score = 0), weak staining (score =1), moderate staining (score = 2) and intense staining (score = 3). The staining extent was scored as 0 (<1%), 1 (1-25%), 2 (26-50%), 3 (51-74%), and 4 (≥75%).

A statistical analysis was performed, the variables of interest (HGF/SF staining intensity and HGF/SF staining extension) were scored as previously indicated. Although the frequency distribution of HGF/SF staining intensity was different between cases and controls (**Table 16**), there was no statistical significance (exact Fisher's test = 0.237). The same can be said for the HGF/SF staining extension (exact Fisher's test = 0.783) (**Table 17**).

Table 16 Frequency distribution of HGF/SF staining intensity.

HGF_INT	Controls	Cases	Total
0	1	6	7
	20.00	35.29	31.82
1	1	8	9
	20.00	47.06	40.91
2	2	1	3
	40.00	5.88	13.64
3	1	2	3
	20.00	11.76	13.64
Total	5	17	22
	100.00	100.00	100.00

Table 17 Frequency distribution of HGF/SF staining extension.

HGF_EXT	Controls	Cases	Total
0	1	6	7
	20.00	35.29	31.82
1	0	3	3
	0.00	17.65	13.64
2	2	2	4
	40.00	11.76	18.18
3	1	3	4
	20.00	17.65	18.18
4	1	3	4
	20.00	17.65	18.18
Total	5	17	22
	100.00	100.00	100.00

Considering the results obtained with this first Ab, we tried to evaluate a panel of homemade Abs. Their protein concentration was determined using BCA assay and all of them were first tested with ELISA assay. Ninety-six well plates were coated with 100 µl/well human or murine HGF/SF (50 nM). All the antibodies were able to bind both human and murine HGF/SF.

Finally, these antibodies were used on colorectal carcinoma samples. Nine of them gave rise to positive but non-specific staining. Only MSH2.B2, MSH2.B6, and EGH2/4C12.1 passed the first screening phase and were also used on liver biopsies with the concentrations reported in **Table 15**. When present, variable HGF/SF expression was detected in the cytoplasm of the hepatocytes while Kupffer cells were still negative for the staining, so the experiment was interrupted without testing further liver biopsies.

Activation of signal transduction pathways

HepG2 and AML12

Both the cell lines were seeded in the evening with 30-40% confluence in 6 well plates. The day after the medium was removed and the HepG2 were first starved for 3 hours with a medium without FBS and later stimulated for 10 minutes with HGF/SF, K1K1, 1K1, NK1 at 3 different concentrations (0.1 nM, 1 nM, 10 nM).

A different protocol was followed for AML12 cells. The original media was removed and changed for 24 hours with one lacking insulin, transferrin, sodium selenite supplements (ITS). After this first incubation, the media was removed and a second one without both FBS and ITS was used for 3-hour starvation. Later AML12 were stimulated for 10 minutes with HGF/SF, K1K1, 1K1, NK1 at 3 different concentration (0.1 nM, 1 nM, 10 nM).

Cell lysates were prepared, stored, and quantified as described in methods section.

Forty micrograms of total protein lysates were loaded on 12% polyacrylamide gels. SDS-PAGE was performed in reducing conditions. Different antibodies were used, and their characteristics are reported in **Table 18.**

Table 18 List of the antibodies used for western blot application.

Name	Antigen	Reactivity	Source	Dilution	Firm
Phospho-Met (Tyr1349) Antibody #3121	p-MET	H, M, R	Rabbit	1:1000	Cell Signaling
Phospho-Met (Tyr1234/1235) (D26) XP® Rabbit mAb #3077	p-MET	H, M, R	Rabbit	1:1000	Cell Signaling
Phospho-Akt (Ser473) Antibody #9271	p-AKT	H, M, R, others	Rabbit	1:1000	Cell Signaling
Phospho-p44/42 MAPK (Erk1/2) (Thr202/Tyr204) (E10) Mouse mAb #9106	p-ERK	H, M, R, others	Mouse	1:5000	Cell Signaling
Met (D1C2) XP® Rabbit mAb #8198	MET total	H	Rabbit	1:1000	Cell Signaling
Akt Antibody #9272	AKT total	H, M, R, others	Rabbit	1:1000	Cell Signaling
Erk V114A	ERK total	H, M	Rabbit	1:5000	Promega
GAPDH antibody GTX100118	GAPDH	H, M, R, others	Rabbit	1:5000	GeneTex
Goat Anti-Rabbit Immunoglobulins/HRP P0448		Rb	Goat	1:1000	Agilent Technologies
Rabbit Anti-Mouse Immunoglobulins/HRP P0260		M	Rabbit	1:1000	Agilent Technologies

After transfer, the membranes were blocked with TBT +5% BSA for 1 hour. The membranes were then cut and incubated overnight at 4 °C with the primary antibodies diluted in blocking buffer. HRP-conjugated secondary antibodies diluted in blocking buffer were later used. TBT was used for the washings and ECL for detection.

Images were collected with Azure c600 Imager and western blot bands intensities were analyzed with ImageJ software. GraphPad was used to create the graphs.

Only HepG2 protein lysates treated with 10 nM and 1 nM protein concentrations were analyzed and GAPDH values were used for normalization (**Fig. 26-27**).

As shown in **Fig. 26** and **27**, when HepG2 cells were treated with 10 nM protein concentrations, both ERK and AKT phosphorylation increased compared to the control, and the cells treated with K1K1 shown the highest level of ERK and AKT phosphorylation. AKT activation was stronger compared to ERK.

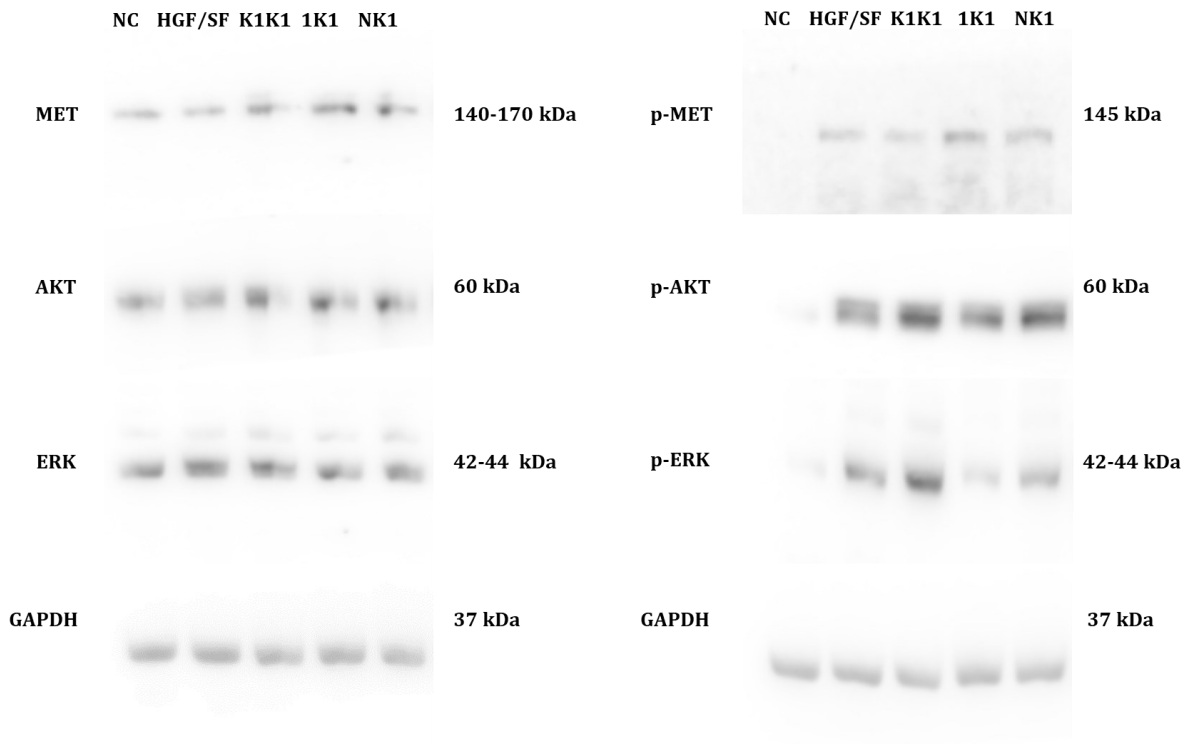

Fig. 26 Western blot images (extracts from HepG2 cells, untreated or stimulated with 10 nM HGF, K1K1, 1K1, NK1 for 10 minutes).

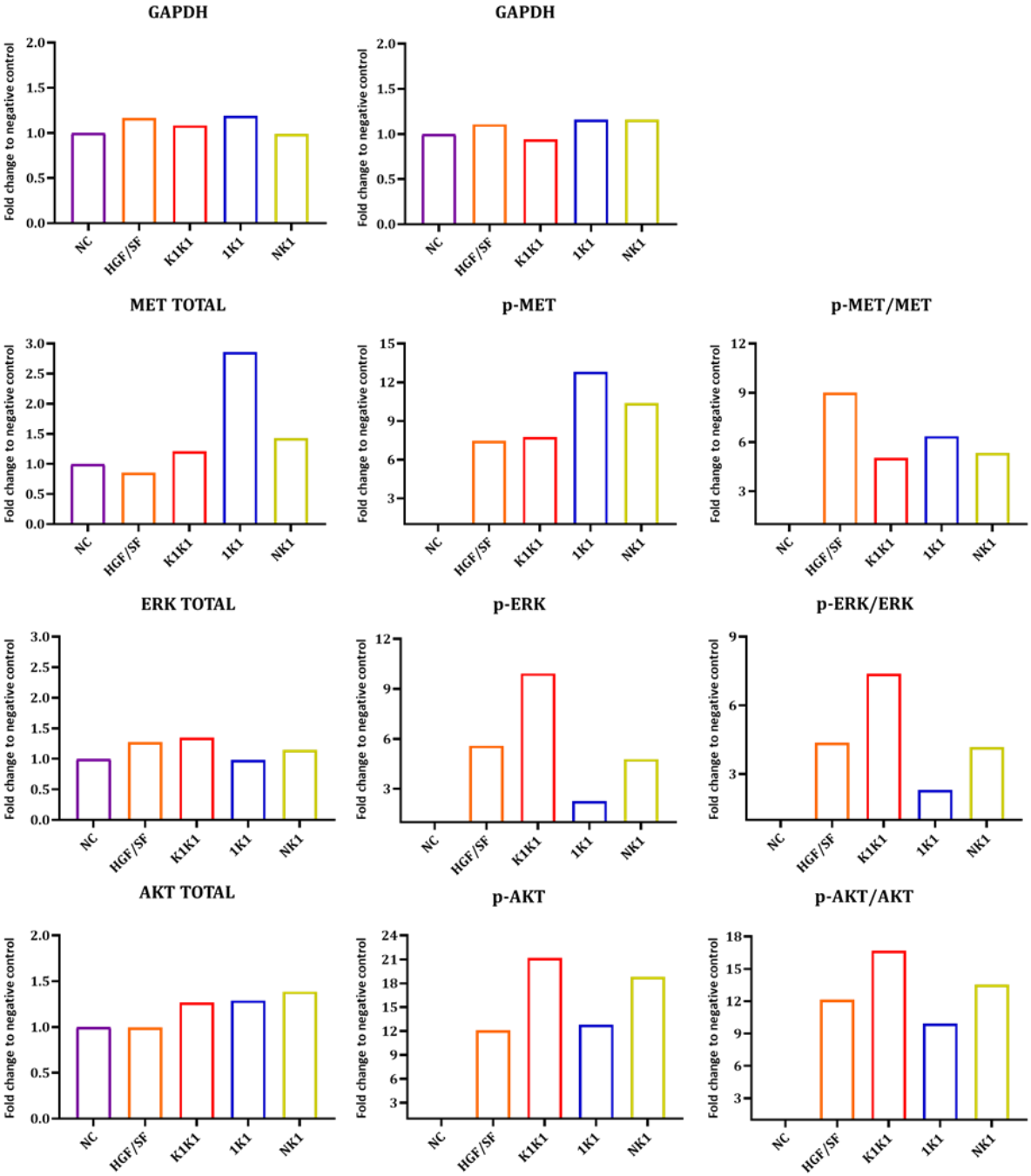

Fig. 27 Western blot analysis of extracts from HepG2 cells, untreated or stimulated with HGF, K1K1, 1K1, NK1, (10 nM for 10 minutes).

When HepG2 cells were treated with 1 nM protein concentrations, both ERK and AKT phosphorylation increased again but this time the cells treated with K1K1 showed the highest level of phosphorylation only for ERK while HGF/SF was able to induce slightly stronger phosphorylation of AKT. This time ERK activation was stronger compared to AKT (**Fig. 28-29**).

Further experiments will be needed to confirm the findings, in particular the results obtained with MET were difficult to interpret.

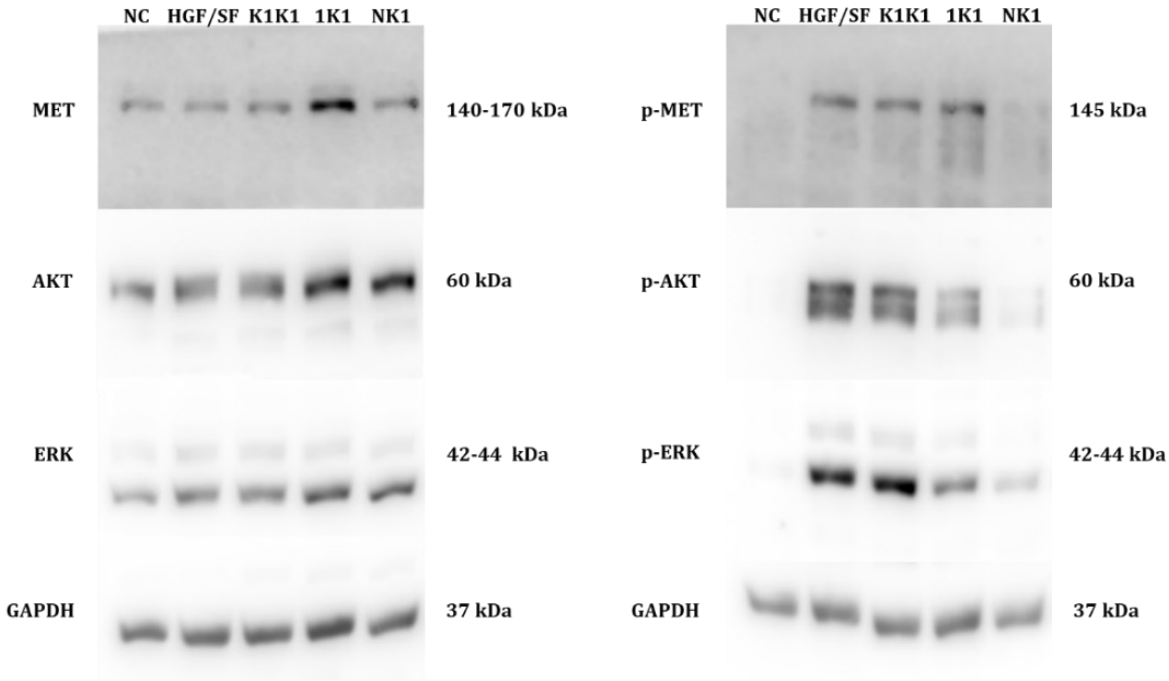

Fig. 28 Western blot images (extracts from HepG2 cells, untreated or stimulated with 1 nM HGF, K1K1, 1K1, NK1 for 10 minutes).

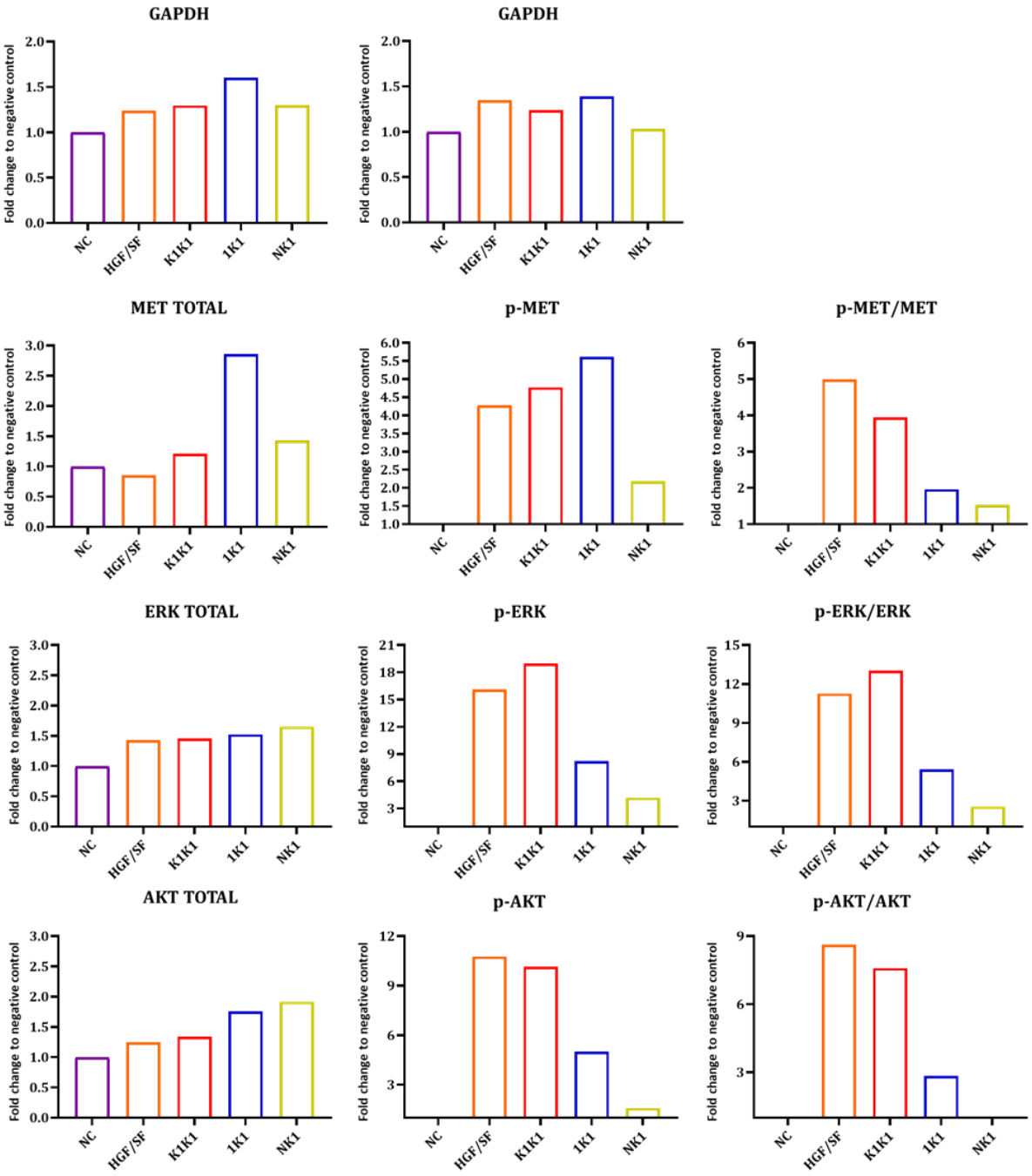

Fig. 29 Western blot analysis of extracts from HepG2 cells, untreated or stimulated with HGF, K1K1, 1K1, NK1, (1 nM for 10 minutes).

Only AML12 protein lysates treated with 10 nM protein concentrations were analyzed and GAPDH values were used for normalization.

When AML12 cells were treated, both ERK and AKT phosphorylation increased but the signals were weaker if compared with the ones registered with HepG2 cells. AKT activation was stronger compared to ERK, as shown also for HepG2 cells treated with 10 nM protein concentrations. This time the cells treated with NK1 shown the highest level of ERK and AKT phosphorylation (**Fig. 30-31**)

Unfortunately, it was not possible to detect total MET and the results obtained with p-MET were of difficult interpretation. Further experiments are therefore needed.

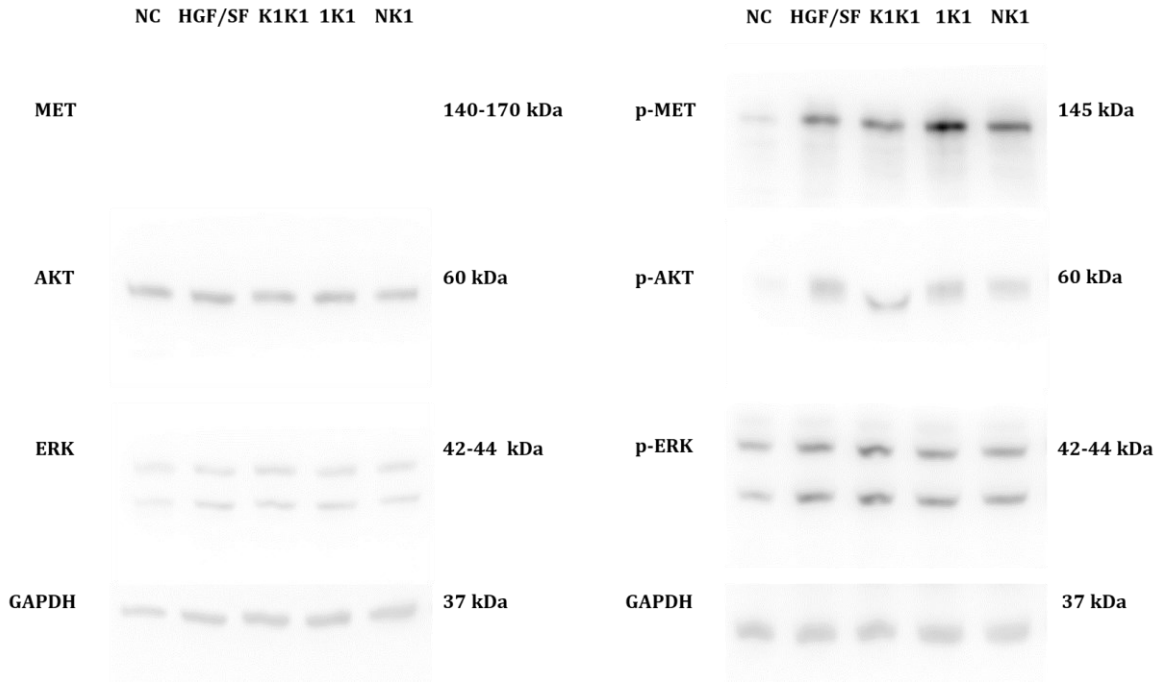

Fig. 30 Western blot images (extracts from AML12 cells, untreated or stimulated with 10 nM HGF, K1K1, 1K1, NK1 for 10 minutes).

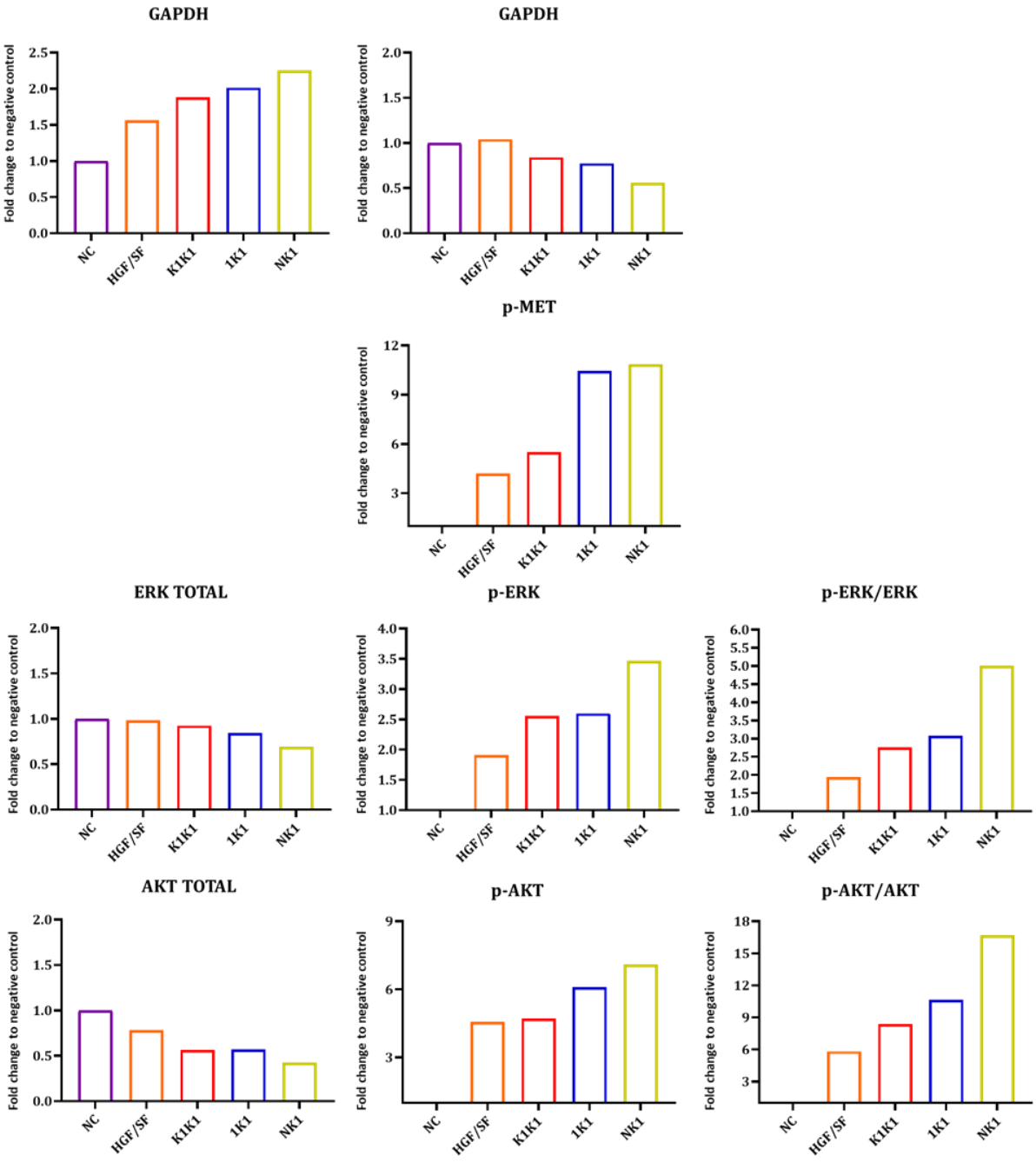

Fig. 31 Western blot analysis of extracts from AML12 cells, untreated or stimulated with HGF, K1K1, 1K1, NK1, (10 nM for 10 minutes).

HGF/SF and K1K1 labeling for *in vivo* studies

The Alexa Fluor ® 488 Microscale Protein Labeling Kit was used for protein labeling as described in the methods section.

With the first experiment 1 M sodium bicarbonate was not added to HGF/SF and K1K1. After protein labeling, HGF/SF and K1K1 concentrations were tested with SHIMADZU UV-Vis spectrometer and the equations described on the kit datasheet were used to find the labeled proteins concentration. Unfortunately, with the first experiment only 26% of HGF/SF and 17% of K1K1 was estimated to be labeled. With the second experiment, 1 M sodium bicarbonate was added to the proteins during the labeling procedure and the percentage of labeled proteins increased to 70% for HGF/SF and to 90% for K1K1. The next steps were performed to understand if the labeled proteins were fluorescent and biologically active.

Protein biological activity was evaluated with MDCK scatter assay, performed as described in the methods section. Native and weakly labeled proteins of the first experiment were compared, there was no evident loss of activity for both HGF/SF and K1K1 after labeling. Both native and labeled HGF/SF were active down to a concentration of 10^{-11} M while K1K1 was able to induce colony scattering as low as 10^{-12} M.

Native and labeled proteins of the second experiment were also compared and this time there was an evident loss of activity for K1K1 after labeling. Both native and labeled HGF/SF were active down to a concentration of 10^{-11} M. Native K1K1 was able to induce colony scattering as low as 10^{-12} M but the labeled version was less active, this protein was able to induce scattering only down to a concentration of 3×10^{-11} M.

As described before, SHIMADZU UV-Vis spectrometer was used to quantify the amount of labeling per protein but was found rather inaccurate and using too much protein. Therefore, cell uptake was used instead to test if both HGF/SF and K1K1 were fluorescent, and two five-channel microfluidic devices (model 1) with cell lines were used. The medium was removed from both channels and EBM-2 plus supplements and 10^{-6} M K1K1, or HGF/SF was added to the inlet channel. The devices were moved to a tilting platform placed inside cell incubator for 15 minutes, then washed with DPBS, incubated for 15 minutes with 4% PFA and washed again 3 times with PBS. Images were collected using fluorescence microscopy. As both proteins were labelled it was possible to detect fluorescence inside HepG2 cells (**Fig. 32**).

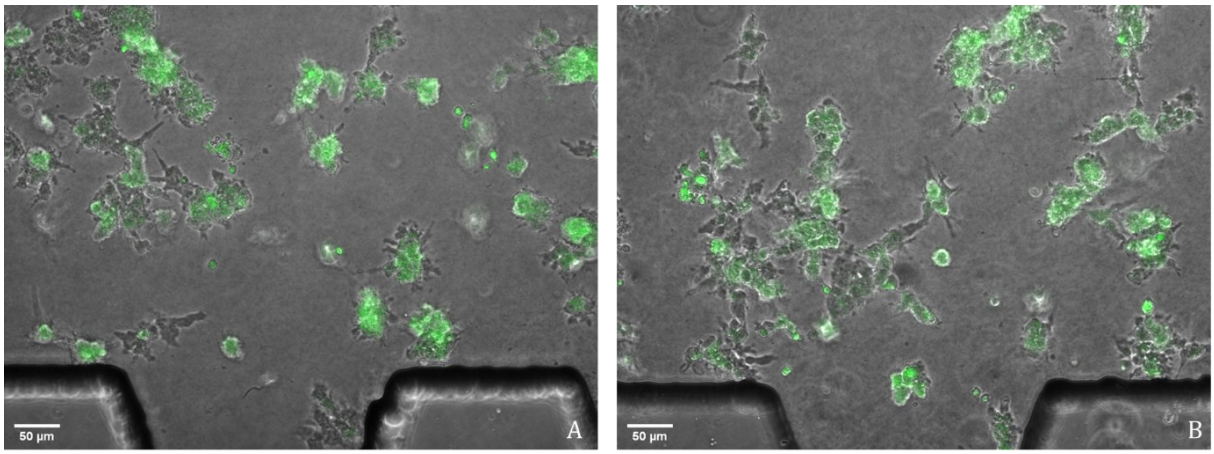

Fig. 32 Representative images showing HepG2 staining after incubation with fluorescent HGF/SF (**A**) or K1K1 (**B**) (magnification 100X).

Development of liver-on-a-chip

As described in methods section, 3 different models were used, all of them were five-channel microfluidic devices. Standard photolithography was used to prepare model 1 while for model 2 and 3 resin 3D printing was used.

Model 1 was the first to be tested with cell lines. After the first experiment it was clear HepG2 and U937 concentration needed to be increased and media composition was also changed to improve HepG2 viability. With the second experiment optimal cells concentrations were used (**Fig. 33**).

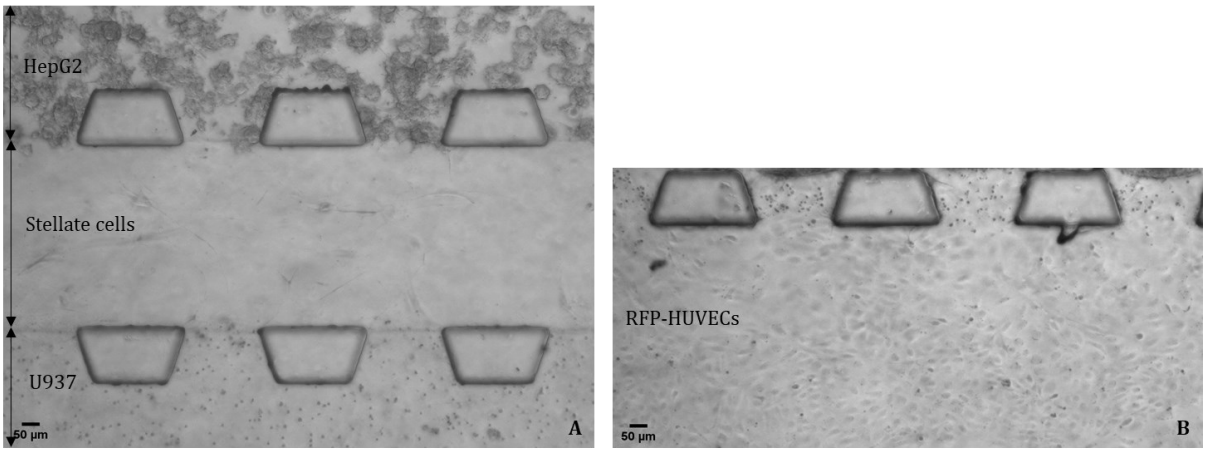

Fig. 33 Representative brightfield microscope images showing HepG2, stellate cells, U937 (**A**) and RFP-HUVECs (**B**) (magnification 40X).

In the collagen matrix U937 had a rounded structure and they expressed their characteristic CD68 protein, while stellate cells were stained positive for Vimentin and showed their characteristic branched structures. HepG2 were stained positive for cytokeratin (**Fig. 34**).

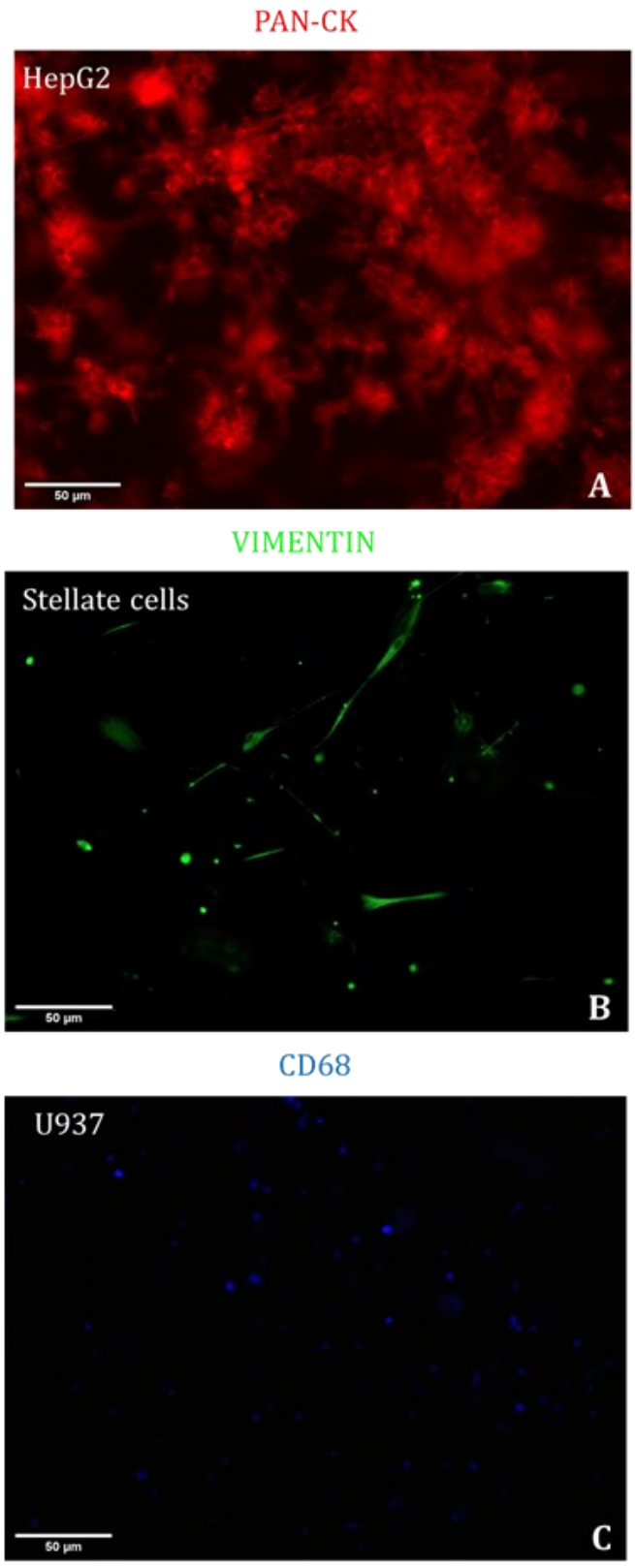

Fig. 34 Specific immunostaining of HepG2 with Alexa Fluor® 647-conjugated anti-CK-pan Ab (**A**), hepatic stellate cells with Alexa Fluor® 488-conjugated anti-vimentin Ab (**B**), U937 with Brilliant Violet 421™- conjugated anti-CD68 Ab (**C**) (magnification 200X).

Viability/cytotoxicity was evaluated 4 days after the seeding of the cells, as described in methods section. The viability (green fluorescence) was above 90% (**Fig. 35**).

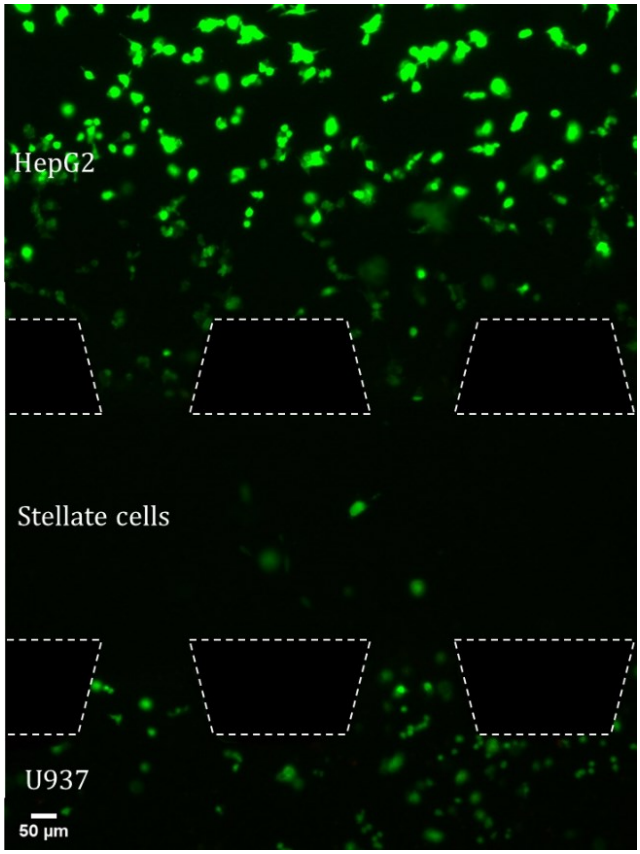

Fig. 35 Viability assay after 4 days from initial culture, model1 (magnification 40X).

Looking at the images collected, it was possible to point out a problem of this first model. The staining faded away when getting closer to the stellate channel, indicating a possible problem of diffusion between channels. The solution considered was reducing the width of the channels. Therefore 2 new models were 3D printed. Model 3 gave better results and as shown in **Fig. 36**, the diffusion problem was solved and more than 90% of the cells were viable. This 3D printed device was therefore used for the final experiment with primary cells.

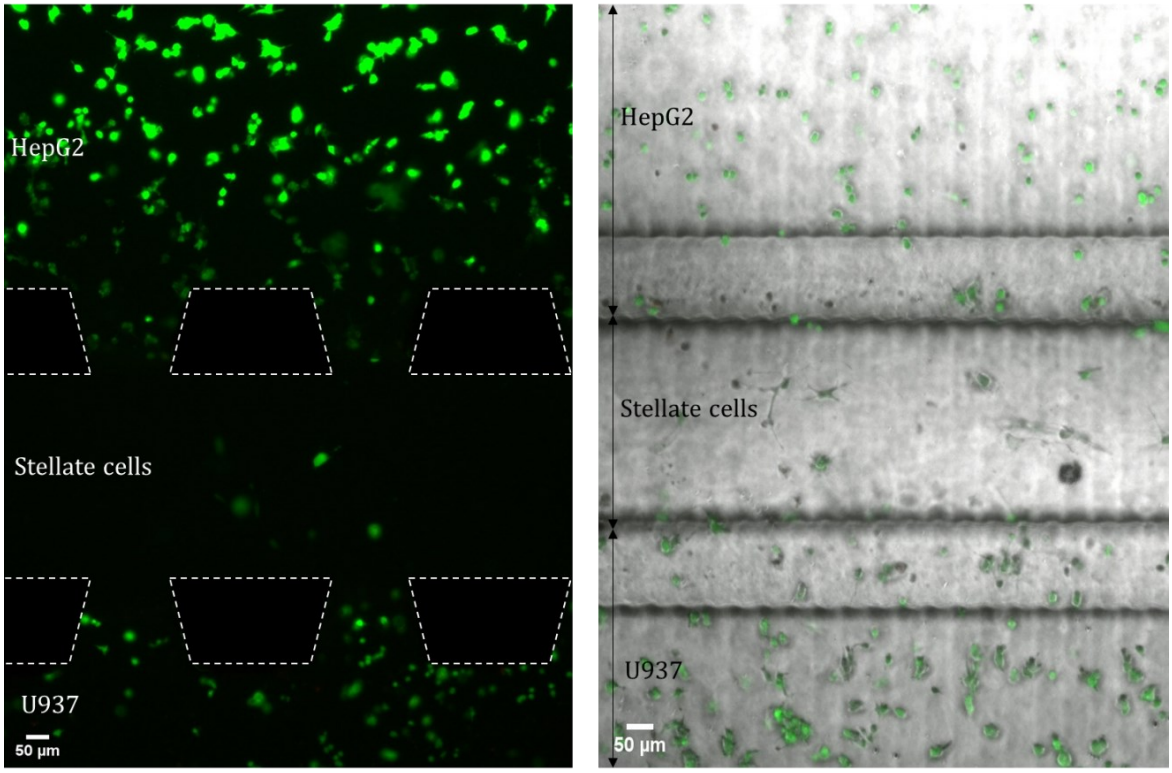

Fig. 36 Viability assay, after 4 days from initial culture. Model 1 (**left**) compared with model 3 (**right**) (magnification 40X).

Test and compare HGF/SF and K1K1 efficacy using the liver-on-a-chip

The first phase of the experiment was the construction of the liver-on-a-chip with primary cells. Initially, 120 five-channel microfluidic devices model 3 were prepared manually and seeded with cells successfully after which, viability was evaluated 3 days after seeding of the cells. The viability was above 90% (**Fig. 37**)

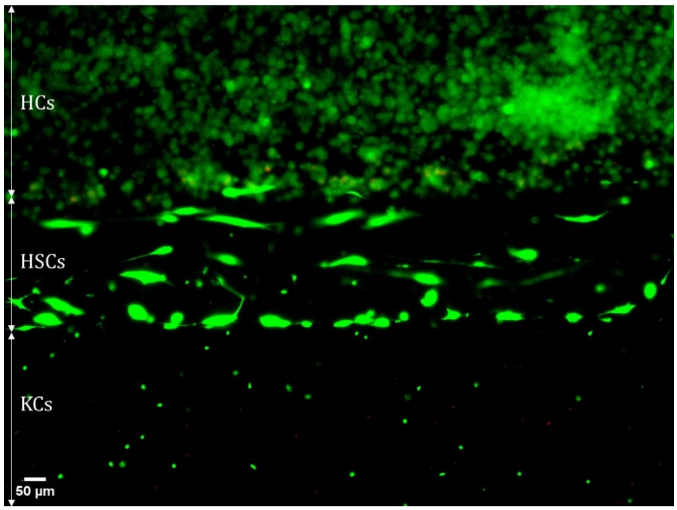

Fig. 37 Viability assay of HCs, HSCs, and KCs after 3 days of initial culture (magnification 40X).

Unfortunately, bacterial contamination was observed after a few days, and it was not possible to proceed with the second phase of the experiment. Therefore, due to the impossibility to restart the experiment with the original model, 41 3D Cell Culture Chips (Aim Biotech) were used. The seeding procedure was performed as described in the methods section and later the devices were divided in 9 groups:

1. Control (6)
2. NASH (6)
3. NASH + 0.1 µM K1K1 (5)
4. NASH + 0.01 µM K1K1(5)
5. NASH + 0.1 µM HGF/SF (4)
6. NASH + 0.1 µM K1K1 + 30 µM TAK-242 (6)
7. NASH + M-CSF/IL4 (3)
8. NASH + 30 µM TAK-242 (3)
9. NASH + 30 µM SR1078 (3)

Treatments were started simultaneously with lipotoxic stress, media was refreshed every 2 days and collected for storage at -80 °C till day 9 after NASH induction. On the same day, all the devices were also sacrificed, the medium was removed from the channels, a quick wash with DPBS was performed followed by fixation with 4% paraformaldehyde at room temperature for 15 min and 3 washes with PBS.

Then it was possible to start evaluating NASH hallmarks including lipid accumulation, cell death, inflammation, and fibrosis.

First, 2 chips for each group were used for lipid staining, following the previously described protocol. A fluorescence microscope was used to take pictures of stained oil globules within hepatocytes (**Fig. 38**).

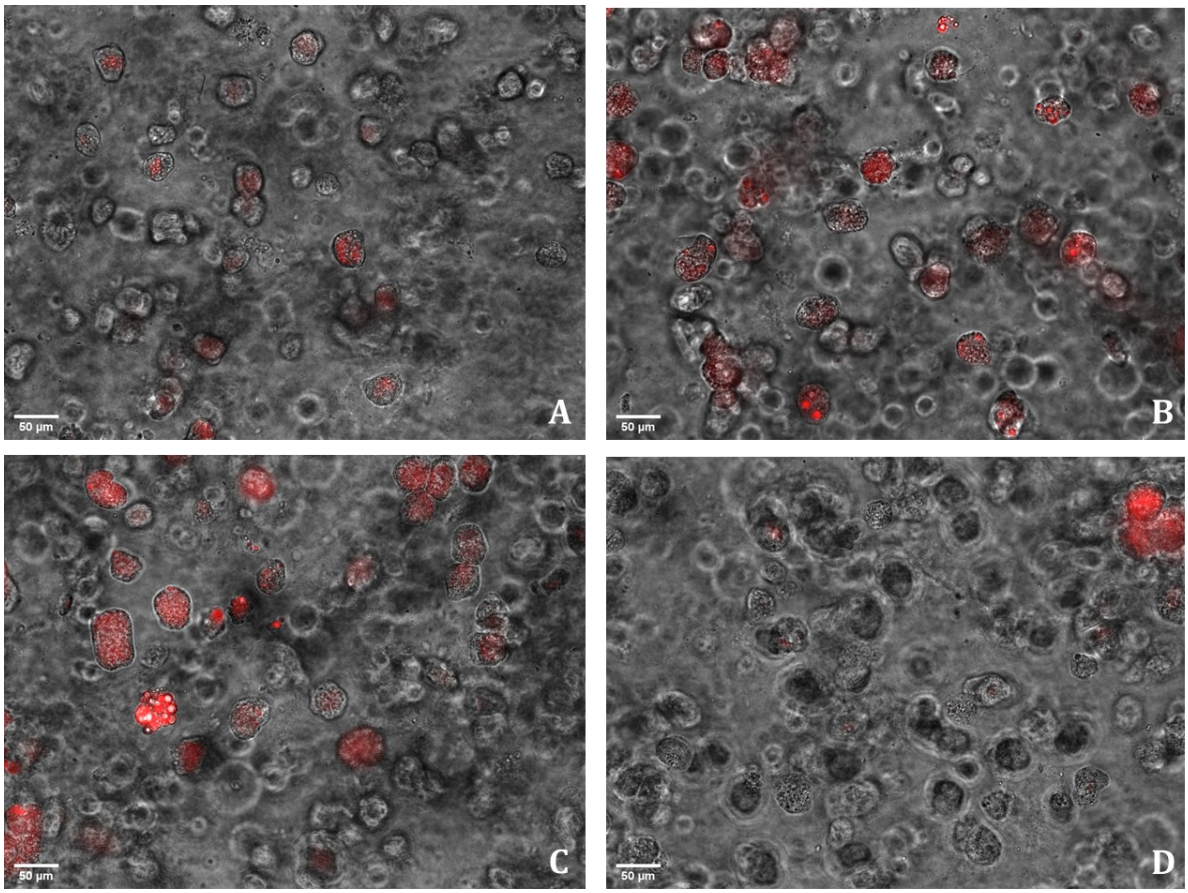

Fig. 38 Representative images of lipid accumulation in HCs of control (**A**), NASH (**B**), NASH+K1K1 (High) (**C**) and NASH+K1K1+TAK-242 (**D**) groups after 9 days of disease induction (magnification 100X).

ImageJ software analysis was used to quantify red fluorescence intensity and statistical analysis was performed with GraphPad (**Fig 39**).

After 9 days of treatment with a high concentration of FFA, there was a significant accumulation of lipids inside HCs of the NASH group compared to the control (~3-fold, P<0.0001), indicating steatosis development (**Fig. 39**). A significative different lipid accumulation was also found when NASH group was compared with groups where drugs were applied, as shown in detail in **Fig. 39.** The treatments with K1K1+TAK-242, HGF/SF, TAK-242 and SR1078 seemed to be the most effective (P<0.0001).

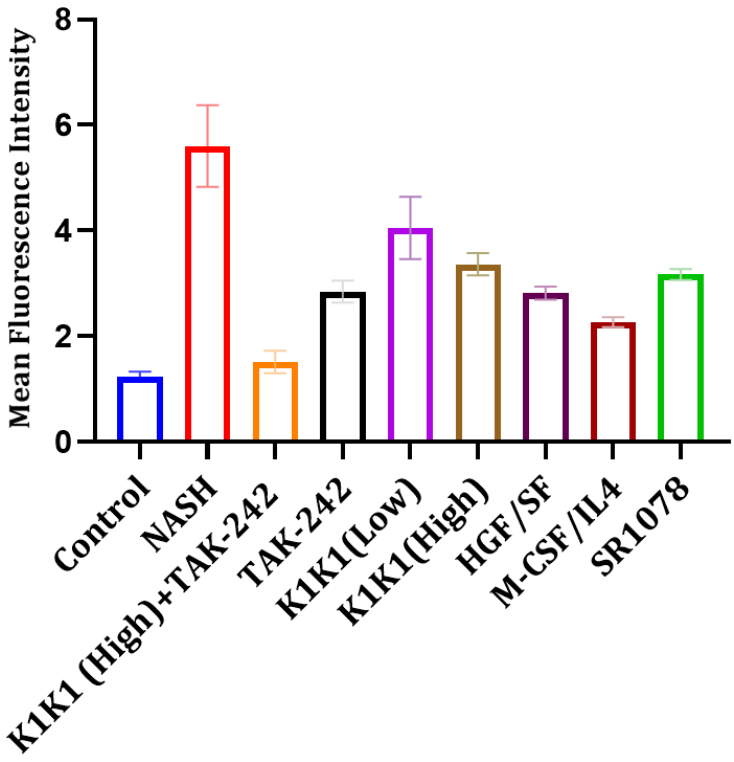

Bonferroni's multiple comparisons test	Summary	Adjusted P Value
Control vs. NASH	****	<0,0001
Control vs. HGF/SF	*	0.0414
Control vs. TAK-242	*	0.0332
Control vs. K1K1(Low)	****	<0,0001
Control vs. K1K1(High)	***	0.0006
Control vs. SR1078	**	0.0029
NASH vs. K1K1 (High)+TAK-242	****	<0,0001
NASH vs. HGF/SF	****	<0,0001
NASH vs. M-CSF/IL4	****	<0,0001
NASH vs. TAK-242	****	<0,0001
NASH vs. K1K1(High)	***	0.0004
NASH vs. SR1078	****	<0,0001
K1K1 (High)+TAK-242 vs. K1K1(Low)	****	<0,0001
K1K1 (High)+TAK-242 vs. K1K1(High)	**	0.0077
K1K1 (High)+TAK-242 vs. SR1078	*	0.0312
M-CSF/IL4 vs. K1K1(Low)	**	0.0089

Fig. 39 Mean fluorescence intensity of neutral lipid staining of HCs quantified and plotted after 9 days of disease induction. Significance was calculated using Bonferroni's multiple comparison test. Each value represents the mean ± SEM (*n*=10 per group).

The second step was to evaluate liver cell apoptosis with cleaved caspase-3 staining. Considering the limited number of devices, only five groups of major interest were used. Cleaved Caspase-3 (Asp175) Antibody Alexa Fluor® 488 Conjugate (green) was used together with Hoechst solution (blue) as described in methods. Pictures were collected with a fluorescence microscope (**Fig. 40**).

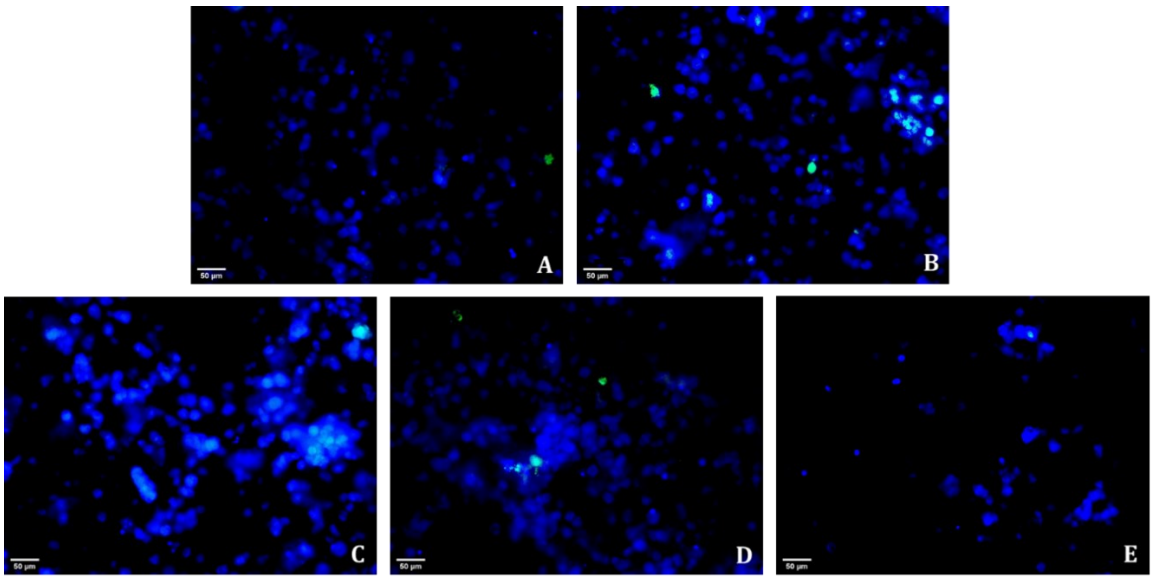

Fig. 40 Representative cleaved caspase-3 staining images of control (**A**), NASH (**B**), NASH+K1K1 (High) (**C**), NASH+TAK-242 (**D**), NASH+K1K1+TAK-242 (**E**) groups after 9 days of disease induction (magnification 100X).

After 9 days of lipotoxic treatment, there was a significant increase of apoptotic cells in the NASH group compared to the control (~3-fold, P<0.0001), indicating the onset of liver injury (**Fig. 41**). A significative difference was also found when NASH group was compared with NASH+K1K1+TAK-242 group (P=0.0021), as shown in detail in **Fig. 41.**

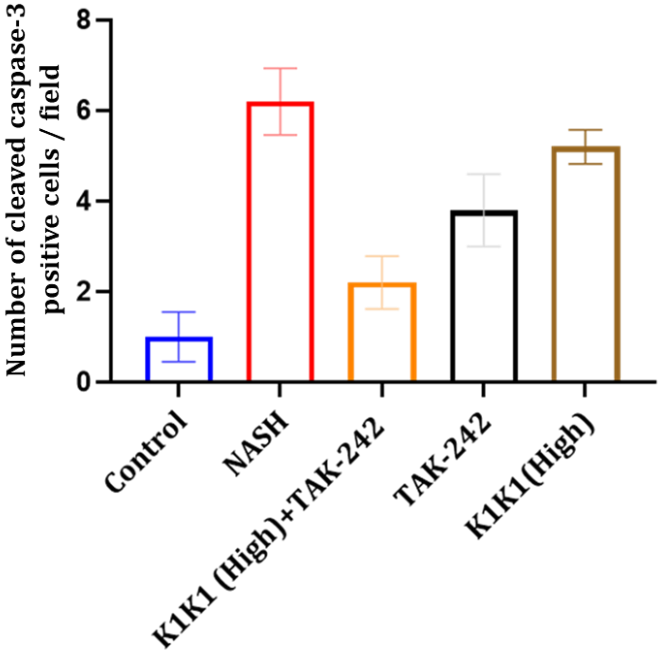

Bonferroni's multiple comparisons test	Summary	Adjusted P Value
Control vs. NASH	****	<0,0001
Control vs. TAK-242	*	0.049
Control vs. K1K1(High)	**	0.0012
NASH vs. K1K1 (High)+TAK-242	**	0.0021
K1K1 (High)+TAK-242 vs. K1K1(High)	*	0.0292

Fig. 41 Number of cleaved caspase-3 positive cells after 9 days of disease induction. Significance was calculated using Bonferroni's multiple comparison test. Each value represents the mean ± SEM (*n*=5 per group).

The third step was to evaluate liver fibrosis, focusing on HSCs which are the main contributors. Increased expression of α-Smooth Muscle Actin (α-SMA) represents a useful marker of HSCs activation and differentiation into myofibroblasts-like cells during NASH progression.

Alpha-SMA(1A4) Antibody Alexa Fluor® 488 Conjugate (green) was used together with Hoechst solution (blue) as described in methods section. Pictures were collected with a fluorescence microscope (**Fig. 42**).

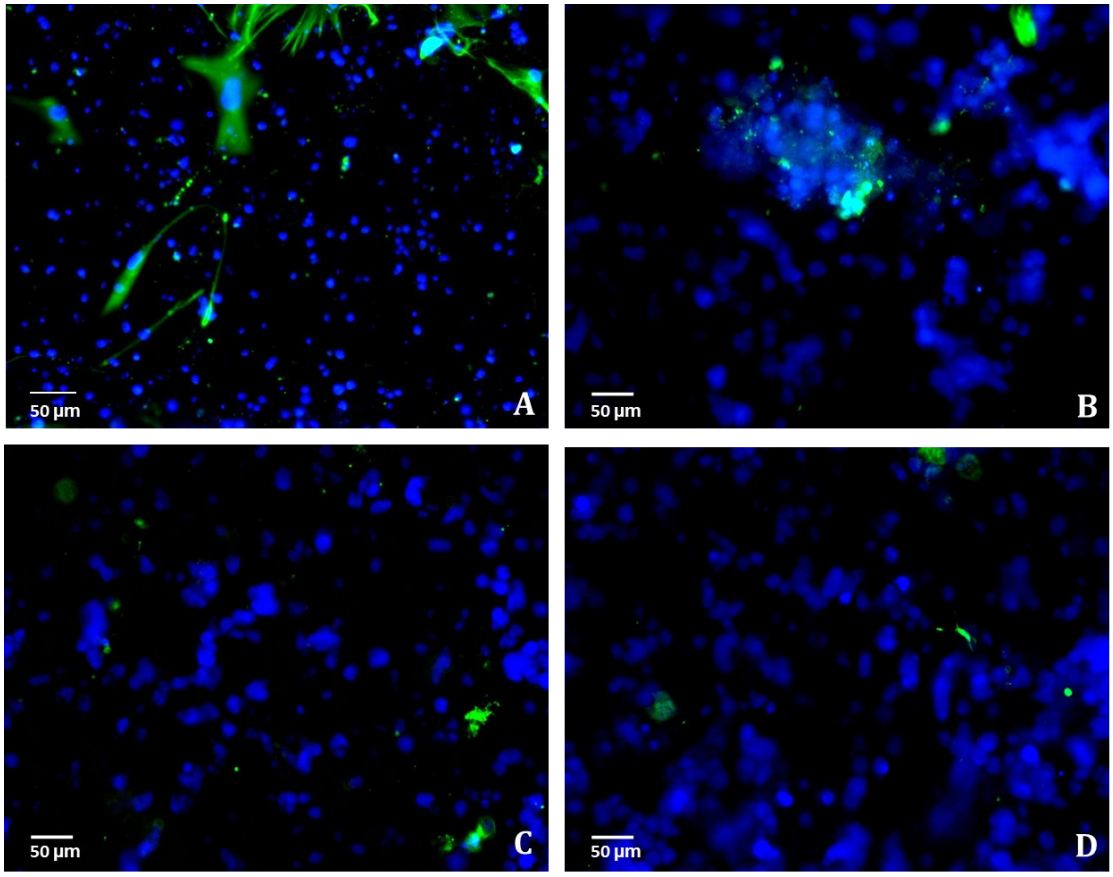

Fig. 42 Representative α-SMA staining images of NASH (**A**), NASH+K1K1 (High) (**B**), NASH+TAK-242 (**C**), and NASH+K1K1+TAK-242 (**D**) groups after 9 days of disease induction (magnification 100X).

Under NASH conditions, HSCs expressed a significant higher level of α-SMA compared to the control group (P<0.0001) (**Fig. 43**).

Significative different expression was also found when NASH group was compared with groups where drugs were applied, as shown in detail in **Fig. 43.** The treatment with K1K1+TAK-242 seemed to be the most effective (P<0.0001) followed by HGF/SF (P=0.0008), TAK-242 (P=0.0015), and K1K1 (Low) (P=0.0044).

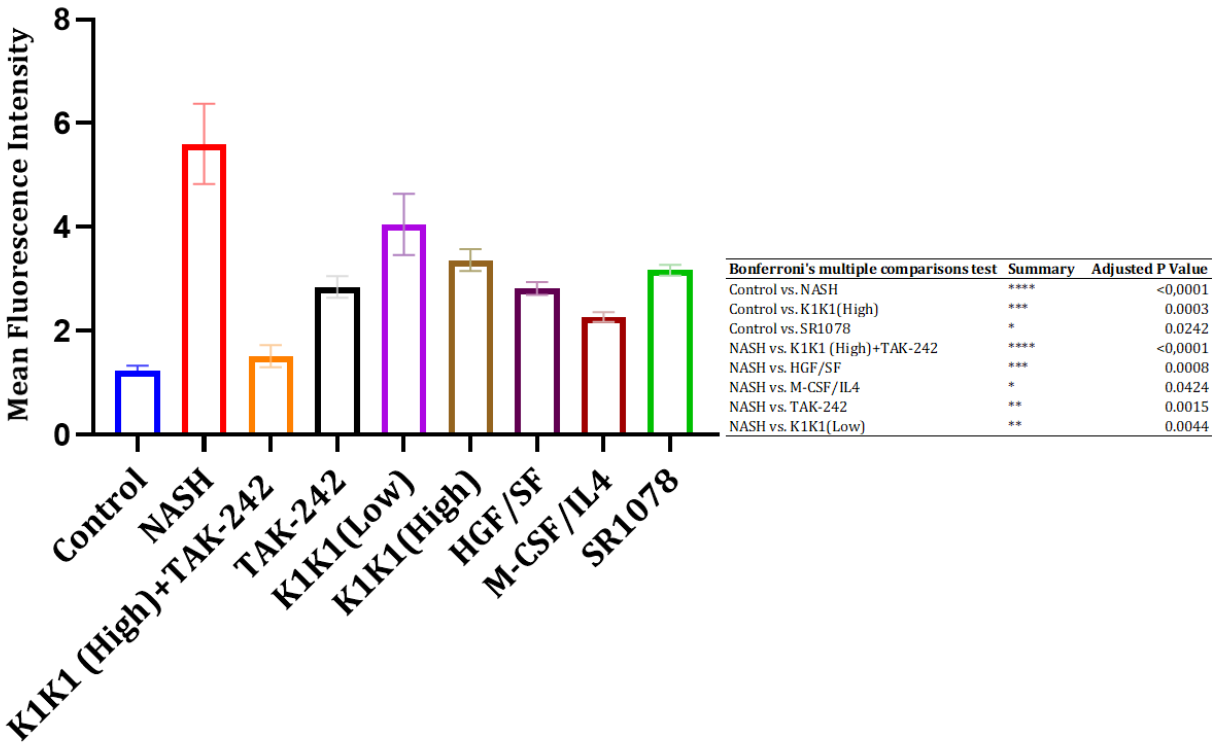

Bonferroni's multiple comparisons test	Summary	Adjusted P Value
Control vs. NASH	****	<0,0001
Control vs. K1K1(High)	***	0.0003
Control vs. SR1078	*	0.0242
NASH vs. K1K1 (High)+TAK-242	****	<0,0001
NASH vs. HGF/SF	***	0.0008
NASH vs. M-CSF/IL4	*	0.0424
NASH vs. TAK-242	**	0.0015
NASH vs. K1K1(Low)	**	0.0044

Fig. 43 Mean fluorescence intensity of α-SMA staining of HSCs quantified and plotted after 9 days of disease induction. Significance was calculated using Bonferroni's multiple comparison test. Each value represents the mean ± SEM (*n*=5 per group).

Finally, inflammatory (TNF-α) and profibrotic biomarkers (TGF-β) were also evaluated using media effluents collected from the devices. Unfortunately, all TGF-β values obtained were below the limit of detection of the kit. For TNF-α, the values obtained were detectable and triplicates were used for each group, but the values obtained were very discordant as shown in **Fig. 44** and none were significant. Unfortunately, this was the last ELISA assay performed and there was no material left to repeat the analysis.

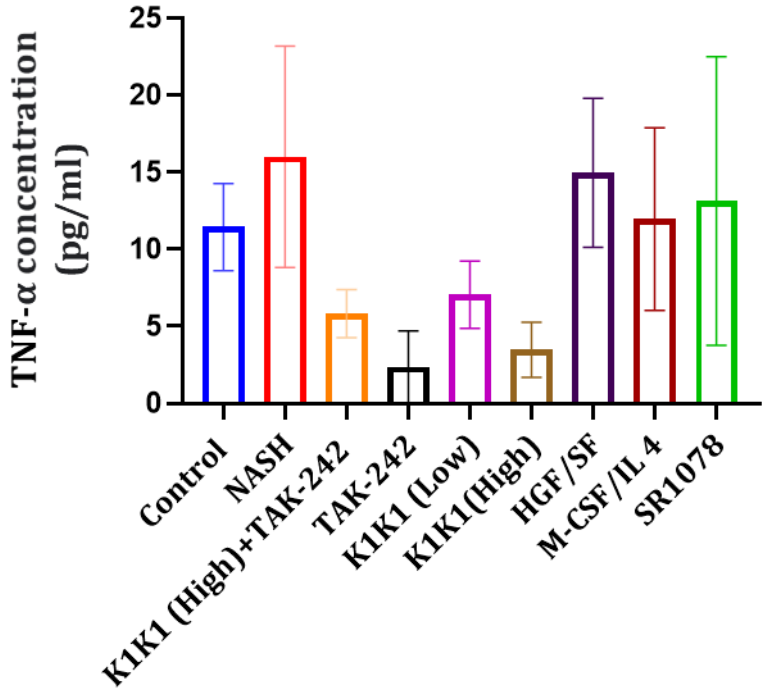

Fig. 44 Concentration levels of TNF-α quantified and plotted after 9 days of disease induction. Significance was calculated using Bonferroni's multiple comparison test.

Discussion

Large-scale production of 1K1, K1K1, and HGF/SF proteins was the first necessary step to start the experiments. Well known and standardized protocol were used [18 25 34]. 1K1 was produced in yeast using transformed GS115 *P. pastoris* cells and its expression and purification was particularly efficient as the protein was secreted in the medium. Also, the yield was the highest of all the protein produced with an average of 5 mg/L. K1K1 was produced in *E. coli* strain *BL21(DE3),* another expression system with a good potential for scaling up. This time the protein was not secreted, but it was stored inside so-called inclusion bodies, requiring a more complex and long extraction procedure compared to 1K1. The protein yield was like the one obtained with 1K1 expression, with an average of 4-5 mg/L but more time was needed to extract the protein from bacterial pellets, and it was only possible to process the pellet originated from 2 L of culture at a time due to requirements to mechanically resuspend and wash the pellet of insoluble material (i.e. the inclusion bodies).

HGF/SF was produced in NS0 myeloma cells. The protein was secreted in the medium, but as expected for large and complex proteins expressed in mammalian expression systems, the protein yield was much lower with an average of 0.1-0.2 mg/L.

1K1 was mainly used for the experiments where proteins stability was compared to HGF/SF and K1K1. The latter two were also used for experiments requiring a labeling procedure.

MET567 was needed for protein crystallography and was expressed in CHO lec 3.2.8.1 cells with also low expression levels needing large volumes of medium (up to 50 liters) to obtain sufficient quantities. I performed protein crystallography using both K1K1 and MET567 to form complexes with different forms of purified heparin. Many attempts were made to obtain good quality crystals of the K1K1/MET567/heparin complex but unfortunately, X-ray diffraction data were poor, and these experiments and results were left out of the thesis.

HGF/SF availability was the limiting factor for most of the experiment because protein yield was very low, it took many weeks to collect enough liters of culture and the growing medium was expensive.

After this first phase of protein production of 6 months, it was possible to start the experiments. As a first goal, we wanted to compare the proteins stability with two different methods, using SDS-PAGE gel and thermal shift assay. We started the experiment

with HGF/SF, 1K1 and K1K1 at a concentration of ten micromolar (10^{-5} M) incubated at 37 °C for 3 weeks. Samples were collected weekly and loaded on a SDS-PAGE gel under reducing conditions.

K1K1 and 1K1 bands were still visible and well defined after 3 weeks of incubation at 37 °C while the HGF/SF bands, in particular the α-chain, seemed to fade after 2 to 3 weeks (**Fig. 17**). This first impression was further confirmed with a western blot performed on HGF/SF samples (**Fig. 18**). After this first evaluation, it seemed HGF/SF was less stable and prone to degradation over time as previously reported [18] [19] but using thermal shift assay, we had different results. Tycho NT.6 was used to measure changes in brightness of aromatic amino acid residues at 330 nm and 350 nm during thermal unfolding. The brightness signals were reported as 350 nm/330 nm ratio and used to calculate the inflection temperature (Ti). Loss or shift of Ti or decrease in Δ ratio with this assay are signals of increased destabilization and unfolding but with this experiment, no observable shift of the Ti or decrease in Δ ratio was reported for the 3 proteins over time Brightness values were also stable for all the proteins during the 3 weeks of incubation (**Fig. 19**). As these results conflicted with the differences in stability observed on gel a further assay was performed.

Protein biological activity was evaluated with MDCK scatter assay, showing there was no evident loss of activity for all the proteins during the 3 weeks of incubation, HGF/SF was active down to a concentration of 3×10^{-12} M while K1K1 was able to induce colony scattering as low as 10^{-12} M. Overall, 1K1 was less active than HGF/SF and K1K1 and the treatment with this protein was able to induce scattering only down to a concentration of 3×10^{-11} M (**Fig. 20**).

Considering the different results obtained using SDS-PAGE gel and thermal shift assay it should be worth repeating the experiment including also thermally unfolded proteins as controls. Another good suggestion could be the use of a third method to evaluate protein stability. Unfortunately, circular dichroism very much depends on structural features such as alpha helixes and beta sheets and none of these are present in K1K1, therefore it is not possible to obtain a nice unfolding pattern. This was confirmed by earlier CD experiments. Instead, fluorescence spectroscopy might be a good option to evaluate protein stability, indeed the use of this technique has some advantages such as high sensitivity, short measurement time, and the relative simplicity of the analysis of the data [62]. The Tycho NT.6 thermal shift assay is a related technique in which the tryptophan fluorescence intensities ratio at 330 nm and 350 nm allows evaluation of unfolding

transitions in proteins. Unfortunately, under certain conditions, the use of this parameter for the analysis of unfolding transitions is not accurate and can leads to the incorrect determination of thermodynamic parameters. Therefore, caution should be used to interpret these results [62].

The last observation concerning this experiment is about the MDCK scatter assay used to evaluate the proteins biological activity. From the results it was clear all the proteins were still active even after 3 weeks of incubation even if we expected a decreased activity of HGF/SF. It should be note than all the protein were incubated at 37 °C in sterile PBS so the experiment conditions are different from what it can be expected *in vivo* where the environment is more complex than the one inside a tube. For example, proteases are present, and they can contribute to protein degradation.

A further *in vitro* characterization and comparison among K1K1 and HGF/SF, 1K1, NK1 was performed evaluating the activation of the MET receptor and the downstream proteins. Briefly, HGF/SF binds to its receptor MET causing its phosphorylation and subsequently, intracellular signaling pathways are activated such as the MAPK and the PI3K–AKT pathways [8 11]. Here the activity of MET and of the downstream protein kinases ERK and AKT was assessed by their phosphorylation status using western blot. Considering our interest in using K1K1 as a treatment for NASH, two commonly used liver cell lines were chosen to study the activation of MET and of the downstream pathways *in vitro*: HepG2 and AML12.

HepG2 were seeded in the evening with 30-40% confluence in 6 well plates. The day after the medium was removed and the HepG2 were first starved for 3 hours with a medium without FBS and later stimulated for 10 minutes with HGF/SF, K1K1, 1K1, NK1 at 3 different concentrations (0.1 nM, 1 nM, and 10 nM). Only HepG2 protein lysates treated with 10 nM and 1 nM protein concentrations were analyzed and GAPDH values were used for normalization.

When HepG2 cells were treated with 1 and 10 nM protein concentrations, both MET, ERK, and AKT phosphorylation increased compared to the control (**Fig. 27-29**). There was a problem with the detection of total MET which needs to be addressed with further experiments.

MET signaling increased when cells were treated with 10 nM or 1nM protein concentrations and in both cases, the treatment with 1K1 gave the highest level of MET phosphorylation (~12.8-fold with 10 nM and ~5.6 with 1 nM). The cells treated with 10 nM of HGF/SF or K1K1 showed nearly the same levels of MET phosphorylation (~7.4-fold

vs ~7.8-fold) and the values were also similar when 1nM protein concentration was used (~4.2-fold vs ~4.7-fold). The treatment with NK1 gave the second-highest level of MET phosphorylation when cells were treated with 10 nM protein concentrations (~10.4-fold) while when they were treated with 1 nM the level of MET phosphorylation was the lowest (~2.2-fold) (**Fig. 27-29**).

Interestingly, ERK signaling increased more when cells were treated with 1nM instead of 10 nM protein concentrations and in both cases the treatment with K1K1 gave the highest level of ERK phosphorylation (~9.9-fold with 10 nM and ~19 with 1 nM). The treatment with HGF/SF gave the second-highest level of ERK phosphorylation (~5.6-fold with 10 nM and ~16.1 with 1 nM) (**Fig. 27-29**).

Finally, AKT signaling was more pronounced when cells were treated with 10 nM instead of 1 nM protein concentrations. The treatment with K1K1 gave the highest level of AKT phosphorylation when cells were treated with 10 nM protein concentrations (~21.5-fold) while when HepG2 cells were treated with 1 nM protein concentrations, HGF/SF was able to induce slightly stronger phosphorylation of AKT compared to K1K1 (~10.7-fold vs ~10.2-fold) (**Fig. 27-29**).

In conclusion, HGF/SF and K1K1 seem to be the most potent agonist being able to induce the highest level of AKT and ERK phosphorylation when the HepG2 cells were treated with 1nM protein concentrations. When cells were treated with higher protein concentrations AKT and ERK phosphorylation were more similar among all the treatments.

AML12 cell line were also used with the same purpose of HepG2 but a different protocol was followed for the preparation of the experiment. The original media was removed and changed for 24 hours with one lacking insulin, transferrin, sodium selenite supplements (ITS). After this first incubation, the media was removed and a second one without both FBS and ITS was used for 3-hour starvation. Later AML12 were stimulated for 10 minutes with HGF/SF, K1K1, 1K1, NK1 at 3 different concentrations (0.1 nM, 1 nM, and 10 nM).

Only AML12 protein lysates treated with 10 nM protein concentrations were analyzed.

When AML12 cells were treated, both ERK and AKT phosphorylation increased but the intensity of the signals compared to the control were weaker when confronted with the ones registered with the HepG2 cells treated with the same protein concentrations. Instead, the intensity of MET phosphorylation signal compared to the control was similar to the one registered with HepG2 cells. AKT activation was stronger compared to ERK, as shown also for HepG2 cells treated with 10 nM protein concentrations. Again, the cells

treated with 10 nM of HGF/SF or K1K1 showed nearly the same levels of MET phosphorylation (~4.2-fold vs ~5.4-fold) and, as shown for HepG2, 1K1 and NK1 were more effective in inducing MET phosphorylation (~10.4-fold and ~10.8-fold) (**Fig. 31**).
This time the cells treated with NK1 showed the highest level of ERK phosphorylation (~3.4-fold), followed very close by the ones treated with 1K1, K1K1 and HGF/SF (~2.6-fold, ~2.5-fold and ~1.9-fold). The same situation was observed for AKT, the cells treated with NK1 showed the highest level of AKT phosphorylation (~7.1-fold), followed very close by the ones treated with 1K1, K1K1 and HGF/SF (~6.1-fold, ~4.7-fold and ~4.6-fold) (**Fig. 31**).
Unfortunately, it was not possible to analyze the cell pellets treated with 1 nM protein concentrations and it would have been interesting to observe if even with AML12, HGF/SF and K1K1 would have been the most potent agonist being able to induce the highest level of AKT and ERK phosphorylation.
Considering the 7-antibodies panel and the limited amount of cell lysates it was not possible to repeat these experiments twice. Therefore, it will be necessary to repeat them to confirm the results, allowing statistical analysis. In Simonneau et al. (Simonneau et al., 2015) MET and downstream signaling activation, after cell stimulation with different MET agonists, were determined. The results of this study showed that different agonists have different signaling activation kinetics [33]. Therefore, it will be interesting to study MET and the kinetics of downstream signaling activation using different MET receptor agonists also in liver-related cell lines. This could lead to a better understanding of our preliminary findings with HepG2 and AML12 cell lines.
After assessing K1K1 stability and its potency in inducing the activation of the MET receptor and of the downstream proteins AKT and ERK in liver-related cell lines, it was necessary to understand if the MET receptor was also present on the target cells in patients, in this case the hepatocytes in patients diagnosed with NAFLD. Therefore, in collaboration with the Unit of Pathology of "Maggiore della Carità" Hospital in Novara, a study on 34 liver biopsies of patients with steatosis or NASH diagnosis has been set up. These 34 cases were part of a more extended database with 41 cases, previously used for another interesting publication on NAFLD [63]. Seven cases did not have adequate biopsy tissue, so they were not included in this preliminary study. The samples were collected at the time of the first diagnosis, and this can partially explain why cases with high grades were less represented.

Six biopsies of normal liver were also included, and two samples of colorectal adenocarcinoma were also used as positive controls. The number of controls was limited because they were strictly selected. Indeed, only those patients without HBV, HCV, HIV, liver cirrhosis or fibrosis, massive steatosis, and liver cancer diagnoses were included. Therefore, normal livers were effectively healthy livers and not histologically normal liver close to a tumour.

The NASH clinical research network (CRN) system was selected for case classification and a composite grade, the NAFLD activity score (NAS) was used as an indication of the severity of the disease. NAS is the unweight sum of steatosis (0-3), lobular inflammation (0-3), and hepatocellular ballooning scores (0-2). Biopsies with NAS ≥5 correlate with a diagnosis of NASH, while biopsies with NAS less than 3 were diagnosed as "not NASH" [60]. Fibrosis was considered separate as the representative for the stage of NAFLD (0-4) [60].

Despite trying different dilutions, incubation times, and different antigen retrieval, all the protocols used to test the two homemade monoclonal antibodies LIF 40-41 and LIF 39-58 failed. These antibodies were previously used with success for other experiments using different methods such as ELISA and western blot but unfortunately, they did not work on FFPE tissues.

A commercial anti-MET antibody was therefore used and after protocol optimization with colorectal carcinoma samples, 5 biopsies of normal liver and 30 liver biopsies of cases were stained. When present, a weak-moderate MET expression was detected in the membrane of the hepatocytes. MET expression in hepatocytes has already been reported in multiple papers, in which the staining was localized within the cytoplasm or the membrane of the hepatocytes, according to the antibody used [64 65].

We mainly focused our attention on hepatocytes, which occupy 78-80% of the liver volume, because this study was performed on liver biopsies that have an extremely low amount of material. The other cells were poorly represented and furthermore, biopsy tissue is compressed due to the harvesting and handling procedures. These alterations make the distinction between different cell populations other than hepatocytes challenging, especially if only haematoxylin-eosin stained slides can be evaluated.

Haematoxylin-eosin stained slides and IHC slides were examined by a pathologist who evaluated IHC staining using a semiquantitative system for both the staining intensity and the percentage of positive cells (i.e. staining extension). The staining intensity was scored as follows: no staining (score = 0), weak staining (score =1), moderate staining (score = 2) and intense staining (score = 3). The staining extent was scored as 0 (<1%), 1 (1-25%),

2 (26-50%), 3 (51-74%), and 4 (≥75%). Statistical analysis was performed, where the variables of interest (MET intensity and MET extension) were scored as previously indicated or transformed into two new variables to minimize the degree of data dispersion, and to try to increase the precision of the estimates. Specifically, the two new variables were created as follows:

- MET intensity (MET-Int01) in which, based on the degree of intensity, code 1 was assigned in the presence of any positive staining of this protein, code 0 otherwise.
- MET extension (MET-Ext01) in which code 1 was assigned in the presence of staining in ≥1% of the cells, code 0 otherwise.

When MET staining intensity and MET staining extension were considered as dichotomized expression variables, interesting findings came out. Indeed, there was a possible association between MET intensity or MET extension and groups belonging (exact Fisher's test = 0.019) because there was a difference in the frequency of positivity between the cases and the controls, respectively equal to 60% and 0% (**Tables 11-12**).

Furthermore, when subjects were divided in subgroups according to disease severity (0 = no pathology; 1 = mild or borderline disease, NAS ≥1 and <5; 2 = severe disease, NAS ≥5) and the relation with MET staining intensity or extension was considered, it was found that MET staining was present in 63% of the subjects with mild or borderline disease and in 54% of the subjects with severe disease while all the subjects with no pathology had absent MET staining (**Tables 13-14**). Therefore, there may be a difference in the intensity or extension of MET protein staining in relation to the severity of the disease, with the significance at the limit of acceptability (exact Fisher's test = 0.05) (**Tables 13-14**).

This was a preliminary study to evaluate MET expression in patients with NAFLD. Unfortunately, the power of the study was not adequate, and the estimate may therefore be biased. Anyway, there are some interesting aspects to highlight. First, even if we had a low number of cases and controls, the number of samples tested was greatly superior if compared to the only other paper where MET expression was evaluated in just 4 NASH samples [47]. Second, a positive aspect of this study was the use of normal liver as the controls. Only a few studies included normal livers [66 67] while most of the time controls were not used or histologically normal liver tissues close to a lesion were chosen [47 65]. Indeed, using normal liver can avoid bias of evaluation but the possibility to find samples of normal liver in patients who underwent liver biopsy is rare. Biopsies are not part of a screening routine, the procedure is invasive and therefore it is performed only if

pathology is suspected. Third, it was interesting to notice that MET expression was upregulated in patients with NAFLD compared to the controls. This is a piece of important evidence because it means the target of our protein, MET receptor, is expressed and therefore these patients can be eligible for the treatment with a MET agonist such as K1K1.

The first goal of our study on liver biopsies of patients with NAFLD was the evaluation of MET expression but considering the availability of these precious samples, we set up a more ambitious goal, evaluating HGF/SF expression, notoriously difficult to detect using IHC. HGF/SF expression was also evaluated in controls and cases and we hypothesized that with the progression of the disease there could be a reduced production of HGF/SF for which we wanted to score the expression within Kupffer cells, the ones who produce the protein within the liver tissue [61 68].

We knew this evaluation could have been challenging because of the limits of using liver biopsies, as described before, and also because in other studies IHC detection has been shown difficult , and only HGF/SF mRNA was detected in Kupffer cells, not HGF/SF protein [64]. Anyway, we proceed using a commercial anti-HGF/SF antibody, and after protocol optimization with colorectal carcinoma samples, 5 biopsies of normal liver and 17 liver biopsies of patients with steatosis or NASH diagnosis were stained. The number of cases was reduced compared to the ones used for MET staining because adequate biopsy tissue was no longer available for 13 cases being first used to assess MET expression. Variable HGF/SF expression was detected in the cytoplasm of the hepatocytes of both cases and controls as already reported in multiple papers where HGF/SF expression was evaluated in different liver pathologies [64 69]. Hepatocytes showed cytoplasmatic staining but unfortunately, Kupffer cells were always negative. Even if these were not the results we expected, haematoxylin-eosin stained slides and IHC slides were examined by a pathologist who evaluated IHC staining as reported in the result section. A statistical analysis was performed, the variables of interest (HGF/SF staining intensity and HGF/SF staining extension) were scored as previously indicated. The frequency distribution of HGF/SF staining intensity or extension was different between cases and controls, but there was no statistical significance (**Tables 16-17**).

Considering the results obtained with this first Ab, we tried to evaluate a panel of 12 homemade Abs to understand if it was possible to visualize HGF/SF expression in Kupffer cells, the ones who produce the protein within the liver tissue [61 68]. Despite trying different dilutions, incubation times, and different antigen retrieval, 9 out of 11 homemade

polyclonal antibodies gave rise to positive but non-specific staining. This lack of specificity can be easily explained considering the polyclonal nature of these Abs; indeed, it is very likely that other non-specific Abs were present together with anti-HGF/SF Abs. MSH2.B2, MSH2.B6, and the only monoclonal EGH2/4C12.1 passed the first screening phase and were used on liver biopsies. Variable HGF/SF expression was detected in the cytoplasm of the hepatocytes while Kupffer cells were still negative for the staining, so the experiment was interrupted without testing further liver biopsies.

There are some interesting aspects to highlight when considering the results of HGF/SF staining. First, to our knowledge, this is the first time HGF/SF expression was evaluated in patients with steatosis and NASH. Second, normal livers were also used for HGF/SF evaluation. Third, some considerations can be made about the localization of HGF/SF staining. Indeed, Kupffer cells are known to produce HGF/SF [61] but they were not stained, this can be due to the fact that HGF/SF expression could be below the detectable level in FFPE tissues. We also know HGF/SF is released in the extracellular space, making its staining with Abs very complicated in FFPE tissues. In the end, hepatocytes do not produce HGF/SF but they expressed MET receptor, therefore the antibody may detect HGF/SF after it is internalized. This could explain why the hepatocytes were positively stained with anti-HGF/SF antibodies [64].

The last part of the experiments took place at the Center for Engineered Therapeutics in Cambridge, US. These experiments were focused on the development of a new liver-on-a-chip platform where NASH can be induced. HGF/SF, K1K1, and other drugs were then tested on this NASH-on-a-chip. As a side project, HGF/SF and K1K1 were labeled with the intent of injecting these fluorescent proteins in mice to study and compare their diffusion and organ localization after defined time periods. Only the first part of this side project was realized with the labeling of K1K1 and HGF/SF with the Alexa Fluor ® 488 Microscale Protein Labeling Kit as described in the methods section.

The reactive dye has a tetrafluorophenylr® (TFP) ester moiety that is more stable in solution than the commonly used succinimidyl (NHS) ester. TFP esters react efficiently with primary amines of proteins to form stable dye-protein conjugates. The addition of 1M sodium bicarbonate is designed to raise the pH of the reaction mixture to ~8, as TFP esters react most efficiently with primary amines at a slightly alkaline pH. HGF/SF isoelectric point (pI) is at a pH of 8.23 and getting close to that might cause the precipitation of the protein, therefore 1 M sodium bicarbonate was not added during the first experiment. Protein activity was preserved as shown with MDCK scatter assay when

native and fluorescent proteins were compared. Only 26% of HGF/SF and 17% of K1K1 were estimated to be labeled, so it was easy to explain why there was no loss of the biological activity. With the second experiment, 1 M sodium bicarbonate was added to the proteins during the labeling procedure and the percentage of labeled proteins increased to 70% for HGF/SF and to 90% for K1K1, with no sign of precipitation or severe loss of protein. This time the efficient labeling partially decreased K1K1 activity as described in results section but HGF/SF activity was not affected. A spectroscopic method was used to quantify the amount of labelling per protein but was found rather inaccurate and using too much protein. Therefore, cell uptake was used instead to test if both HGF/SF and K1K1 were fluorescent, two five-channel microfluidic devices (model 1) with cell lines were used as described in result section. As it was possible to detect fluorescence inside the HepG2 cells (**Fig. 32**) and U937 (not shown) while stellate cells were not stained (not shown), we concluded that both proteins were labeled and able to bind the MET receptor. Later both proteins were flash frozen in nitrogen for storage at -80 °C.

There are some interesting aspects to highlight after these experiments. First, it will be important to test the biological activity of the 2 proteins after the storage at -80 °C to understand if they are still active and if they are not, trying different storage conditions. Second and most important aspect, TFP esters react efficiently with primary amines of proteins to form stable dye-protein conjugates so, since we determined the structure of K1K1, we can identify lysines on the surface and predict where this binding will take place and judge if indeed the labeling can affect MET receptor and/or heparin binding.

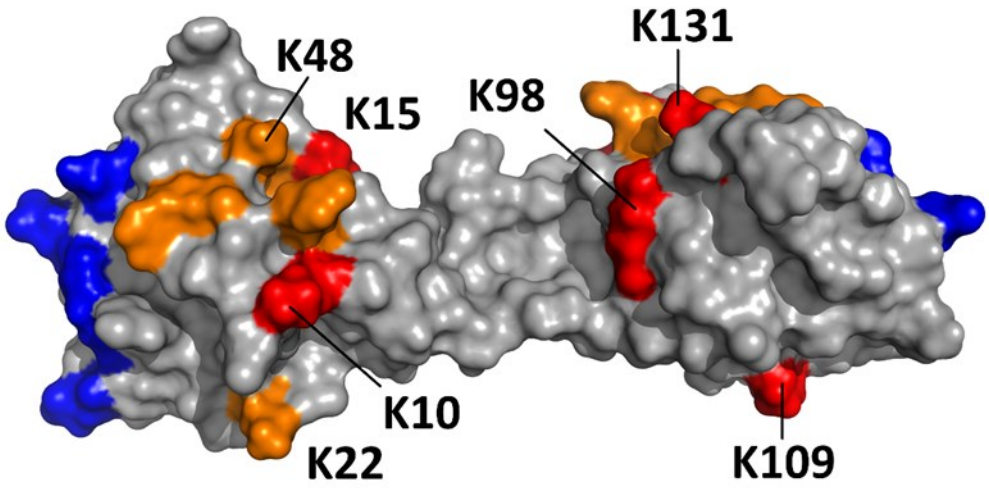

Fig. 45 Surface representation of K1K1 with the MET binding site indicated in blue, the residues interacting with heparin in orange, including four lysine residues, and additional lysine residues in red.

As previously described, HGF/SF has a high-affinity for HSPG and its analogue heparin, and two binding sites were identified, a high-affinity binding site in the N-domain and a low-affinity binding site within the K1 domain [18]. K1K1 instead has a significantly reduced heparin affinity due to the elimination of the N-domain, a characteristic that has improved the protein penetration and distribution *in vivo* [34]. If the dye-protein conjugates interfere with heparin binding sites, the comparison between HGF/SF and K1K1 diffusion and organ localization will be difficult. Therefore, before going *in vivo* an additional step will be needed using for instance Surface Plasmon Resonance (SPR) to analyze whether the labelling has affected MET receptor or heparin binding. By using SPR it could be possible to compare the receptor and heparin affinity of the native proteins and the labeled ones.

As previously stated, the main topic of the experiments at the Center for Engineered Therapeutics in Cambridge, US was the development of a new liver-on-a-chip platform where NASH can be induced and where it could be possible to test the efficacy of drugs.

Many factors make NASH drug development very complicated and one of the most important limitations is the lack of valuable *in vitro* and *in vivo* models that can fully recapitulate all the hallmarks of this complex disease. During the last 10 years, microfluidic-based 3D organ-on-a-chip platforms have been developed making possible the creation of 3D organs in miniature able to recapitulate key physiological features of the liver microenvironment and overcoming therefore the limitations of the previous models [45] [46]. The liver-on-a-chip devices created at the Center for Engineered Therapeutics were 3D vascularized, immune-integrated NASH-on-a-chip with 5 channels. These models were built with the intent of recapitulating the spatial arrangements of the different cell populations of the liver (hepatocytes, stellate cells, Kupffer cells) in a 3D liver tissue matrix. Another key element of these devices was the creation of vasculature in the microfluidic channel (inlet channel), indeed the liver is a highly vascularized organ and the accumulation of circulating fatty acids is a starting point for NASH. Therefore, the endothelial channel can be used to flow the fatty acids to develop NASH and to diffuse new drugs.

In the end, these models of NASH-on-a-chip had the potential to be used to study NASH progression with high fidelity, and for testing drug regimens.

Going deeply inside the experiment, 3 different five-channel models were created with different channel widths (**Fig. 10**), all of them consisting of three hydrogel channels

surrounded by inlet and outlet channels. Standard photolithography was used to prepare model 1 while for model 2 and 3 resin 3D printing was used. Cell lines were used for preliminary tests instead of primary cells to initially study the behavior of the cells inside the channels, to find the most appropriate cells concentration, and to monitor their viability during time. Model 1 was the first to be tested with cell lines, and thanks to these preliminary tests it was possible to define the most appropriate cells concentration, and to assess cell viability. The viability was above 90% 4 days after the seeding but looking at the images collected, it was possible to point out a problem in this first model. The staining faded away when getting closer to the stellate cells channel, indicating a possible problem of diffusion. Therefore, the solution considered was to create model 2 and 3 with reduced width of the channels. This time resin 3D printing was used, the diffusion problem was solved and model 3 was chosen for the final experiment with primary cells. For this experiment 120 five-channel microfluidic devices were prepared but bacterial contamination was reported immediately after NASH induction. Therefore, with great disappointing after 5 months of work, it was not possible to test and compare HGF/SF and K1K1 on these innovative devices. With limited time remaining a solution was found using a simpler 3-channel NASH-on-a-chip as used by Freag et al. (Freag et al., 2020) with success.

In this study, HCs, HSCs, and KCs were mixed with collagen and injected within the middle channel of the devices. NASH was induced by perfusing FFA through the endothelialized inlet microfluidic channel. These devices were under disease-inducing conditions for 10 days, simulating the key hallmarks of NASH, such as accumulation of intracellular lipids inside the hepatocytes, hepatocellular ballooning, and production of inflammatory and profibrotic markers. Elafibranor efficacy was also tested on this platform [45].

It was not possible to use this exact model, but commercial 3D Cell Culture Chips (Aim Biotech) were very similar, immediately available, and ready for cell seeding. Therefore, it was possible to proceed with NASH induction and with the creation of 9 different groups, as reported here:

1. Control
2. NASH
3. NASH + 0.1 μM K1K1
4. NASH + 0.01 μM K1K1
5. NASH + 0.1 μM HGF/SF
6. NASH + 0.1 μM K1K1 + 30 μM TAK-242
7. NASH + M-CSF/IL4
8. NASH + 30 μM TAK-242
9. NASH + 30 μM SR1078

Two different concentrations of K1K1 were used but, considering the low number of devices, it was not possible to test 2 different concentrations of HGF/SF. Drugs concentrations were chosen considering previous experiments where these concentrations were found to be the most effective in reducing apoptosis and converting M1 macrophage/Kupffer cell to M2. Together with HGF/SF and K1K1 other two drugs were tested, TAK-242 and SR1078. TAK-242 is a small-molecule–specific inhibitor of Toll-like receptor (TLR) 4 signaling, it binds to the intracellular domain of TLR4 and inhibits the production of lipopolysaccharide-induced inflammatory mediators such as nitric oxide (NO), TNF-α and Interleukin-6 (IL-6) [53 54]. SR1078 is a synthetic agonist that binds to and modulates the activity of the retinoic acid receptor-related orphan receptors α and γ (RORα and RORγ). These receptors are involved in the regulation of immune functions and metabolism [55]. Both TAK-242 and SR1078 have the potential to switch macrophage/Kupffer cell phenotype from M1 to M2 and were therefore used for this experiment [56 57 58]. The group treated with M-CSF and IL4 was a control group because both factors are known to be strong inducers of the M2 phenotype [58].

Treatments were started simultaneously with lipotoxic stress, media was refreshed every 2 days and collected for storage at -80 °C till day 9 after NASH induction. All the devices were also sacrificed that day to start evaluating NASH hallmarks including lipid accumulation, cell death, inflammation, and fibrosis.

As previously reported, there was a significant accumulation of lipids inside HCs of the NASH group compared to the control (~3-fold, $P<0.0001$), indicating steatosis development. A significative different lipid accumulation was also found when NASH group was compared with groups where drugs were applied (**Fig. 39**).

K1K1 and HGF/SF were both able to reduce lipid accumulation in hepatocytes, even if HGF/SF action seemed to be slightly superior. The findings for K1K1 were in agreement with a previous work where the treatment with K1K1 significantly decreased the steatosis in Lieber DeCarli (LDC) mice models fed with alcohol [34].

The protective role of the HGF/SF-MET pathway in NASH is well known and it was also studied in *in vivo* mice models, showing that one of the consequences of the genetic knockout of MET receptor was increased liver steatosis [47] [48]. In another paper, wild-type C57BL/6 mice were fed a choline-deficient amino acid defined (CDAA) diet and were treated with recombinant feline HGF/SF. The treatment with HGF/SF was effective in reducing liver steatosis [70].

TAK-242, SR1078, HGF/SF and probably also K1K1 have the potential to switch macrophage/Kupffer cell phenotype from M1 to M2 [56] [57] [58] [59]. Here, all of them were able to reduce lipid accumulation in hepatocytes. The efficacy of these drugs in reducing steatosis can be explained by the conversion of M1 macrophages in M2. In Han et al. (Han et al., 2017) paper the roles of M1 and M2 macrophages in the liver were efficiently described as follows: "in the liver, M1 KCs contribute to the pathogenesis of hepatic steatosis and inflammation by secreting cytokines such as TNF-a and IL-1b. In contrast, inactivation of the alternative M2 KCs exacerbates hepatic steatosis and insulin resistance in the HFD-fed mice. M2 KCs promote apoptosis of M1 KCs, thereby protecting hepatocytes against NASH in mice" [58]. The protective role of M2 macrophages was also demonstrated in humans. Indeed, patients with simple steatosis have higher levels of M2 macrophages in the liver compared to patients with severe steatohepatitis [58]. To our knowledge, there are no studies where TAK-242 was used in NASH models while more data are present for SR1078. In Han et al. (Han et al., 2017) it was reported that: "RORα has anti-lipogenic and antioxidative stress functions in the liver, thus protecting against the development of NASH. Treatment with activating ligands of RORα, such as cholesterol sulfates (CSs), SR1078, and JC1-40, may improve the symptoms of NASH and insulin resistance" [58].

Finally, as expected, the combination of K1K1 and TAK-242 was also able to reduce lipid accumulation, and as it showed the strongest reduction of steatosis of all tested conditions there might be an indication for synergistic activity.

The second analysis performed was the evaluation of liver cell apoptosis with cleaved caspase-3 staining. Unfortunately, the number of devices was a limiting factor and only five groups of major interest were used (control, NASH, NASH+K1K1, NASH+TAK-242, and NASH+K1K1+TAK-242 groups). There was a significant increase of apoptotic cells in the NASH group compared to the control (~3-fold, $P<0.0001$), indicating the onset of liver injury. This time the single drug treatments were not effective in reducing the number of

apoptotic cells, but significative difference was found when NASH group was compared with NASH+K1K1+TAK-242 group (P=0.0021) (**Fig. 41**).

The antiapoptotic activity of HGF/SF in the liver is well known, both in normal conditions and in response to liver injuries [8 15 16 17]. The antiapoptotic activity of K1K1 was less studied compared to the parent molecule but it was found that the treatment with K1K1 was more effective than HGF/SF in preventing motor neurons loss in an *in vitro* model of ALS*.* Indeed, when motor neurons were treated with K1K1, there was a total recovery of the viability at a ten-times lower concentration compared to HGF/SF treatment [38].

K1K1 antiapoptotic activity was also tested performing a cell viability assay based on MDCK cells incubated overnight with different concentrations of HGF/SF, K1K1, and NK1 in the presence of the apoptosis inducer anisomycin. This time HGF/SF was more effective but K1K1 was more potent than NK1 in preventing cell death [34].

As stated before, TAK-242, HGF/SF, and probably K1K1 have the potential to switch macrophage/Kupffer cell phenotype from M1 to M2 and it was found that altering polarization towards an M2 phenotype partially reversed steatosis and hepatocyte apoptosis [51 56 57 59]. Therefore, the efficacy of the treatment with these two drugs could be explained by the capability to hit two key drivers of NASH progression, and there might be an indication for synergistic activity.

The third analysis performed was the evaluation of liver fibrosis, another important hallmark of NASH. As discussed before, hepatocyte apoptosis due to lipotoxic stress together with activated M1 Kupffer cells can induce the activation of hepatic stellate cells into myofibroblasts that start producing matrix proteins faster than they are degraded, leading to fibrosis [40].

Increased expression of α-Smooth Muscle Actin (α-SMA) represents a useful marker of HSCs activation and differentiation into myofibroblasts-like cells during NASH progression [45]. In our *in vitro* model, under NASH conditions, HSCs expressed a significantly higher level of α-SMA compared to the control group (P<0.0001). Significative different expression was also found when NASH group was compared with groups where drugs were applied. The treatment with K1K1+TAK-242 seemed to be the most effective (P<0.0001) followed by HGF/SF (P=0.0008), TAK-242 (P=0.0015), and K1K1 (Low) (P=0.0044) (**Fig. 43**).

Here again, the combination of a macrophage-focused immunotherapeutic drug with MET agonist was the most effective treatment. This evidence could be explained by the

capability to hit two key drivers of NASH progression, therefore preventing the development of fibrosis.

Both HGF/SF and K1K1 alone were able to reduce α-SMA expression. This confirm the protective role of the HGF/SF-MET pathway in NASH, where its activation plays an important role in repressing liver fibrosis [47 48 71 72].

Finally, TNF-α was also evaluated using media effluents collected from the devices. In the liver, M1 KCs are known to contribute to the development of steatosis and inflammation by secreting proinflammatory cytokines such as TNF-α, and it was therefore interesting to evaluate this marker using our *in vitro* platform. From literature, TAK-242 and SR1078 treatments were found to be effective in reducing TNF-α, by converting M1 macrophages to M2 in *in vitro* models [53 54 58].

The effect of the activation of the HGF/SF-MET pathway on TNF-α production was studied both *in vitro* and *in vivo*. In M1 bone marrow-derived macrophages (BMDMs) isolated from mice, it was found that HGF/SF-MET signaling was able to induce the expression of Arg-1 mRNA and secretion of IL-10 and TGF-b1 and to downregulate the mRNA expression of iNOS, TNF-α, and IL-6 [59]. In mice models, one of the consequences of the genetic knockout of MET receptor was the increased expression of TNF-α mRNA [47].

K1K1 *in vivo* efficacy was tested on a validated mouse model of subchronic alcohol exposure, the adapted Lieber DeCarli (LDC) model. K1K1 treatment was not only able to decrease steatosis, but the highest doses of K1K1 (2 and 10μg) were also able to significantly decrease the mRNA expression of the proinflammatory cytokines TNFα and IL-6 [34]. K1K1 was also tested in a superoxide dismutase 1 G93A (SOD1G93A) transgenic mice model. Here, K1K1 was not able to reduce the transcript levels of the pro-inflammatory cytokine TNF-α but K1K1 treatment was instead effective in increasing the mRNA expression of anti-inflammatory interleukin 4 (IL-4) [38].

In our NASH-on-a-chip model, we expected to find a significant higher level of TNF-α under NASH conditions compared to the control group, but this was not the case. No significative different expression was also found when NASH group was compared with groups where drugs were applied. Triplicates were used for each group, but the values obtained were very discordant as shown in **Fig 44**. Unfortunately, this was the last ELISA assay that could be performed as there was no material left to repeat the analysis.

These preliminary experiments led to interesting findings. Nevertheless, it should also be highlighted that these studies on NASH-on-a-chip have some limitations. First, according to the original plan, 120 devices should have been used but we ended up using only 41,

therefore with less devices for each group of study and with a reduced possibility to test more drug concentrations and more drug combinations. Second, it would have been necessary to repeat the experiment to confirm the results, but it was not possible because the experiment was performed less than one month before the end of my time in Cambridge.

Conclusions and future perspectives

These preliminary *in vitro* studies on K1K1 were useful to compare its stability and biological activity to the parent molecule HGF/SF, highlighting K1K1 superiority.

As previously reported, two different methods were used to compare the stability of the three proteins with conflicting results. On one hand, SDS-PAGE gel showed HGF/SF was less stable and prone to degradation over time while on the other hand, Tycho NT.6 analysis did not show increased destabilization and unfolding of HGF/SF during the three weeks of incubation. At that time, it was not possible to use triplicates for each protein because HGF/SF availability was the limiting factor, therefore it should be worth repeating the experiment using triplicates for each protein and including thermally unfolded proteins as controls. Another good suggestion could be the use of a third method to evaluate protein stability.

After the experiments dedicated to the evaluation of proteins stability, it was possible to study pathways activation in two liver cell lines after stimulation with K1K1, HGF/SF, and other recombinant proteins, showing both K1K1 and HGF/SF were the most potent agonist being able to induce a high level of AKT and ERK phosphorylation also when the cells were treated with the lowest protein concentrations.

Assessment of MET protein expression with IHC in FFPE liver samples of patients with NAFLD was also important to show that MET receptor is expressed on the hepatocytes and therefore K1K1 could be tested for future therapy in such a liver disease.

A valid concern with such treatments using potent growth factors is the stimulation/induction of tumor growth, however previous clinical trials with HGF/SF have not revealed such side effect and no excess cancer mortality was reported [73]. This might be explained by the fact that in many cases the tumor growth is driven by MET activating mutations and/or MET amplification leading to ligand independent receptor activation [74].

Finally, we have evaluated the protective effect of K1K1 and its combination with macrophage immunotherapy on a NASH-on-a-chip model. The combination therapy was found to be the most effective in reducing steatosis, apoptosis, and fibrosis.

The NASH-on-a-chip model used here could represent a major innovation to study NASH progression and for testing new drugs. These complex devices can work as a bridge between simple *in vitro* assays and *in vivo* experiments; therefore, it will be interesting to follow their future development.

A continued collaboration with Oleg Melnyk and Jérôme Vicogne at the university of Lille has been expanded with a collaboration between Boehringer and the university of Paris which will hopefully soon yield more information to support the use of K1K1 in regenerative medicine.

References

1. Roth, G. A. *et al.* Global, regional, and national age-sex-specific mortality for 282 causes of death in 195 countries and territories, 1980–2017: a systematic analysis for the Global Burden of Disease Study 2017. *Lancet* **392**, 1736–1788 (2018).
2. Lozano, R. *et al.* Global and regional mortality from 235 causes of death for 20 age groups in 1990 and 2010: A systematic analysis for the Global Burden of Disease Study 2010. *Lancet* **380**, 2095–2128 (2012).
3. Blair, N. F., Frith, T. J. R. & Barbaric, I. Regenerative medicine: Advances from developmental to degenerative diseases. *Adv. Exp. Med. Biol.* **1007**, 225–239 (2017).
4. Ren, X., Zhao, M., Lash, B., Martino, M. M. & Julier, Z. Growth Factor Engineering Strategies for Regenerative Medicine Applications. *Front. Bioeng. Biotechnol.* **7**, 1–9 (2020).
5. Nakamura, T. *et al.* Molecular cloning and expression of human hepatocyte growth factor. *Nature* **342**, 440–443 (1989).
6. Stoker, M., Gherardi, E., Perryman, M. & Gray, J. Scatter factor is a fibroblast-derived modulator of epithelial cell mobility. *Nature* **327**, 239–242 (1987).
7. Puerta, A. B. F., Prado, M. M., Frampton, A. E. & Jiao, L. R. Gene of the month: HGF. *J. Clin. Pathol.* **69**, 575–579 (2016).
8. Nakamura, T., Sakai, K., Nakamura, T. & Matsumoto, K. *Hepatocyte growth factor twenty years on: Much more than a growth factor*. *Journal of Gastroenterology and Hepatology (Australia)* vol. 26 (2011).
9. Imamura, R. & Matsumoto, K. Hepatocyte growth factor in physiology and infectious diseases. *Cytokine* **98**, 97–106 (2017).
10. Mungunsukh, O., McCart, E. A. & Day, R. M. Hepatocyte growth factor isoforms in tissue repair, cancer, and fibrotic remodeling. *Biomedicines* **2**, 301–326 (2014).
11. Garajová, I., Giovannetti, E., Biasco, G. & Peters, G. J. c-Met as a target for personalized therapy. *Transl. Oncogenomics* **2015**, 13–31 (2015).
12. Matsumoto, K., Umitsu, M., De Silva, D. M., Roy, A. & Bottaro, D. P. Hepatocyte growth factor/MET in cancer progression and biomarker discovery. *Cancer Sci.* **108**, 296–307 (2017).
13. Skead, G. & Govender, D. Gene of the month: MET. *J. Clin. Pathol.* **68**, 405–409 (2015).
14. Petrini, I. Biology of MET: A double life between normal tissue repair and tumor progression. *Ann. Transl. Med.* **3**, (2015).
15. Huh, C. G. *et al.* Hepatocyte growth factor/c-met signaling pathway is required for efficient liver regeneration and repair. *Proc. Natl. Acad. Sci. U. S. A.* **101**, 4477–4482 (2004).
16. Borowiak, M. *et al.* Met provides essential signals for liver regeneration. *Proc. Natl. Acad. Sci. U. S. A.* **101**, 10608–10613 (2004).
17. Giebeler, A. *et al.* c-Met Confers Protection Against Chronic Liver Tissue Damage and Fibrosis Progression After Bile Duct Ligation in Mice. *Gastroenterology* **137**, 297-308.e4 (2009).
18. Ross, J. *et al.* Protein engineered variants of hepatocyte growth factor/scatter factor promote proliferation of primary human hepatocytes and in rodent liver. *Gastroenterology* **142**, 897–906 (2012).

19. Roos, F., Ryan, A. M., Chamow, S. M., Bennett, G. L. & Schwall, R. H. Induction of liver growth in normal mice by infusion of hepatocyte growth factor/scatter factor. *Am. J. Physiol. - Gastrointest. Liver Physiol.* **268**, (1995).
20. Hartmann, G. *et al.* Engineered mutants of HGF/SF with reduced binding to heparan sulphate proteoglycans, decreased clearance and enhanced activity in vivo. *Curr. Biol.* **8**, 125–135 (1998).
21. Cioce, V. *et al.* Hepatocyte growth factor (HGF)/NK1 is a naturally occurring HGF/scatter factor variant with partial agonist/antagonist activity. *J. Biol. Chem.* **271**, 13110–13115 (1996).
22. Chan, A. M. L. *et al.* Identification of a competitive HGF antagonist encoded by an alternative transcript. *Science (80-.).* **254**, 1382–1385 (1991).
23. MIYAZAWA, K., KITAMURA, A., NAKA, D. & KITAMURA, N. An alternatively processed mRNA generated from human hepatocyte growth factor gene. *Eur. J. Biochem.* **197**, 15–22 (1991).
24. Jakubczak, J. L., Larochelle, W. J. & Merlino, G. NK1, a Natural Splice Variant of Hepatocyte Growth Factor/Scatter Factor, Is a Partial Agonist In Vivo. *Mol. Cell. Biol.* **18**, 1275–1283 (1998).
25. Gherardi, E. *et al.* Structural basis of hepatocyte growth factor/scatter factor and MET signalling. *Proc. Natl. Acad. Sci. U. S. A.* **103**, 4046–4051 (2006).
26. Gherardi, E. *et al.* Functional map and domain structure of MET, the product of the c-met protooncogene and receptor for hepatocyte growth factor/scatter factor. *Proc. Natl. Acad. Sci. U. S. A.* **100**, 12039–12044 (2003).
27. Tolbert, W. D., Daugherty-Holtrop, J., Gherardi, E., Vande Woude, G. & Xu, H. E. Structural basis for agonism and antagonism of hepatocyte growth factor. *Proc. Natl. Acad. Sci. U. S. A.* **107**, 13264–13269 (2010).
28. Holmes, O. *et al.* Insights into the Structure/Function of Hepatocyte Growth Factor/Scatter Factor from Studies with Individual Domains. *J. Mol. Biol.* **367**, 395–408 (2007).
29. Chirgadze, D. Y. *et al.* Crystal structure of the NK1 fragment of HGF/SF suggests a novel mode for growth factor dimerization and receptor binding. *Nat. Struct. Biol.* **6**, 72–79 (1999).
30. Blaszczyk, M., Harmer, N. J., Chirgadze, D. Y., Ascher, D. B. & Blundell, T. L. Achieving high signal-to-noise in cell regulatory systems: Spatial organization of multiprotein transmembrane assemblies of FGFR and MET receptors. *Prog. Biophys. Mol. Biol.* **118**, 103–111 (2015).
31. Donate, L. E. *et al.* Molecular evolution and domain structure of plasminogen-related growth factors (HGF/SF and HGF1/MSP). *Protein Sci.* **3**, 2378–2394 (1994).
32. Lokker, N. A., Presta, L. G. & Godowski, P. J. Mutational analysis and molecular modeling of the n-terminal kringle-containing domain of hepatocyte growth factor identifies amino acid side chains important for interaction with the c-metreceptor. *Protein Eng. Des. Sel.* **7**, 895–903 (1994).
33. Simonneau, C. *et al.* Semi-synthesis of a HGF/SF kringle one (K1) domain scaffold generates a potent in vivo MET receptor agonist. *Chem. Sci.* **6**, 2110–2121 (2015).
34. Leclercq, B. *et al.* A minimal hepatocyte growth factor mimic acting as a powerful agonist of the MET receptor tyrosine kinase for regeneration of epithelial tissues and organs. *bioRxiv* (2020) doi:10.1101/2020.07.20.212654.
35. Ultsch, M., Lokker, N. A., Godowski, P. J. & De Vos, A. M. Crystal structure of the NK1 fragment of human hepatocyte growth factor at 2.0 Å resolution. *Structure* **6**, 1383–1393 (1998).
36. Schwall, R. H. *et al.* Heparin induces dimerization and confers proliferative activity onto the

hepatocyte growth factor antagonists NK1 and NK2. *J. Cell Biol.* **133**, 709–718 (1996).

37. Sakata, H. *et al.* Heparin binding and oligomerization of hepatocyte growth factor/scatter factor isoforms. Heparan sulfate glycosaminoglycan requirement for Met binding and signaling. *J. Biol. Chem.* **272**, 9457–9463 (1997).
38. Vallarola, A. *et al.* A novel HGF/SF receptor (MET) agonist transiently delays the disease progression in an amyotrophic lateral sclerosis mouse model by promoting neuronal survival and dampening the immune dysregulation. *Int. J. Mol. Sci.* **21**, 1–20 (2020).
39. Romero, F. A., Jones, C. T., Xu, Y., Fenaux, M. & Halcomb, R. L. The Race to Bash NASH: Emerging Targets and Drug Development in a Complex Liver Disease. *J. Med. Chem.* **63**, 5031–5073 (2020).
40. Friedman, S. L., Neuschwander-Tetri, B. A., Rinella, M. & Sanyal, A. J. *Mechanisms of NAFLD development and therapeutic strategies*. *Nature Medicine* vol. 24 (2018).
41. Drew, L. Drug development: Sprint finish. *Nature* **551**, S86–S89 (2017).
42. Younossi, Z. *et al.* Global Perspectives on Nonalcoholic Fatty Liver Disease and Nonalcoholic Steatohepatitis. *Hepatology* **69**, 2672–2682 (2019).
43. Ratziu, V., Goodman, Z. & Sanyal, A. Current efforts and trends in the treatment of NASH. *J. Hepatol.* **62**, S65–S75 (2015).
44. Müller, F. A. & Sturla, S. J. Human in vitro models of nonalcoholic fatty liver disease. *Curr. Opin. Toxicol.* **16**, 9–16 (2019).
45. Freag, M. S. *et al.* Human Nonalcoholic Steatohepatitis on a Chip. *Hepatol. Commun.* **5**, 217–233 (2021).
46. Sosa-Hernández, J. E. *et al.* Organs-on-a-chip module: A review from the development and applications perspective. *Micromachines* **9**, (2018).
47. Drescher, H. K. *et al.* c-Met signaling protects from nonalcoholic steatohepatitis- (NASH-) induced fibrosis in different liver cell types. *Oxid. Med. Cell. Longev.* **2018**, (2018).
48. Kroy, D. C. *et al.* Hepatocyte specific deletion of c-Met leads to the development of severe non-alcoholic steatohepatitis in mice. *J. Hepatol.* **61**, 883–890 (2014).
49. Kazankov, K. *et al.* The role of macrophages in nonalcoholic fatty liver disease and nonalcoholic steatohepatitis. *Nat. Rev. Gastroenterol. Hepatol.* **16**, 145–159 (2019).
50. Mehal, W. Z. The inflammasome in liver injury and non-alcoholic fatty liver disease. *Dig. Dis.* **32**, 507–515 (2014).
51. Wan, J. *et al.* M2 Kupffer cells promote M1 Kupffer cell apoptosis: A protective mechanism against alcoholic and nonalcoholic fatty liver disease. *Hepatology* **59**, 130–142 (2014).
52. Svendsen, P. *et al.* Antibody-Directed Glucocorticoid Targeting to CD163 in M2-type Macrophages Attenuates Fructose-Induced Liver Inflammatory Changes. *Mol. Ther. - Methods Clin. Dev.* **4**, 50–61 (2017).
53. Yamada, M. *et al.* Discovery of novel and potent small-molecule inhibitors of NO and cytokine production as antisepsis agents: Synthesis and biological activity of alkyl 6-(N-substituted sulfamoyl)cyclohex-1-ene-1-carboxylate. *J. Med. Chem.* **48**, 7457–7467 (2005).
54. Matsunaga, N., Tsuchimori, N., Matsumoto, T. & Ii, M. TAK-242 (resatorvid), a small-molecule inhibitor of Toll-like receptor (TLR) 4 signaling, binds selectively to TLR4 and interferes with interactions between TLR4 and its adaptor molecules. *Mol. Pharmacol.* **79**, 34–41 (2011).

55. Wang, Y. *et al.* Identification of SR1078, a synthetic agonist for the orphan nuclear receptors RORα and RORγ. *ACS Chem. Biol.* **5**, 1029–1034 (2010).
56. Wu, L. *et al.* Multiwalled carbon nanotubes prevent tumor metastasis through switching M2-polarized macrophages to M1 via TLR4 activation. *J. Biomed. Nanotechnol.* **15**, 138–150 (2019).
57. Yamaguchi, T. *et al.* Low-dose paclitaxel suppresses the induction of M2 macrophages in gastric cancer. *Oncol. Rep.* **37**, 3341–3350 (2017).
58. Han, Y. H. *et al.* RORα Induces KLF4-Mediated M2 Polarization in the Liver Macrophages that Protect against Nonalcoholic Steatohepatitis. *Cell Rep.* **20**, 124–135 (2017).
59. Nishikoba, N. *et al.* HGF-MET Signaling Shifts M1 Macrophages Toward an M2-Like Phenotype Through PI3K-Mediated Induction of Arginase-1 Expression. *Front. Immunol.* **11**, 1–10 (2020).
60. Kleiner, D. E. *et al.* Histology of NAFLD and NASH in Adults and Children. **20**, 293–312 (2017).
61. Nakamura, T. Structure and function of hepatocyte growth factor. *Prog. Growth Factor Res.* **3**, 67–85 (1991).
62. Žoldák, G., Jancura, D. & Sedlák, E. The fluorescence intensities ratio is not a reliable parameter for evaluation of protein unfolding transitions. *Protein Sci.* **26**, 1236–1239 (2017).
63. Bruzzì, S. *et al.* B2-Lymphocyte responses to oxidative stress-derived antigens contribute to the evolution of nonalcoholic fatty liver disease (NAFLD). *Free Radic. Biol. Med.* **124**, 249–259 (2018).
64. J-i, O., Okano, J., Shiota, G. & Kawasaki, H. Second Department of Internal Medicine, Tottori University School of Medicine, Yonago 683, Japan. 151–159 (1999).
65. D'Errico, A. *et al.* Liver hepatocyte growth factor does not always correlate with hepatocellular proliferation in human liver lesions: Its specific receptor c- met does. *Hepatology* **24**, 60–64 (1996).
66. Terada, T., Nakanuma, Y. & Sirica, A. E. Immunohistochemical demonstration of MET overexpression in human intrahepatic cholangiocarcinoma and in hepatolithiasis. *Hum. Pathol.* **29**, 175–180 (1998).
67. Szparecki, G., Ilczuk, T., Gabzdyl, N., Stocka-ŁAbno, E. & Górnicka, B. Expression of c-MET protein in various subtypes of hepatocellular adenoma compared to hepatocellular carcinoma and non-neoplastic liver in human tissue. *Folia Biol. (Czech Republic)* **63**, 146–154 (2017).
68. Takeishi, T. *et al.* The role of Kupffer cells in liver regeneration. *Archives of Histology and Cytology* vol. 62 413–422 (1999).
69. Tangtrongchitr, P. *et al.* Hepatic expression of HGF/C-met and native liver survival in biliary atresia. *Pediatr. Surg. Int.* **36**, 597–602 (2020).
70. Yang, Y. M. *et al.* Interventional potential of recombinant feline hepatocyte growth factor in a mouse model of non-alcoholic steatohepatitis. *Front. Endocrinol. (Lausanne).* **9**, 1–10 (2018).
71. Tojima, H. *et al.* Hepatocyte growth factor overexpression ameliorates liver inflammation and fibrosis in a mouse model of nonalcoholic steatohepatitis. *Hepatol. Int.* **6**, 620–630 (2012).
72. Kiyama, S. *et al.* Reduction of fibrosis in a rat model of non-alcoholic steatohepatitis cirrhosis by human HGF gene transfection using electroporation. *J. Gastroenterol. Hepatol.* **23**, (2008).
73. Cui, Y. L. *et al.* Recombinant human hepatocyte growth factor for liver failure. *Contemp. Clin. Trials* **29**, 696–704 (2008).

74. Moosavi, F., Giovannetti, E., Saso, L. & Firuzi, O. HGF/MET pathway aberrations as diagnostic, prognostic, and predictive biomarkers in human cancers. *Crit. Rev. Clin. Lab. Sci.* **56**, 533–566 (2019).

Scientific production arisen from this thesis

Vallarola, A. et al. A Novel HGF/SF Receptor (MET) Agonist Transiently Delays the Disease Progression in an Amyotrophic Lateral Sclerosis Mouse Model by Promoting Neuronal Survival and Dampening the Immune Dysregulation. Int J Mol Sci. 21(22):8542 (2020).

Acknowledgements

“Everything will be okay in the end. If it's not okay, it's not the end.” —John Lennon

This PhD was a disappointing experience, but I think such kind of things can help you understand you have to change something in your life and move on. Anyway, I had the possibility to know amazing people during these three years and I really want to thank them so….

Thank you, Lorenzo. You were always by my side even when we were 6000 km away, thank you for your love and for your patience.

Thank you, Elena. Thank you for your support even during the darkest hours when I was away from home.

Thank you, Rosangela and Alberto. I hope you are proud of me.

Thank you, Giuseppe, Antonio, Emilia. Finally, and officially, a part of my family!

Thank you, Hugo. I am here today, writing the acknowledgments just because of you. Thank you because you never gave up on me.

Thank you, Luisa, Michele, and Cristina. You are the heart of the GFG group.

Thank you, Sasha, Martina, Elisa, Michela, Giulia, Filippo, and Michele. Saturday’s evenings with you were amazingly funny even if the cocktails were from hell!

Thank you, Michaela. You were the half part of the “Europe team”. A friend and an amazing scientist. I loved our holiday in Washington!

Thank you, Tanmoy. An amazing scientist and a good guy. It was an honor to meet you.

Thank you, Monica. Thank you for your messages when I was in the US. I loved working with you even if it was for a short time!

Thank you, Cristian. Thank you for your friendship and for cheering me up.

Thank you, Alessia, Claudia, Priscilla, Michela, and Prof. Boldorini. Somehow, I keep on coming back to Novara every time!

Thank you, Prof. Gherardi, Prof. Sengupta, Prof. Valente, Prof. Carini and Prof. Vicogne.

Thank you to all the professors and researchers of the Department of Molecular Medicine, Division of Immunology and General Pathology.

I am sure I forgot someone maybe it was intentional or maybe it was not. Who knows? In the end, I would like to thank everyone who helped me get this PhD. Thank you!!

Appendix

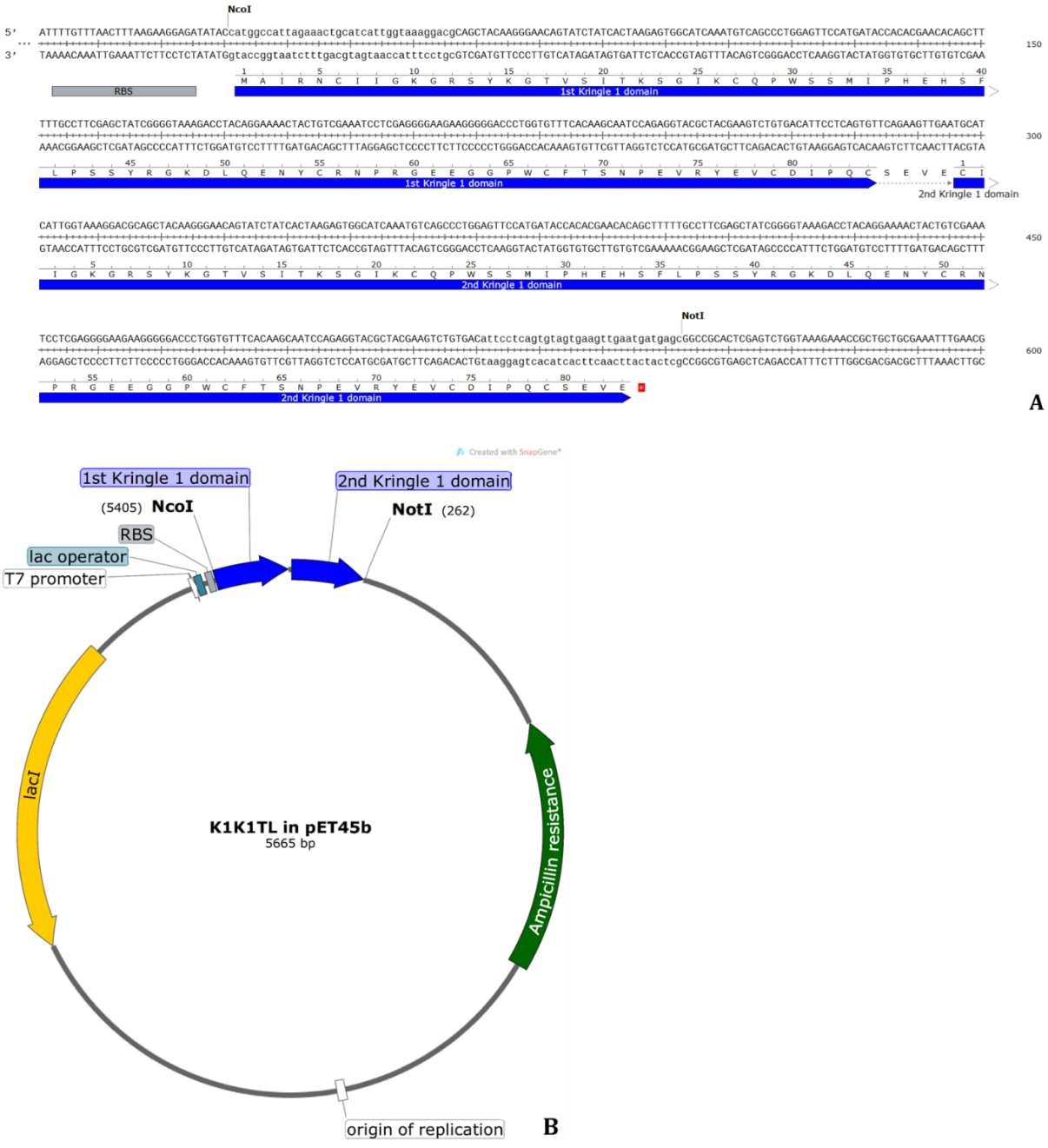

Fig. 46 K1K1 insert (**A**) inside multiple cloning site of pET45b (+) expression vector (**B**).

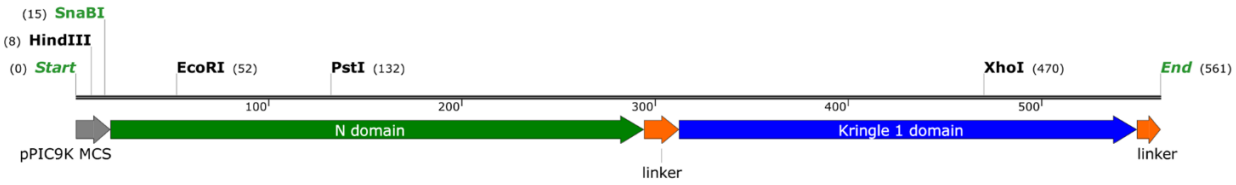

Fig. 47 1K1 insert inside multiple cloning site of pPIC9K expression vector.

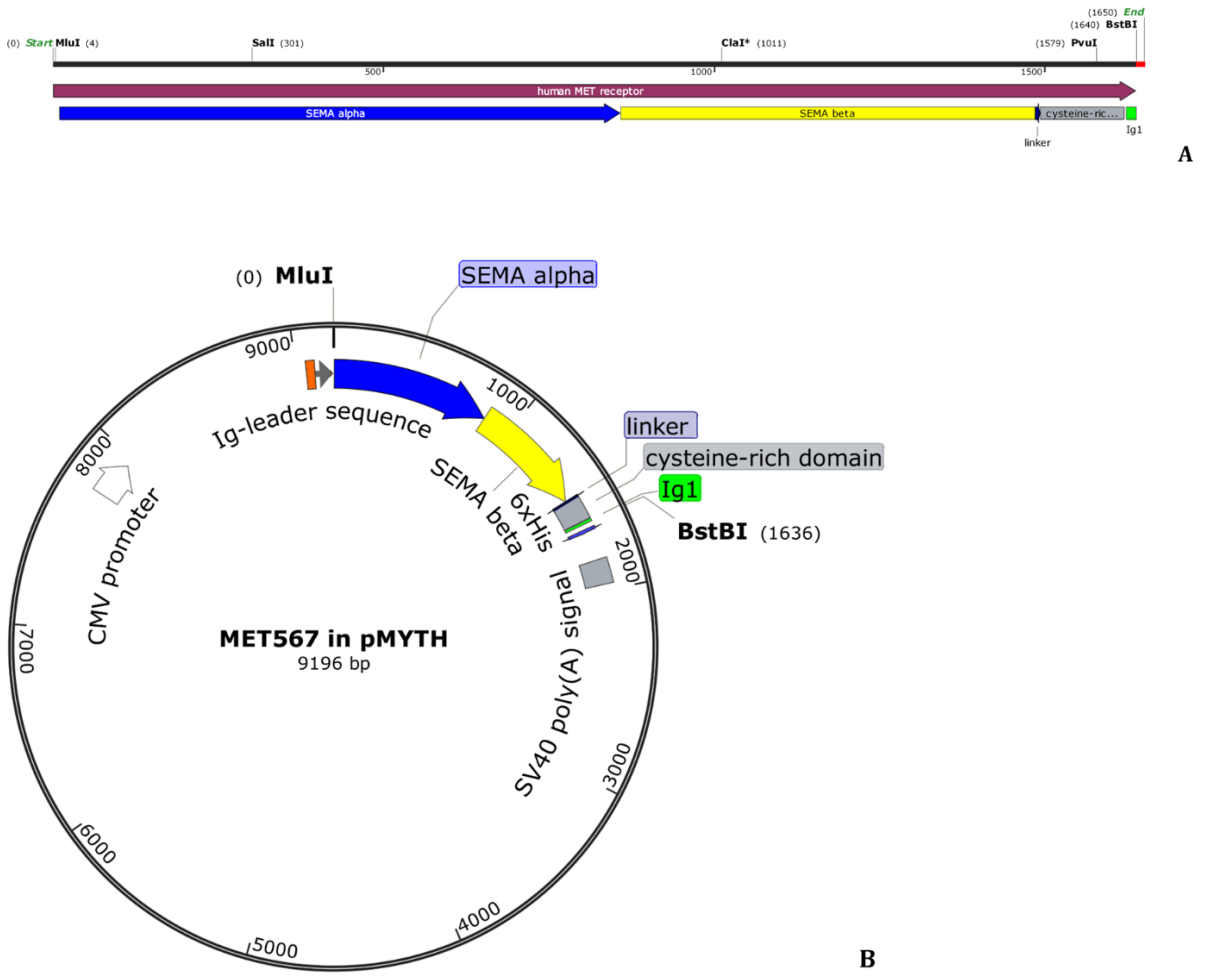

Fig. 48 MET567 insert (**A**) inside multiple cloning site of proprietary pMYTH expression vector (**B**).